Entangled Polymer Melts in Extensional Flow

Hengeller, Ludovica; Hassager, Ole; Skov, Anne Ladegaard; Almdal, Kristoffer

Publication date:
2016

Document Version
Peer reviewed version

Entangled Polymer Melts in Extensional Flow

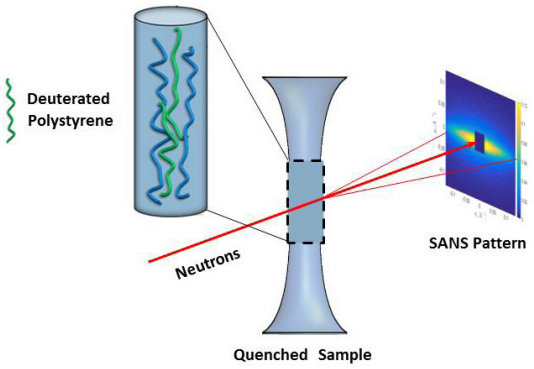

Ludovica Hengeller

PhD Thesis

March 2016

DTU Chemical Engineering
Department of Chemical and Biochemical Engineering

Entangled Polymer Melts in Extensional Flow

Ludovica Hengeller

Ph.D. Thesis

March 2016

Department of Chemical and Biochemical Engineering
Danish Polymer Centre
Technical University of Denmark
Søltofts Plads, Building 227
DK-2800 Kongens Lyngby, Denmark

Acknowledgements

This thesis presents the results of my Ph.D. project. The work was carried out at the Danish Polymer Centre, Department of Chemical and Biochemical Engineering, Technical University of Denmark from April 2013 to March 2016 under the supervision of Professor Ole Hassager, Associate Professor Anne Ladegaard Skov at DTU Chemical and Biochemical Engineering and Professor Kristoffer Almdal at DTU Nanotech. The research leading to these results has received funding from three financing sources: 1/3 by the Danish Council for Independent Research - Natural Sciences (Det Frie Faskningsråd / Natur od Univers)(FNU) under EPMEF on Grant 0602-02179B , 1/3 by Kemiteknik (Technical University of Denmark) and 1/3 by Danish Polymer Centre (DPC) co-financing.

I have truly enjoyed my three years as a Ph.D. student in Denmark and that has been for me not only a work but a life experience that has changed me deeply. First and foremost I would like to express my gratitude to my main supervisor Professor Ole Hassager for giving me the opportunity to perform this study in the Danish Polymer Centre. I am very grateful for his efforts to help, inspire, advise and support me throughout these three years. I have really enjoyed working and spending time with him whether it was discussing about science or hicking/biking in Bornholm and Capri. I would like to thank my co-advisor Associate Professor Anne Ladegaard Skov for her help, support and encouragement; and Professor Kristoffer Almdal for fruitful and stimulating discussions about my project.

A special thanks goes to Dr. Qian Huang who has been of crucial importance to me and my work. Her encouragement in critical moments and guidance in the experimental work have been decisive for the success of my Ph.D.

I would also like to thank Associate Professor Nicolas Alvarez for our fruitful and stim-

ulating discussions and for the guidance throughout the first part of my Ph.D. and Dr. Irakli Javakhishvili for the moral support, the understanding and the scientific discussions. Also in this regard I will thank all the Hassager Group: Sara, Aamir and Martin. It has been great to learn from our group meeting, discussions about experimental rheology and the endless amount of new ideas for novel experimental procedures.

I am grateful also for the pleasant working environment. Thanks to all my nice colleagues at the Danish Polymer Centre. In particular I would like to thank Kim Chi Szabo for running SEC and DSC for my samples. I would also like to thank Hanne for helping me in filling in travel claims and find accommodations. Without her organization skills I could not have concentrated on my research work. I am thankful to the Workshop staff for all the invaluable work on the apparatus and for the preparation of the neutron scattering samples and the sample's holder.

Special thanks go to my EPMEF colleagues.

I thank all my friends for giving me the important balance between free time and work. Finally I wish to express my deepest gratitude to all my nearest and dearest for their moral support: my dad Mario, my brother Carlo, my aunt Chiara and especially my mum Teresa who has bear me all the way and given outsider's view to my research problems.

Kgs. Lyngby, March 2016

Ludovica Hengeller

Abstract

Many commercial materials derived from synthetic polymers exhibit a complex response under different processing operations such as fiber formation, injection moulding, film blowing, film casting or coatings. They can be processed both in the solid or in the melted state. Often they may contain two or more different polymers in addition to additives, fillers or solvents in order to modify the properties of the final product. Usually, it is also desired to improve the processability. For example the supplement of a high molecular weight component improves the stability in elongational flows. On the other hand, addition of low-volatility solvents to polymers is also a common industrial practice that offers a means for lowering the T_g of the polymers. Moreover industrial polymers present a wide distribution of chain lengths and/or branched architectures that strongly influence their response.

Understanding the behaviour of polymer melts and solutions in complex non-linear flows is crucial for the design of polymeric materials and polymer processes. Through rheological characterization, in shear and extensional flow, of model polymer systems, i.e. narrow molar mass distribution polymer melts and solutions or well defined polymer molecules architecture, researchers develop constitutive equations that can relate the stress induced into a material with its flow deformation history. Indeed experiments on samples with well-defined structure supply data that can be compared with models.

Current models have been shown to be quite successful in describing the dynamics of polymers although they are still continuously challenged by new experimental data on model polymer systems. At the same time, new methods for generating extensional flows [McKinley and Sridhar (2002), Sentmanat (2004), Bach *et al.* (2003b)] are being constantly refined to improve the quality of the data and to explore a wider range of rates and deformations. Moreover, recently rheometry methods have been supplemented by other techniques such as dielectric spectroscopy that can probe chain

dynamics and neutron scattering which can monitor macromolecular chain orientation associated with induced flow fields.

This work concerns linear and non-linear rheology of polystyrene melts and solutions coupled with neutron scattering experiments. The aim of this thesis is to investigate the extensional properties of well characterized polymer samples and provide new experimental data on extensional rheology that can validate constitutive models. Moreover we show how the extensional technique may be used in combination with small-angle neutron scattering (SANS) to perform single chain structural studies after uniaxial elongation both after steady extensional flow and at several times during true stress relaxation. Extensional experiments have been performed on a Filament Stretching Rheometer (FSR), placed at the Technical University of Denmark (DTU), equipped with an online controlled scheme that allows to operate in controlled strain rate or controlled stress mode. High temperatures measurements can be performed due to an oven that surrounds the sample environment. Also a new implemented version of the device, named VADER 1000, has been employed to prepare the neutron scattering samples. The reduced dimension, compared to the FSR, and the particular design of the oven meets the requirement of fast cooling of the sample, so that it can freeze the particular molecular orientation of the chains at different stages of the stretching or relaxing of the sample.

Resumé

Reologiske og strukturelle undersøgelser af kædeindviklede polymerer i forlængelse

Mange kommercielle materialer, der stammer fra syntetiske polymerer udviser en kompleks respons under forskellige behandlinger, såsom fiberdannelse, sprøjtestøbning, filmblæsning, og film-støbning eller belægning. Polymererne kan forarbejdes både i fast eller smeltet form. Ofte kan materialerne indeholde to eller flere forskellige polymerer foruden additiver, fyldstoffer eller opløsningsmidler for at modificere egenskaberne af det endelige produkt. Sædvanligvis er det også ønskeligt at forbedre procesegenskaberne. F.eks. forbedres stabiliteten i forlængelsesstrømning ved at tilføre en højmolekylær komponent. Tilsætning af lav-volatile opløsningsmidler til polymerer er også en almindelig industriel praksis, der anvendes til sænkning af glasovergangstemperaturen (T_g) af polymererne. Desuden har industrielle polymerer ofte en bred fordeling af kædelængder og/eller forgrenede arkitekturer, som stærkt påvirker deres mekaniske egenskaber.

Forståelsen af polymer-smelter og -opløsninger i komplekse ikke-lineære flow er afgørende for designet af polymer-materialer og polymer-forarbejdning. Gennem reologisk karakterisering, i forskydnings- og forlængelsesstrømning af model polymersystemer, er der udviklet ligninger, som kan relatere stress induceret i et materiale med dens flow deformation. Målinger af polymerer med veldefineret struktur passer med de udviklede modeller.

Nuværende modeller har vist sig at være ganske succesfulde i at beskrive polymerdynamikken, selvom modellerne stadig bliver udfordret af nye eksperimentelle data af polymersystemer. Samtidig, bliver nye eksperimentelle metoder til at generere forlængelsesstrømning [McKinley and Sridhar (2002), Sentmanat (2004), Bach *et al.*

(2003b)] konstant forbedret for at højne kvaliteten af data, samt at udforske en bredere vifte af strækhastigheder og deformationer. Desuden er nyere reometri blevet suppleret med andre teknikker, såsom dielektrisk spektroskopi der kan måle polymerkædedynamik, og neutronspredning som kan måle makromolekylær kædeorientering forbundet med inducerede flow felter.

Denne afhandling omhandler lineær og ikke-lineær- reologi samt neutronspredning af polystyren smelter og opløsninger. Formålet med denne afhandling er at undersøge egenskaber af velkarakteriserede polymerer i forlængelse og at ekstrahere eksperimentel data om forlængelsesreologi reologi, der kan validere konstitutive modeller. Endvidere viser vi, hvordan den eksperimentelle metode kan anvendes i kombination med små-vinkel neutronspredning (SANS) til at udføre studier af enkeltkædede strukturer efter uniaksial stræk både efter konstant strømning og under spændingsrelaksation.

Eksperimenterne blev udført med et Filament Stretching Rheometer (FSR) på Danmarks Tekniske Universitet (DTU). FSR er udstyret med en kontrolenhed, som tillader at måle prøverne ved kontrolleret deformationshastighed eller stress. Målinger ved højere temperaturer blev udført vha. en ovn, der omslutter instrumentet. Ydermere har en ny-implementeret enhed, VADER 1000, muliggjort at klargøre prøverne til neutronspredning. Den reducerede størrelse af VADER 1000, sammenlignet med FSR, og den særlige udformning af ovnen opfylder kravet om hurtig afkøling af prøven, således at den kan fryse den særlige molekylære orientering af kæderne på forskellige stadier af strækning eller relaksation af prøven.

Contents

CHAPTER 1

Introduction

1.1 General Introduction to Polymer Rheology

The objective of rheology is to relate the stress induced within a flow deformation with the deformation that has caused it. The response of the material is physically attributed to its molecular structure. In particular the mechanical response of polymers, either in a solution or in melt state, is highly sensitive to their structure on the molecular level.

The presumed origin of the complex mechanical and rheological behaviour exhibited by polymers are the entanglements, i.e. topological interactions between the chains, which arise when chains are long enough to overlap. Chain topology can be linear, branched or dendritic. Depending on the branch distribution the effect on the rheological response can be dramatically different.

In rheological modelling the aim is to derive, by means of the microscopic physics of the polymers, constitutive equations able to predict the experimentally measured macroscopic stresses from the deformation history of the material. To achieve the goal a physical characterization of polymer conformation is needed rather than an actual chemical description. In the following approach a polymer chain is described by a generic bead-spring model that does not account for the different chemistries.

1.2 Molecular Theories for Melts and Solutions

1.2.1 Unentangled Polymers

Throughout the past sixty years a number of molecular models that describe the polymer dynamics in solution and in melt have been proposed. They are based on assumptions on molecular interaction and motion of molecules and aim to capture the dynamic of polymers in melts and solutions. Among bead-spring models the Rouse model [Rouse (1953)] is the one that takes into account the overall interactions of the polymer molecule with the surrounding solvent distributing the frictional force between a series of points. It considers the molecule composed of beads connected by springs (see figure 1 .1). The beads experience a Brownian motion and a drag force moving through the solvent while the springs represent the constraints. Originally this theory was proposed to explain the linear viscoelasticity of polymers in dilute solutions, since ignores intra-molecular uncrossability, excluded volume and hydrodynamic interactions but it turned out to well describe unentangled melts (i.e. low molecular weight).

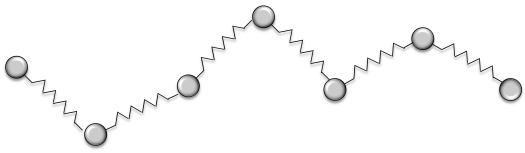

Figure 1.1: Illustration of the bead-spring chain in the Rouse Model

In presence of an imposed flow field the dynamic of the chain in solution can be described by a system of N independent differential equations (one on each dumbell) whose analytic solution enables the decomposition of the chain motion into a spectrum of different modes. Each mode has its own characteristic relaxation time which contributes to the overall relaxation modulus of the chain [Doi (1996)], given by:

$$G(t) = \nu k_B T \sum_{p=1}^{\infty} \exp\left(-2t/\tau_p\right) \tag{1.1}$$

where $G_N^0 = \nu k_B T$ is the elastic modulus, $\nu = N/V$ is the number of chains N per unit volume V, k_B is the Boltzmann constant and T is the temperature. The characteristic relaxation time τ_p of each mode is defined as:

$$\tau_p = \frac{\zeta N^2 b^2}{p^2 3\pi k_B T} \tag{1.2}$$

where ζ is the friction coefficient, b is the length of a Kuhn segment (distance between the centers of two adjacent beads) and p is the mode number. The longest relaxation time, i. e. the relaxation time of the whole chain, τ_R, also called Rouse time, can be found by setting $p = 1$ in equation 1.2:

$$\tau_R = \tau_1 = \frac{\zeta N^2 b^2}{3\pi k_B T} \tag{1.3}$$

The Rouse theory predicts a scaling of τ_R with the molecular weight as $\tau_R \propto M^2$ and a scaling of the zero-shear viscosity as $\eta_0 \propto M$. However, it was shown by experiments that chains diluted in a θ solvent exhibit a scaling with the power of 1.5 [Berry *et al.* (1968), Colby *et al.* (1987)]. In dilute solutions, the Rouse model takes into account the frictional interactions along the chain but disregards their effect on solvent veloc-ity, where the hydrodynamic interaction produces a disturbance altering the flow rate. Therefore it requires Zimm's correction to account for hydrodynamic interactions.

The Rouse Model instead describes well the dynamics of concentrated solutions and melts where chain are not entangled, i.e. their molecular weight is below the critical molecular weight $M < M_c$.

Figure 1.2 shows the Rouse model predictions for the storage modulus G' and the loss modulus G" as function of frequency ω. The modes distribution generates the typical slopes of the moduli, which are respectively 2 and 1 in the low frequency range, also called terminal regime. Eventually they collapse on a unique line, in the high frequency regime, with a slope of 0.5.

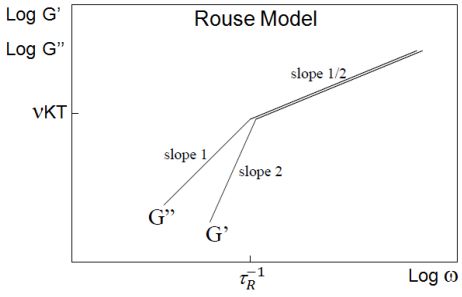

Figure 1.2: Illustration of the frequency response of the polymer chains in the Rouse Model.

Despite its limitations the Rouse model, and more in particular the Rouse time, is still a powerful tool broadly used to study the rheological behaviour of melts and concentrated solutions.

1.2.2 Entangled Polymers

In the framework of entangled polymer melts and solutions, where polymer chains exceed a critical molecular weight M_c ($M > M_c$) to generate an impermanent polymer network, the motion of each chain is not anymore independent from the surrounding ones. Therefore, the polymer dynamics become a cooperative and many-body problem. A simplified picture was proposed by Edwards (1967). He considered a test chain where Brownian motion is restricted due to the presence of topological interactions, the entanglements, with the neighbouring molecules. The entanglements thus constitute a tube-like region, characterized by a primitive path that defines its axis, which limits the movement of the chain along a plane orthogonal to the central axis of the tube. At equilibrium, the primitive path is a random of walk of step length a. a is also defined as the tube diameter (distance between two entanglements). The length of the tube at equilibrium can be expressed as $L_{eq} = aZ$, where $Z = M/M_e$ is the number of entanglements.

Shortly after de Gennes (1971) described the chain relaxation in an entangled poly-mer melt as being possible through a sliding mechanism back and forth along the tube axis. This movement, called reptation is treated as a 1-D diffusion problem and was the base for the work of Doi and Edwards (1986) which derived the molecular constitu-tive equations that express the mechanism. The reptation model can describe well the terminal relaxation and ultimately the zero-shear viscosity η_0 but it cannot capture the high-frequency region conversely from the Rouse model.

The behaviour of G' and G" (see figure 1.3) shows the right slopes of 2 and 1 in the terminal regime, at low frequencies, while at intermediate frequencies G" does not capture the slope of $-1/4$ experimentally observed but approaches instead a slope of $-1/2$. This picture suggests that the reptation model alone is inadequate to describe the linear viscoelasticity of polymers.

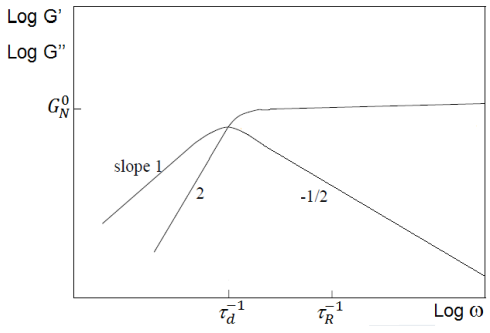

Figure 1.3: Illustration of the frequency response of the chains in the Reptation Model.

The Doi and Edwards (1986) (DE) model, known as tube model, describes the relaxation process of stresses caused only from an orientation of the segments; it assumes that the molecules cannot be stretched by the deformation field. As the chain diffuses, new tube segments are created while old ones are forgotten. The tube looses memory of its original configuration. Each end segment is not correlated with the others. Hence it is possible to derive the fraction of polymer still constrained in the tube, also called 'memory function'. The corresponding predicted relaxation modulus for the unrelaxed portion is:

$$G(t) = G_N^0 \sum_{p=odd} \frac{8}{p^2\pi^2} \exp\left(-\frac{tp^2}{\tau_d}\right) \tag{1.4}$$

Where τ_d is the reptation time defined as:

$$\tau_d = \frac{Z^2 a^2 \zeta_0 N}{\pi^2 k_B T} \tag{1.5}$$

and ζ_0 is the monomeric friction.

The model predicts a scaling for the zero-shear viscosity η_0 with the molecular weight of $\eta_0 \propto M^3$ close to the experimental observations which show a power law dependence of 3.4 [Berry *et al.* (1968), Colby *et al.* (1987)]. The explanation is that the chain-end fluctuations inside the tube where neglected. The plateau modulus has been defined in the DE model as:

$$G_N^0 = \frac{4}{5}\frac{\rho RT}{M_e} \tag{1.6}$$

were M_e is the molecular weight of a strand between two entanglements and its relaxation time is:

$$\tau_e = \frac{a^2 \zeta_0 N}{3\pi k_B T}. \tag{1.7}$$

Those two parameters are independent of M in the tube model for linear viscoelasticity (i. e. when deformations are small and the system is close to the equilibrium configuration).

In figure 1.4 the frequency response of G' and G" predicted from the tube model with the slopes corresponding to each region is shown.

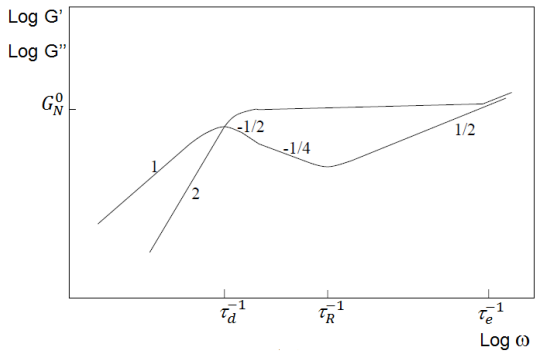

Figure 1.4: Illustration of the frequency response of the chains in the Tube Model.

While the reptation idea of de Gennes (1971) gave the input for interpreting the behaviour in the linear viscoelastic region, the real novelty introduced by Doi and Edwards has been the formulation of a constitutive equation for non-linear viscoelasticity based on reptation and tube ideas [Doi and Edwards (1978)].

Taking the case of stress relaxation after a large step strain the relaxation modulus $G(t, \gamma)$ is function not only of time but also of the strain applied. The time-dependent component of the response is controlled by reptation while the strain-dependent component is dominated by a chain-retraction mechanism, activated just in non-linear deformations that involve only orientation, not stretching, of the molecules. This novel dynamics is a Rouse-like process governed by the Rouse time (τ_R) that takes place instantaneously, much before the reptation process starts. Hence the large-strain relaxation occurs basically in two steps: a fast stretch-relaxation process that only involves friction and not topological constraints. It is governed by a Rouse time where the chain wants to retract to the original tube length (to regain equilibrium tension and monomer density). And a second step: the orientation relaxation happening at the reptation time (τ_d).

Over the years, the original DE model has been extensively modified by including additional relaxation and non-reptative processes to improve its accuracy. Two disengagement movements have been incorporated to obtain quantitative predictions of the linear viscoelasticity of monodisperse melts. The contour length fluctuations (CLF) mechanism [Doi (1981)] which considers the discrepancy in the dynamic of relaxation experienced by the middle chain segments respect to the chain-ends. The latter ones are less constrained in the movements and their fluctuations are faster than the reptation process. Hence they release faster the stress renewing the tube orientation and decrease

the viscosity with respect to reptation prediction (only the fraction of the tube that survives has to relax by reptation [Likhtman and McLeish (2002), Milner and McLeish (1998)]). Chain-end fluctuations are more effective in short chains. As the chain length increases, the effect of the chain-end fluctuations progressively looses importance.

The second correction is the constraint release (CR) which gives a better description of the entanglements and the restrictions of the test chain with the molecules that form the tube. In the original DE theory the deformation of the tube axis is affine and the tube diameter remains fixed at equilibrium value. This would imply a non-mobility of the surrounding chains that are imposing their constraints. Although is unrealistic that the tube will remain static while there is simultaneous relaxation of the other molecules. Many attempts have been done to describe this process [Graessley (1982), Marrucci (1985), Tsenoglou C. (1987), des Cloizeaux (1988), Viovy *et al.* (1991)].

Several versions of the tube model in the linear regime including both CLF and CR exist, i.e. the Likhtmann-Mcleish model [Likhtman and McLeish (2002)] and the time-marching algorithm [van Ruymbeke *et al.* (2007)]. Their predictions can capture the 3.4 power dependency of the viscosity from the molecular weight.

In the original Doi and Edwards theory, a crucial difference between stretch and orientation was introduced. Indeed the problem was simplified by setting $\tau_R = 0$, i.e. by assuming that chains retract virtually instantly and stress is simply due to orientation. Nonetheless, if the flow has a rate larger than the inverse of the Rouse time, then also chain stretch becomes important in determining the stress and it cannot be assumed to relax instantaneously. Hence is needed to decouple stretch and orientation contributions. The chain stretch is defined as $\lambda = L/L_0$, where L is the tube length and L_0 is the tube length at equilibrium. The polymer molecule stretches due to the drag arising from the convection exerted from the flow on the surrounding molecules. The result is an increase of the tube length as well as an additional stress [Marrucci and Grizzuti (1988)].

Another non-linear effect that has been included in constitutive equations for entangled polymers is the so called Convective Constraint Release (CCR) [Marrucci (1996), Marrucci and Ianniruberto (1996), Marrucci and Ianniruberto (2000)]. CCR arises from chain retraction and it is very similar to the release process that occurs in the linear regime. Indeed, retraction of any given chain removes entanglements from other chains, which can then relax the orientation more quickly than in the absence of the CCR mechanism.

1.3 Rheological Characterization

In order to characterize constitutive equations a series of rheometric flows are generally used. The most common ones are shear, uniaxial elongation and planar extensional flows. The main focus of this work is on the first two kinds of experiments. It is indeed possible to get different kind of informations about the fluid behaviour due to the dissimilar relative motion of the particles.

Even though the response to flow of a material is governed by the structure on the molecular level, on a larger scale flow motion it is common to consider the polymer melt as a continuum medium in which it is possible to define intermolecular forces as macroscopic stresses. For each kind of flow we have the definitions of velocity gradient tensor $\underline{\underline{K}}$ and a deformation gradient tensor $\underline{\underline{E}}$, usually used to write constitutive equations for viscoelastic materials. However it is usual to plot the stress normalized by the deformation rate rather than the measured stress. The resulting quantity would be a time-dependent stress growth coefficient, either in shear:

$$\eta = \frac{\sigma_{xy}}{\dot{\gamma}} \tag{1.8}$$

or in uniaxial elongation:

$$\bar{\eta} = \frac{\sigma_{zz} - \sigma_{xx}}{\dot{\varepsilon}} \tag{1.9}$$

Using the coordinate system shown in Figure 1.5.

1.3.1 Shear and Extensional Flow

In a shear experiment the polymeric material is placed between two parallel plates with a certain gap and the deformation of the upper one establishes a velocity field:

$$\begin{aligned} v_x &= \dot{\gamma}_{xy} y \\ v_y &= 0 \\ v_z &= 0 \end{aligned} \tag{1.10}$$

$\dot{\gamma}_{xy}$ is the velocity gradient or shear rate [Bird *et al.* (1987)]. That can be expressed in

tensorial terms as:

$$\underline{\underline{K}}(t) = \begin{bmatrix} 0 & \dot{\gamma} & 0 \\ 0 & 0 & 0 \\ 0 & 0 & 0 \end{bmatrix} \tag{1.11}$$

while the corresponding deformation gradient tensor is:

$$\underline{\underline{E}}(t, t') = \begin{bmatrix} 0 & \gamma & 0 \\ 0 & 0 & 0 \\ 0 & 0 & 0 \end{bmatrix} \tag{1.12}$$

Uniaxial extension flow is the simplest among extensional flows. The velocity field (making the assumption of incompressibility) in that case is expressed by the equations:

$$\begin{aligned} v_x &= -(\dot{\varepsilon}/2)\, x \\ v_y &= -(\dot{\varepsilon}/2)\, y \\ v_z &= \dot{\varepsilon} z \end{aligned} \tag{1.13}$$

where $\dot{\varepsilon}$ is the elongational strain rate. It is possible to define a velocity gradient:

$$\underline{\underline{K}} = \begin{bmatrix} -\dot{\varepsilon}/2 & 0 & 0 \\ 0 & -\dot{\varepsilon}/2 & 0 \\ 0 & 0 & \dot{\varepsilon} \end{bmatrix} \tag{1.14}$$

and a deformation gradient:

$$\underline{\underline{E}} = \begin{bmatrix} e^{-\varepsilon/2} & 0 & 0 \\ 0 & e^{-\varepsilon/2} & 0 \\ 0 & 0 & e^{\varepsilon} \end{bmatrix} \tag{1.15}$$

A description of ideal uniaxial extensional flow is represented in Figure 1.5 where a cylinder of initial height L_0 and initial radius R_0 at time $t = 0$ is pulled in z direction (and at the same time is subject to the same compression in x and y directions) to the final height $L(t)$. For an incompressible material, i.e. melt or solution, the volume is constant:

$$V = \pi R_0^2 L_0 = \pi R(t)^2 L(t) \tag{1.16}$$

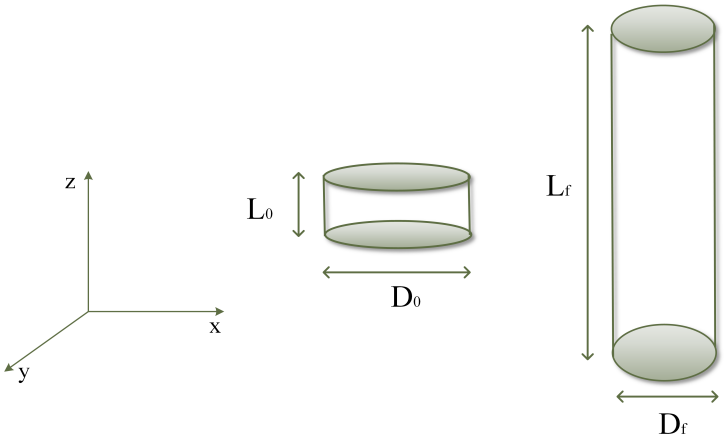

Figure 1.5: Illustration of uniaxial extension.

The velocity in the z-direction can be then expressed as:

$$v_z = \frac{dL}{dt} = \dot{\varepsilon} L(t) \tag{1.17}$$

and the final length of the sample will then be:

$$L(t) = L_0 \exp(\dot{\varepsilon} t) = L_0 \exp(\varepsilon) \tag{1.18}$$

where $\varepsilon = \dot{\varepsilon} t$ is the Hencky strain and can be written as:

$$\varepsilon = \dot{\varepsilon} t = \ln(L(t)/L_0) = -2 \ln(R(t)/R_0) \tag{1.19}$$

From which we can calculate the radius:

$$R = R_0 \exp[-(\dot{\varepsilon}/2) t] = R_0 \exp(-\varepsilon/2) \tag{1.20}$$

It is also possible to define the stretch ratio as the ratio of the final height of the cylinder

over the initial one:

$$\lambda = L(t)/L_0 = [R_0/R(t)]^2 \tag{1.21}$$

On the microscopic level we can define other parameters such as the maximum stretch ratio:

$$\lambda_{\max} = \frac{R_{\max}}{R_{eq}} = \frac{bN}{aN/N_e} = N_e^{1/2} \tag{1.22}$$

1.3.2 Linear and Non-Linear Viscoelasticity

Polymers are composed by very long molecules that above a critical molecular weight starts to interact with each other forming constraints that cause their so-called viscoelastic behaviour. They exhibit an intermediate response between the one of a viscous liquid, governed by the Newton's law, where the shear stress is proportional to the deformation rate and the fluid has no memory, and the one of an elastic solid, described by the Hooke's law, where as the deformation γ_{yx} depends on both t_0 (starting time) and t (final time) there is a memory stored in the material:

$$Newton's \quad Law \quad \sigma_{yx} = \eta\dot{\gamma}_{yx}(t) \tag{1.23}$$

$$Hooke's \quad Law \quad \sigma_{yx} = G\gamma_{yx}(t_0, t) \tag{1.24}$$

σ_{yx} is the stress, η is the viscosity and G is the elastic or shear modulus.

The deformation is defined as:

$$\gamma_{yx}(t_0, t) = \int_{t_0}^{t} \dot{\gamma}_{yx}(t')dt' \tag{1.25}$$

while the deformation rate definition is :

$$\dot{\gamma}_{yx}(t) = \frac{\partial}{\partial t}\gamma_{yx}(t_0, t) \tag{1.26}$$

The equations 1.23 and 1.24 describe the stress induced in a Newtonian fluid and in a Hookean solid. They can be combined in series leading to an empirical model also known as Maxwell model. The consequence of this coupling has as result that the stress of each contribution (newtonian and hookean) is equal and uniform:

$$\sigma_{yx} = \sigma_{yx,N} = \sigma_{yx,H} \tag{1.27}$$

while the total deformation becomes a sum of the two contributions, newtonian $\gamma_{yx,N}$ and hookean $\gamma_{yx,H}$ as well as the deformation rate:

$$\gamma_{yx} = \gamma_{yx,N} + \gamma_{yx,H} \tag{1.28}$$

$$\dot{\gamma}_{yx} = \dot{\gamma}_{yx,N} + \dot{\gamma}_{yx,H} \tag{1.29}$$

Inserting equation 1.23 and equation 1.24 differentiated in equation 1.29 we get:

$$\sigma_{yx} + \frac{\eta}{G}\frac{\partial \sigma_{yx}}{\partial t} = \eta \dot{\gamma}_{yx} \tag{1.30}$$

where the ratio $\eta/G = \lambda$ is defined as the relaxation time of the material (if $\lambda \to 0$ gives back the Newtonian model whether if $\lambda \to \infty$ gives back to the Hookean model). The Maxwell model is the simplest viscoelastic model that describes the linear behaviour of liquid-like materials. Substituting η with the zero-shear viscosity η_0 and considering as integration boundary conditions all the past deformations from $t' =]-\infty; t]$ where $t = t'$ is the present time and the corresponding strain rate is $\dot{\gamma}_{yx}(t')$ we can integrate the differential equation 1.30 obtaining the solution:

$$\sigma_{yx}(t) = \int_{-\infty}^{t} \left[\frac{\eta_0}{\lambda} \exp\left(\frac{-(t-t')}{\lambda}\right)\right] \dot{\gamma}_{yx}(t')\, dt' \tag{1.31}$$

The stress can be expressed with the general form of the linear viscoelastic model as:

$$\sigma_{yx}(t) = \int_{-\infty}^{t} G(t-t')\, \dot{\gamma}_{yx}(t')\, dt' \tag{1.32}$$

where $G(t-t')$ is the response function, i.e. the relaxation modulus (which is decreasing with time).

In a shear experiment with constant shear rate the viscosity η is defined as:

$$\eta = \frac{\sigma_{yx}}{\dot{\gamma}_{yx}} = \int_{-\infty}^{t} G\left(t - t'\right) dt' = \int_{0}^{\infty} G\left(s\right) ds \tag{1.33}$$

with $s = t - t'$.

In shear flows, where the deformation applied to the melted material is small or the shear rates applied are slow, the polymer molecules are only slightly deformed from their equilibrium configuration. The chains have time to relax by rotation along the backbone and by reptation throughout their surrounding, those motions are generally called Brownian motions. In order to quantify the inherent viscous and elastic contribution to the stress of a viscoelastic material it is used a small amplitude oscillatory experiment (also called frequency sweep test). A time-dependent sinusoidal strain of the form:

$$\gamma\left(t\right) = \gamma_0 \sin \omega t \tag{1.34}$$

is applied to the material, where γ_0 is the strain amplitude and ω is the angular frequency. The resulting stress induced in the material is out of phase with the strain and is expressed as:

$$\sigma_{yx} = \sigma_{yx,0} \sin\left(\omega t + \delta\right) \tag{1.35}$$

where δ is the phase shift between stress and strain. Furthermore it is possible to decompose the total stress in two components:

$$\sigma_{yx}\left(t, \omega\right) = \gamma_0 G'\left(\omega\right) \sin\left(\omega t\right) + \gamma_0 G''\left(\omega\right) \cos\left(\omega t\right) \tag{1.36}$$

The in-phase component corresponds to the elastic contribution and is named storage modulus G', while the out-of-phase component is a measure of the loss of energy due to viscous dissipation, also referred to as loss modulus G''. Under oscillatory shear flow the velocity gradient can be expressed in complex variables, and using the general expression for the stress in the linear viscoelastic range (see equation 1.32) we get:

$$\sigma_{yx}\left(t, \omega\right) = i\omega\gamma\left(t\right) \int_{0}^{\infty} G\left(s\right) e^{-i\omega s} ds \tag{1.37}$$

Introducing the definition of complex modulus as the LaPlace transform of the stress relaxation modulus (eq. 1.32) multiplied by $i\omega$ we can write:

$$G^*(\omega) = i\omega \int_{-\infty}^{t} e^{-i\omega(t-t')} G(t-t')\, dt' \tag{1.38}$$

at this point equation 1.37 can be rewritten as:

$$\sigma_{yx}(t,\omega) = \gamma(t)\, G^*(\omega) \tag{1.39}$$

It is possible either to specify the modulus $G(t)$ or give the moduli $G'(\omega)$ and $G''(\omega)$

$$G'(\omega) = \omega \int_0^{\infty} \sin(\omega t)\, G(t)\, dt \tag{1.40}$$

$$G''(\omega) = \omega \int_0^{\infty} \cos(\omega t)\, G(t)\, dt \tag{1.41}$$

So one can switch between the stress relaxation and the storage and loss moduli responses by performing a Fourier transform. To probe the entire linear viscoelastic response of the material the measurements must span on a large range of frequencies. Moving to a uniaxial extensional experiment the general expression for the stress in the linear viscoelasticity can be again obtained from the general expression in tensorial form:

$$\underline{\underline{\sigma}} = \int_{-\infty}^{t} G(t-t')\dot{\underline{\underline{\gamma}}}(t')\, dt' \tag{1.42}$$

where, in the case of uniaxial elongational flow, the rate of strain components are given as:

$$\dot{\gamma}_{xx} = \dot{\gamma}_{yy} = -\dot{\varepsilon} \quad and \quad \dot{\gamma}_{zz} = 2\dot{\varepsilon} \tag{1.43}$$

In the start up of extensional flow (for $t > 0$) at constant stretch rate $\underline{\underline{\dot{\gamma}}}(t') = \dot{\varepsilon}$ the stress growth coefficient is defined as:

$$\bar{\eta}^{+} = \frac{\sigma_{zz} - \sigma_{xx}}{\dot{\varepsilon}} \tag{1.44}$$

If we insert them in the equation 1.32 we get the two expressions for σ_{rr} and σ_{zz}:

$$\sigma_{rr} = -\dot{\varepsilon} \int_{-\infty}^{t} G(t - t')dt' \tag{1.45}$$

$$\sigma_{zz} = 2\dot{\varepsilon} \int_{-\infty}^{t} G(t - t')dt' \tag{1.46}$$

that combined together gives:

$$\sigma_{zz} - \sigma_{xx} = 3 \int_{0}^{t} G(t - t')\,\dot{\varepsilon}dt' \tag{1.47}$$

The stress growth coefficient is then rewritten in the integral form as:

$$\bar{\eta}^{+} = 3 \int_{-\infty}^{t} G(t - t')\,dt' \tag{1.48}$$

and comparing this expression with the linear viscoelastic stress growth coefficient equation 1.33 we get the relationship between stress growth coefficient in extension and in shear flow, also defined as Trouton ratio:

$$\bar{\eta}^{+} = 3\eta \tag{1.49}$$

Trouton's ratio links extensional properties with shear properties. Figure 1.6 shows a typical uniaxial extension experiment. In the linear region (i. e. at low Hencky strain rates $\dot{\varepsilon}$) the data obey the linear viscoelastic envelope (solid line), which is 3 times the shear viscosity (see Equation 1.49). The transient stress growth coefficient $\bar{\eta}^{+}(t)$ approaches at long times a constant value, the steady-state elongational viscosity $\bar{\eta}_s$, which equals the zero-elongation-rate viscosity $\bar{\eta}_0$ [Bird *et al.* (1987)](according to

equation 1.49 we have $\bar{\eta}_0 = 3\eta_0$, where η_0 is zero-shear-rate viscosity and $\bar{\eta}_0$ is the zero-elongation-rate viscosity). As the stretch rate $\dot{\varepsilon}$ is increased data enter the non-linear regime. The extensional non-linearity is recognisable as a deviation from the LVE. Polymer melts and solutions, which are strain hardening materials, show a sudden upturn in the curve before levelling off to a steady-state value $\bar{\eta}_s$ (not always observable in experimental data due to limitations of the rheometers or sample's instabilities) which becomes a function of the stretch rate.

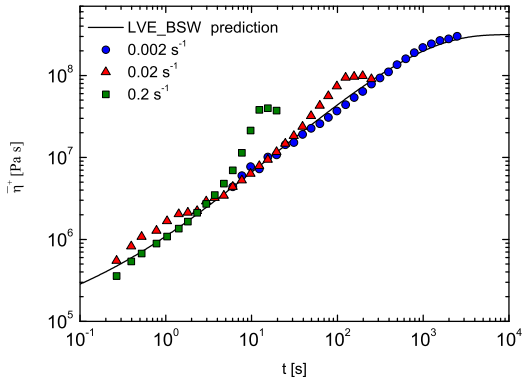

Figure 1.6: Stress growth coefficient data of linear PS-150k performed at 130 °C at three different strain rates.

Shear rheology experiments have been the benchmark for the validation of different theoretical molecular models and for the experimental study of polymeric materials. Mainly experimental measurements occur in the linear viscoelastic regime (LVE). From these kind of experiments the linear viscoelastic properties and the zero-shear-rate viscosity η_0 (which is the viscosity of the liquid obtained in the limit of shear rate $\dot{\gamma}$ tending to zero and the material viscosity is still in the linear response regime) are usually obtained. Nevertheless also non-linear viscoelastic behaviour can be measured with rotational rheometers, for example in a step-strain experiment or in a steady strain rate experiment. The polymer chains experience a high degree of orientation. However in shear rheology is difficult to induce chain stretching and reproduce what polymer molecules experience during polymer processing operations (where extensional properties are totally dominating or they are in combination with shear properties). If the shear rate or the deformation amplitude exceed a critical value, the polymer chains start to orient and reorganize along the flow and they are not anymore close to the equilibrium configurations, i.e. they exceed the LVE limits. The deformations occurring in a number of polymer processing operations are huge and fast and result in a non-linear response of the material. Thus the study of a complex material in the non-linear region is more complicated since deformation rate, magnitude and the kinematics of

the deformation need to be accounted. Moreover, besides the importance in industrial applications, elongational flows are of interest in the validation of constitutive models.

1.4 State of the Art: Extensional Rheometers

Experimental research in extensional rheology has been for many years very limited due to the difficulties in produce accurate data in extensional experiments.

Careful and reliable extensional measurements are very challenging to perform due to experimental limitations in addition to a number of instabilities arising during the experiments. For example: a. The interactions of the polymer sample with any adjacent walls or solid interface would introduce a shear component, resulting in a not pure extensional flow. b . Problems associated with gravitation and surface tension rise in absence of walls. c. The dimensions of the sample increases exponentially with actual strain and handling this increasing dimension puts limitation to obtainable strains, indeed measurements are limited to small deformations.

Throughout the years many different experimental setups have been designed. The clamping system, introduced by Cogswell (1969), represents the first attempt to perform extensional experiments. The system was composed of two belts, pulling in opposite directions, and the strip-shaped sample was fixed at the extremities of the belts with clamps. One problem was that the deformation was simply imposed without any observable confirmation of the actual strain while the force was recorded. Also, measurements were limited to small strains, due to the difficulty in performing an exponentially increased speed of the clamps. A following version [Meissner (1972)] tried to solve the rate problem introducing rotational clamps. They were fixed on wheels rotating opposite to each other at a constant speed such that the resulting strain rate imposed on the sample was also constant. Gravitational effects were avoided placing the sample in a bath of silicone oil. Other improvements brought at constant strain rate experiments with Hencky strain up to $\varepsilon = 7$. An even newer design of the Meissner rheometer [Meissner and Hostettler (1994)], where nitrogen was used as a fluid bed for the sample and the clamps where replaced with conveyor belts, was commercialized by Rheometric Scientific with the name 'Rheometrics Melt Extensiometer' (RME). It has been the most used device to measure elongational flow of polymer melts until the birth of the filament stretching rheometers.

The Münstedt Tensile Rheometer (MTR) [Münstedt (1979)] is another type of rheometer based always on the clamping system. For the first time it was possible to perform measurements at constant strain rate, constant stress and stress relaxation in extensional flow. An oil bath was used to avoid gravitational sagging but the max strain reachable was $\varepsilon = 4$ because of the increasing dimension of the sample.

The Sentmanat Extensional Rheometer (SER) [Sentmanat (2004)] is a testing equipment that can be adapted easily to various type of rheometers to stretch polymer melts under uniform extensional deformation. It incorporates dual wind-up drums. The versatility and simple manipulation quickly made SER become one of the most popular extensional rheometers. A similar device was soon designed by TA Instruments with the name Extensional Viscosity Fixture (EVF). However, both SER and EVF can only reach a maximum Hencky strain of around 3.5.

Filament Stretching Rheometers

To encounter the problem of measuring the extensional properties of polymer solutions, which are more difficult to handle in experimental setups due to the low viscosity, first some methods as opposing jets or spin-line rheometers were proposed. However they generate a flow with a strong shear component that makes very difficult to obtain an accurate measure of the extensional viscosity. In the last two decades, filament stretching rheometers have been used increasingly as a means for measuring accurately the extensional viscosity of polymer solutions[Matta and Tytus (1990), Sridhar *et al.* (1991), Tirtaatmadja and Sridhar (1993), Spiegelberg *et al.* (1996)]. In a filament stretching device, a sample is placed between two rigid end-plates and an elongated fluid filament is formed by a rapid separation of the plates. A force transducer attached to one of the end plates measures the tensile force generated by the elongation and a laser micrometer measures the evolution in the diameter of the fluid column at the filament mid-plane. The middle part of the filament during stretching is considered to be subject to solely elongational flow. A very detailed review on filament stretching rheometry has been written by McKinley and Sridhar (2002). A number of different experimental configurations have been introduced: (a) Both plates accelerate symmetrically in opposite directions with user-imposed profiles, such that the axial mid-plane remains stationary at z=0 and the radius decreases exponentially in time (b) The bottom plate remains stationary and the top plate accelerates upwards. The mid-plane thus also accelerates upwards (c) The top plate remains stationary and the lower plate accelerates downwards [Matta and Tytus (1990), Sridhar *et al.* (1991)].

In the work of Matta and Tytus (1990), the lower plate was accelerate under the application of a constant force (gravity) rather than a constant strain rate. Sridhar *et al.* (1991) introduced a device to visually measure the diameter and attached a motor to the bottom plate such that the velocity of the moving plate could be controlled. During the stretching, while the distance between the plates increased exponentially in time, the central part of the diameter did not decrease exponentially as the ideal case, due to the no-slip boundary at the end-plates. Therefore no overall constant strain rate at the center part was observed. Tirtaatmadja and Sridhar (1993) throughout the online observation of the mid-diameter during stretching could adjusted the speed of the plates, so that the strain rate in the middle is kept constant. The iterative procedure requires a series of experiments to get the aimed separation speed of the end plates. Anna *et al.* (1999) were the first having the idea of introducing a closed loop instead of using

an open loop to control the end plates separation from the online observation of the mid-diameter.

The Filament Stretching Rheometer (FSR)

The Filament Stretching Rheometer (FSR) used in this Ph.D. project has been designed and developed by Bach *et al.* (2003b) at the Technical University of Denmark. The main novelty in its design is the vertical oven that surrounds the sample environment and ensures measurements not only of solutions but also melts at high temperatures ($T \in [15\,°C; 200\,°C]$). Some efforts during the past 10 years have been done to assure a stable and uniform temperature in the oven. The heat exchange with the surrounding environment was limited by the add of an insulating shell. Nitrogen is injected from holes placed at the bottom of the oven to avoid sample degradation during the experiment. A laser is used for on-line determination of the the mid-filament diameter and a weight cell, connected with the bottom plate, detects the force exerted by the sample during the experiment. The sample is placed between of two cylindrical steel plates. The bottom plate is stationary while the top plate stretches the sample vertically. The laser moves at the half of the speed of the top plate in order to stay at the mid-filament p lane. In the updated version of the device the laser and the upper plate are driven by two independent motors. The peculiarity of this device, compared to the others filament stretching rheometers, is the particular online control scheme [Bach *et al.* (2003b)], supplied with a feedback loop (subsequently updated by Román Marín *et al.* (2013)), that ensures a constant Hencky strain rate. This method avoids the iterative (trial and error) experimental procedure [Tirtaatmadja and Sridhar (1993), Orr and Sridhar (1999)]. Where more than one experiment is needed to obtain the separation rate of the end plates based on the filament sample response. The FSR can also operate in a controlled stress mode and the original version of the control scheme has been implemented by Alvarez *et al.* (2013). The types of experiments that can be performed on the FSR are: constant strain rate, stress relaxation, constant stress (creep), reversed flow and small amplitude o scillation. In this work both constant strain rate and stress relaxation experiments will be presented.

Very recently a new commercial version of the device (VADER 1000) has been developed by Alvarez and Román Marín, which is a smallest variant of the original FSR. Due to the reduced dimension of the vertical oven it is possible to measure only polymer melts or concentrated solutions. Conversely to this limitation it allows a much better control of the temperature as well as much faster heating/cooling process during experiments which saves a lot of time. Moreover its particular cylindrical shape and the lifting up mechanism make possible to quench stretched filaments in a very short time. The quenched samples will then be used for further investigation in neutron scattering facilities. A description of the quenching procedure with an estimation of the quenching time is reported Appendix 1.

The average of the difference between the axial and the radial stress in the mid-plane

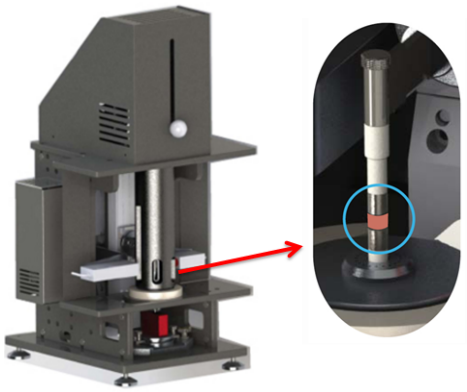

Figure 1.7: Illustration of the mini-FSR.

filament (where the deformation is assumed to be solely elongational) is obtained from a general force balance [Szabo (1997)]. At high hencky strain the expression is:

$$\langle \sigma_{zz} - \sigma_{rr} \rangle = \frac{F(t) - \frac{1}{2}mg}{\pi R(t)^2} \tag{1.50}$$

where $F(t)$ is the force detected by the weight cell, $R(t)$ is the half of the mid-diameter measured by the laser, g is the gravitational acceleration and m is the mass of the sample. Several assumptions have been done: symmetry over the mid-plane of the filament and a rotational axis-symmetry. Moreover inertia and surface tension are negligible.

Conversely, for small strains, an extra stress contribution σ_{rz} arises from the shear component, due to the small aspect ratios ($\Lambda_0 = L_0/R_0$, where R_0 and L_0 are the initial radius and length of the specimen) at the beginning of the experiment. Therefore it needs to be taken into account with a correction factor defined in Rasmussen *et al.* (2010):

$$\langle \sigma_{zz} - \sigma_{rr} \rangle_{corr} = \frac{F(t) - \frac{1}{2}mg}{\pi R(t)^2} \left(1 + \frac{\exp\left(-5\varepsilon/3 - \Lambda_0^{-3}\right)}{3\Lambda_0^2} \right)^{-1} \tag{1.51}$$

For larger Henky strains the extra shear contribution becomes negligible [Kolte *et al.* (1997)]. By dividing the mean difference stress value by the Hencky strain rate we

obtain the extensional stress growth coefficient:

$$\bar{\eta}^{+} = \frac{\langle \sigma_{zz} - \sigma_{rr} \rangle_{corr}}{\dot{\varepsilon}} \tag{1.52}$$

1.5 Neutron Scattering and Polymer Dynamics

Shear and extensional rheology of polymers are just an indirect way to probe the conformation that molecules assume under flow. In the last years, an increased interest in understanding and exploring complex polymeric systems and colloidal solutions, has lead to the use of complementary techniques that can provide details on structural as well as thermodynamic properties of the samples. Determining molecular structures or relative positions of atoms in a bulk sample of liquid or solid present intrinsic limitations: we need somehow to look inside the material with a suitable 'magnifying lens'.

Small-angle scattering techniques have been shown to be some among the most important experimental tools in soft matter research to probe length scale from 1 to 500 nm, which are the sizes relevant to study structural properties of single molecules and molecular aggregates. Small-angle scattering by X ray, SAXS, and by neutrons, SANS, are complementary methods in the study of the systems mentioned above. X rays technique has the advantage that sources are more available, the radiation flux is very high and the instrumental resolution is not comparable with the one obtainable with neutrons. In contrast, neutron scattering facilities are more rare and the flux is weaker.

The advantage of neutrons arises from their basic properties. They have both particle as well as wave-character. The use of scattering techniques for determining structural properties rely on the second one. The de Broglie wavelength of thermal neutrons, is calculated from the following equation $\lambda = \frac{h}{m_n v}$, where h is the Planck constant, m_n is the neutron mass and v is the velocity of the particle. The quantity obtained is of the order of interatomic distances in liquids and solids, therefore interference effects between radiation scattered from different sites in the material will yield information on the structure of the system analysed. Neutrons are uncharged particles and their electric dipole moment is very small, meaning that they can penetrate far better into the target than charged particles. Furthermore, they interact with atoms by nuclear forces, rather than electrical forces, which are very short range and since the distance between scattered centers (scattering nuclei) is much larger than the dimension of the single center they can travel deeply in the matter without being scattered or absorbed. This feature of neutrons has positive as well as negative aspects. On one side, a neutron beam can penetrate deep in a sample even if it has to pass first through a container (usually aluminium). On the other side, they are known to only weakly scattered once they hit the target and usually the neutron beams have very low intensities. Combination of those

two features make neutron scattering a signal limited technique. Often a big volume of sample is required to have a good statistics of the experimental data. Neutron scattering provides more evident informations on the extent to which the molecules have been unraveled and eventually stretched by the flow field. In order to perform this kind of experiments it is necessary to label polymer molecules, wholly or partially, by replacing hydrogen atoms with deuterium ones. That will result in having a contrast due to different interactions of the neutron beam with the two kind of isotopes. The scattered pattern will then provide, depending on the intensity, the shape and the scattering angle, knowledge of the chains conformation. Figure 1.8 shows the SANS 1 instrument at the Paul Sherrer Institute in Switzerland (Villigen) where some of the experiments reported in chapter 5 have been performed. Figure 1.9 shows the sample holders placed in correspondence of the neutron beam.

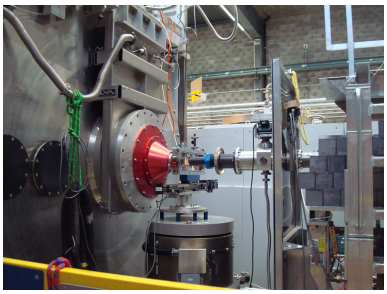

Figure 1.8: Small-angle neutron scattering instrument at Paul Sherrer Institute.

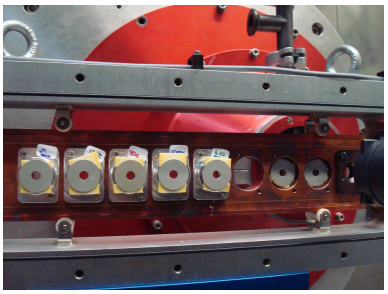

Figure 1.9: SANS sample holder.

1.6 Thesis Outline

With this Ph.D project we hope to contribute to the ongoing work of relating macroscopic quantities of rheology to microscopic dynamics of the individual chains. Studies on the shear and extensional flow behaviour of well characterized polymer samples have been performed. Particular emphasis has been put on the extensional rheological response of polymers, where chains are expected to assume configurations difficult to reach in shear experiments. Also, more deep investigations on the spacial disposition assumed after stretching have been made with neutron scattering experiments on quenched samples.

The material employed in this work is essentially linear polystyrenes with narrow molar mass distributions (NMMD) in a very broad range of molecular weights, going from oligomer OS-4k to PS-3280k. They have been used in well designed experiments with the goal of solving some of the still not understood behaviour of polymer melts and solutions in uniaxial extensional flow. The measurements have been carried out with the Filameent Stretching Rheometer (FSR) described in section 1.4 and results for constant strain rate mode and stress relaxation after uniaxial extensional flow are presented.

Chapters 2-5 have been written in the format of scientific articles containing separate abstracts, introductions, experimental sections, discussions and conclusions to rationalize the process of subsequent publishing.

Chapter 2 deals with the study of the experimentally observed discrepancy in the trend of the steady-state stress growth coefficient between concentrated polymer solutions and melts (entangled) [Bhattacharjee *et al.* (2002), Bach *et al.* (2003a), Sridhar *et al.* (2014)]. Previous studies [Huang *et al.* (2013a), Huang *et al.* (2013b)] investigated the influence of the entanglement molecular weight M_e and the stretch/orientation reduced reduction of monomeric friction as possible explanations for the difference behaviour of the two systems. Here we compare the non-linear extensional rheology of a series of polystyrene solutions with wide concentration ranging between 10% and 100% (melt). All the solutions measured have the same number of entanglements per chain and are diluted in the same solvent (oligomeric styrene OS-4k) in order to determine the key missing physics that can account for dilution effects.

In Chapter 3 a series of polymer solutions with the same long component PS-545k and the same composition 10% (the high molecular weight chain in the blend/solution and its percentage are fixed) and different length of the short chains (OS-10k, PS-25k, PS-60k and PS-95k) have been measured in the FSR at constant strain rates at the same temperature distance from the glass transition temperature $T-T_g$. A convincing plateau in extensional viscosity was found for all polymer solutions at all strain rates presented, except one for the solution PS-545k/25k at $0.1s^{-1}$ where the plateau was not achieved. The results suggest that the steady-state value of the extensional viscosity is determined

by the high molecular weight component.

In Chapter 4 a bi-disperse 50% by weight blend of 95k and 545k molecular weight polystyrene has been used to investigate the mutual influence of the two polymer chains through both uniaxial extension and stress relaxation experiments (following steady extensional flow and after fixed flow time). Data for the blend are also compared to data for the pure components.

Finally in Chapter 5 we compare two systems: the same bi-disperse melt presented in Chapter 4 and a pure melt of the short polystyrene chains. In both systems a fraction of the short chains is deuterated and thus allows for direct comparison of the short chains relaxation in these two scenarios. The purpose is to investigate the structural relaxation behaviour of the short components when mixed with long chains (bi-disperse polymer melt) and when in presence of themself (pure NMMD melt) during relaxation after fast uniaxial elongational flow.

Chapter 2, 4 and 5 are journal articles in their published or submitted version. The relative joint author statements are included in Appendix C. In Appendix A the techniques employed in the experimental procedure and the parameters that may affect the accuracy of the measurements are presented. In Appendix B the details of the preparation of the neutron scattering samples used in the work of Chapter 5 are reported.

CHAPTER 2

Bridging the Gap between Polymer Melts and Solutions in Extensional Rheology

Since its inception, the tube model of polymer dynamics has undergone several modifications to account for observed experimental trends. One trend that has yet to be captured by a modified version of the tube model is the observed experimental difference between concentrated polymer solutions and polymer melts. We compare the nonlinear extensional rheology of a series of polystyrene solutions with wide concentration range between 10% and 100% (melt) in order to determine the key missing physics that can account for dilution effects. All solutions studied have the same number of entanglements per chain, and are diluted in the same solvent (oligomeric styrene). We show that the difference in nonlinear rheological behavior between polystyrene melts reported by Bach *et al.* (2003a), and polystyrene solutions reported by Bhattacharjee *et al.* (2002) and Sridhar *et al.* (2014), can be bridged by changing the polystyrene concentration. The results presented represent a unique benchmark for all future modifications to the tube model.

2.1 Introduction

The tube model [Doi and Edwards (1986)] is the most prolific model used to date to describe the dynamics of entangled polymer systems. Since its inception, several modifications have been made to the original theory in order to account for the observed experimental trends. For example, modifications including the concept of constraint release (CR) [Daoud and de Gennes (1979)] and contour length fluctuations (CLF) [Doi (1981)], were introduced to the tube model in order to quantitatively address experimentally observed aspects in linear viscoelastic (LVE) properties for linear entangled polymer melts and solutions. More mechanisms such as chain stretch [Marrucci and Grizzuti (1988)] and convective constraint release (CCR) [Marrucci (1996)] were introduced to account for non-linear behavior of dilute entangled polymer solutions in extensional flow, such as the polystyrene solutions with concentrations lower than 20% reported by Bhattacharjee *et al.* (2002) and Sridhar *et al.* (2014).

Despite the introduction of the above mentioned mechanisms and physics, the tube model does not correctly predict the non-linear extensional rheology of polymer melts [Bach *et al.* (2003a)]. Bach and coworkers were the first to show that polystyrene melts in extensional rheology show significant extensional strain rate thinning [Bach *et al.* (2003a)], which was the exact opposite trend reported for polystyrene solutions by Bhattacharjee *et al.* (2002) and Sridhar *et al.* (2014). Polystyrene solutions show significant extensional strain rate thickening at the same Weissenberg numbers. At present there are no modifications to the tube model that can account for this difference. This has left many open questions and a search for new physics that will correctly predict both the observed experimental results for polymer solutions as well as polymer melts.

The focus of our recent work has been to attempt to determine experimentally why polymer solutions and melts behave differently, i.e. experimentally determine the missing physics. The concept of universality in polymer dynamics underlies the fundamental tube model theory and states that any two systems with the same physical parameters must exhibit identical linear and nonlinear dynamics. Using this fundamental understanding, Huang and coworkers [Huang *et al.* (2013a,b)] compared polystyrene solutions (higher concentration than previously studied) and melts with the same number of entanglements. Congruent with universality, the data shows that the linear rheological behavior of both polystyrene solution and melt are identical when the moduli are scaled by the plateau modulus and frequency is normalized by the inverse relaxation time of one entanglement. Contrary to universality, the polymer melt and solution behave very differently in nonlinear extensional rheology even though the number of entanglements are identical. To complicate the issue further, the higher concentration solutions using a different molecular weight polystyrene in the Huang et al. study show very different nonlinear behavior than Bhattacharjee *et al.* (2002) and Sridhar *et al.* (2014); suggesting that the nonlinear behavior of concentrated solutions depend on concentration

and/or molecular weight.

It would appear that these recent findings have complicated the issue rather than narrow down the missing physics. However, there is an important parameter, which accounts for the flexibility of the polymer chain, which fundamentally changes with dilution/concentration. The flexibility of a polymer chain, also known as the finite extensibility of the chain, $\lambda_{\max}$, increases upon dilution; meaning that a polymer chain can in principle be stretched more in a dilute environment than a concentrated one. Therefore, from melt [Bach *et al.* (2003a)], to concentrated solution [Huang *et al.* (2013a,b)], and to dilute solutions [Bhattacharjee *et al.* (2002); Sridhar *et al.* (2014)] there is a steady increase in the flexibility of the chain. The three data sets in fact show that the amount of extension rate thickening increases with decreasing polymer concentration, which is in-line with increasing flexibility. This suggests that the degree of extension rate thickening in a polymer sample (solution or melt) increases with increasing flexibility and is one half of the key physics that must be properly accounted for in the tube model to accurately predict polymer dynamics. The other half of the key physics must account for the stretch/orientation induced reduction of friction as proposed by Yaoita *et al.* (2012) and Ianniruberto *et al.* (2012).

The goal of the present work is to determine the dependency of nonlinear extensional dynamics on the flexibility of the chain and bridge the gap between polymer melts and dilute polymer solutions. We show that the steady-state extensional viscosity of polystyrene solutions changes from stretch rate thinning to stretch rate thickening by decreasing the polystyrene concentration, i.e. increasing chain flexibility. When the concentration is low enough and the flexibility of the chain large enough, the data can be described by the modified tube model that was used to compare to the dilute solutions of the Sridhar group. In addition to experimentally explaining the difference between polymer melts and solutions, the data shown here provides a unique bench mark for all future modifications to the tube model where all parameters are fixed except chain flexibility.

2.2 Experimental Details

Polystyrenes of four different molecular weights, PS-545k, PS-900k, PS-1760k and PS-3280k, were separately diluted in an oligomeric styrene, OS-4k, to make four polystyrene solutions. PS-545k was synthesized by living anionic polymerization and is identical to the material used in Ref. Huang *et al.* (2013a). PS-900k was bought from ChemcoPlus. PS-1760k, PS-3280k and OS-4k were bought from Polymer Standards Service (PSS). All the purchased materials were checked by size exclusion chromatography (SEC) to confirm the molecular weight. Table 2.1 summarizes the weight average molecular weight M_w and the polydispersity index PDI provided by the suppliers as

well as obtained from our SEC.

Table 2.1: The molecular weight of the polystyrenes and the styrene oligomer

Sample Name	M_w[g/mol] (from suppliers)	PDI (from suppliers)	M_w[g/mol]	PDI
PS-545k	–	–	545000	1.12
PS-900k	900000	1.10	910000	1.16
PS-1760k	1760000	1.04	1880000	1.13
PS-3280k	3280000	1.11	3140000	1.38
OS-4k	4330	1.04	3630	1.06

The PS solutions were prepared using the same procedure described in Ref. Huang *et al.* (2013a). The concentrations of all the solutions were confirmed by the peak areas of the bimodal curve in SEC. Table 2.2 summarizes the components, the weight fraction ϕ and the glass transition temperature T_g of the solutions. The density of the polystyrenes and the styrene oligomer is assumed independent of molecular weight, and therefore the the weight fraction is equivalent to the volume fraction.

Table 2.2: The components and the glass transition temperatures of the polystyrene solutions. Data for PS-285k is taken from Ref. Huang *et al.* (2013a) and data for PS-545k/4k-52 is taken from Ref. Huang *et al.* (2013b).

Sample Name	Components	ϕ[wt% of PS]	T_g[°C]
PS-285k	285k	100%	107.5
PS-545k/4k-52	545k+4k	52%(±1%)	98.6
PS-900k/4k-33	900k+4k	33%(±1%)	92.1
PS-1760k/4k-18	1760k+4k	18%(±1%)	89.0
PS-3280k/4k-13	3280k+4k	13%(±1%)	88.4

The concentrations in Table 2.2 were chosen in order to keep the number of entanglements per chain Z the same for all the samples (higher molecular weight requires more dilution). We showed in the previous study [Huang *et al.* (2013a)] that samples with identical Z have the same linear viscoelastic properties. Figure 2.1 shows the linear rheology at the reference temperature 130 °C for all the samples including a polystyrene melt (PS-285k) with the same Z. For the solutions with the concentration lower than 50%, influence of the solvent viscosity is considered and the values of the loss modulus G'' in the figure are corrected by

$$G''_{corr} = G'' - \phi_s \eta_s \omega, \tag{2.1}$$

where ϕ_s is the volume fraction of OS-4k and η_s = 248Pa.s is the viscosity of OS-4k at 130 °C. LVE data for OS-4k can be found in the appendix. The lines in the figure repre-

sent the Baumgaertel-Schausberger-Winter (BSW) relaxation spectrum [Baumgaertel *et al.* (1990)], which will be used to predict the linear behavior in uniaxial constant strain rate extensional flow. The values of the BSW parameters, n_e, n_g, G_N^0, τ_c and τ_m, are listed in Table 2.3. For nearly monodisperse melts and solutions, the values of n_e and n_g are fixed to 0.23 and 0.70, respectively [Jackson and Winter (1995)]. The adjustable parameters, i.e. the plateau modulus G_N^0, the relaxation time of one entangled segment τ_c and the maximum relaxation time of the polymer chain τ_m, are found by least squares fitting to the LVE data. Details about the meaning of the BSW parameters and their relation to tube model parameters are explained in Ref. Huang *et al.* (2013a). It is found that the values of G_N^0 reported in Table 2.3 follow the scaling rule of $G_N^0 \propto \phi^{1+\alpha}$ with $\alpha = 1$. Details can be found in the appendix. The number of entanglements per chain Z for the solutions is obtained from the relation $\tau_m/\tau_c \propto Z^{3.4}$ and $Z = 41.0$ for PS-545k [Huang *et al.* (2013a)]. Values of Z are also listed in Table 2.3. Figure 2.2 compares the LVE data under the dimensionless parameters where the angular frequency ω is normalized by $1/\tau_c$ and the storage modulus G' and loss modulus G'' are normalized by G_N^0. A master curve is obtained as shown in Figure 2.2, confirming all the samples have the same number of entanglements per chain.

Furthermore, the LVE data in Figure 2.1 was measured at different temperatures and shifted to the reference temperature using the time–temperature superposition procedure. Although the polystyrene solutions have different T_g, it is found that the temperature shift factor a_T for each solution can be described by one Williams-Landel-Ferry (WLF) equation, which agrees with the observation reported in Ref.Wagner (2014). Details can be found in the appendix.

Table 2.3: Material properties obtained from the BSW spectrum at 130 °C. Data for PS-285k is taken from Ref. Huang *et al.* (2013a); Data for PS-545k/4k-52 is taken from Ref. Huang *et al.* (2013b).

Sample Name	n_e	n_g	G_N^0[Pa]	τ_c[s]	τ_m[s]	Z	λ_{max}	N_e
PS-285k	0.23	0.7	252040	0.444	6846	21.4	4.7	22.1
PS-545k/4k-52	0.23	0.7	68900	0.200	3180	21.6	6.5	42.3
PS-900k/4k-33	0.23	0.7	27320	0.320	5844	22.5	8.2	67.2
PS-1760k/4k-18	0.23	0.7	6850	0.661	12615	22.8	11.1	123.2
PS-3280k/4k-13	0.23	0.7	2790	1.511	26373	22.2	13.0	169.0

The uniaxial extensional stress was measured by a filament stretching rheometer (FSR) [Bach *et al.* (2003b)]. Prior to making a measurement, the samples were molded into cylindrical test specimens with a fixed radius of either $R_0 = 2.7$mm or $R_0 = 4.0$mm. The initial length L_0 of the cylindrical test specimens was controlled by the addition of a given mass of the sample into the mold. The aspect ratio $\Lambda_0 = L_0/R_0$ is between 0.48 and 0.59. The samples were pressed at $140 - 150\,^\circ$C and annealed at the same temperature under vacuum until the polymer chains were completely relaxed.

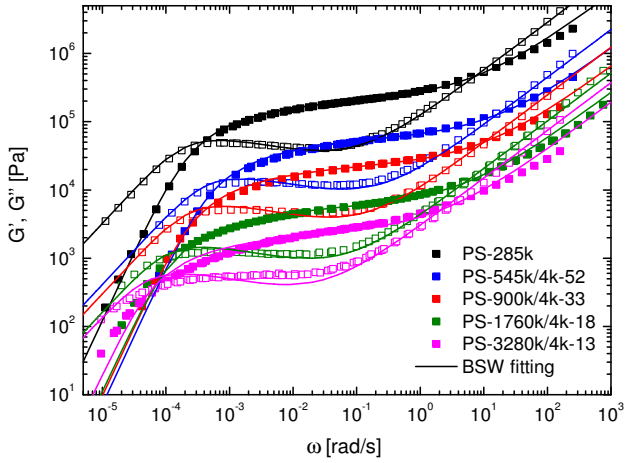

Figure 2.1: Storage modulus G' and loss modulus G'' as a function of angular frequency ω fitted with the BSW spectrum at 130 °C for the polystyrene solutions. Data for PS-285k is taken from Ref. Huang *et al.* (2013a); Data for PS-545k/4k-52 is taken from Ref. Huang *et al.* (2013b).

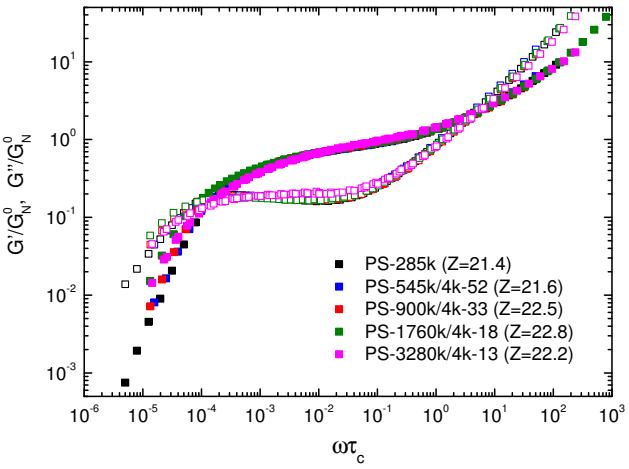

Figure 2.2: Normalized LVE data for polystyrene solutions from Figure 2.1.

All the samples were pre-stretched to a radius R_p ranging from 1.2 mm to 3 mm at elevated temperatures, 150 − 160 °C prior to the extensional experiments. After pre-stretching, the temperature was decreased to 130 °C for the extensional stress measurements. The samples were kept under a nitrogen atmosphere at all times. After the experiments, the samples were checked by SEC to ensure that no degradation or concentration changes occurred during testing. No changes were observed for all the samples except PS-3280k with showing a shift from *PDI* 1.38 to 1.77, signifying degradation of the long chains during experiments.

The samples were subject to constant uniaxial Hencky strain rate $\dot{\varepsilon}$, and the stress at the mid-filament plane was measured as a function of time. This is denoted as extensional stress growth coefficient and is defined as $\bar{\eta}^+ = \langle \sigma_{zz} - \sigma_{rr} \rangle / \dot{\varepsilon}$. Details are given in Ref. Huang *et al.* (2013a).

2.3 Results and Discussions

Figure 2.3 shows the measured extensional stress growth coefficient $\bar{\eta}^+$ as a function of time at 130 °C for all the PS solutions. The solid lines in the figure are predictions from the LVE parameters listed in Table 2.3. For each solution except PS-3280k/4k-13, $\bar{\eta}^+$ reaches a clear steady-state value when brittle fracture does not occur. $\bar{\eta}^+$ at the high rates for PS-3280k/4k-13 (and also the highest rate for PS-1760k/4k-18) tends to a steady-state value at the end of the measurements, but the steady-state viscosity is not very clear even under a large deformation up to Hencky strain 5. In this case we take the highest value of $\bar{\eta}^+$ as the steady-state viscosity.

Figure 2.4 compares the solutions under dimensionless parameters which are normalized the same way as we did in Figure 2.2. The LVE envelopes (solid lines) in the figure overlap each other as expected. For each solution, the normalized transient data also overlaps each other when stretch rate is relatively low. However, at high stretch rate, each solution shows a different behavior. The solution with lower concentration shows obviously higher strain hardening than the solution with higher concentration.

The difference is clearer in Figure 2.5 where the normalized steady-state viscosity is plotted as a function of the normalized stretch rate. The Rouse time can be estimated as $\tau_R = Z^2 \tau_c$ [Huang *et al.* (2013a)]. Since $Z \approx 22$ for all the samples, stretching faster than inverse Rouse time means the normalized stretch rate $\dot{\varepsilon}\tau_c > 0.002$ in Figure 2.5. In this region, it is clear that the steady-state viscosity of PS-285k is stretch rate thinning, which agrees with the observations reported by Bach *et al.* (2003a) for PS-200k and PS-390k. When the concentration of PS decreases from 100% to 52%, the trend of the steady-state viscosity changes from stretch rate thinning to stretch rate constant and followed by thinning again. When the concentration further decreases to

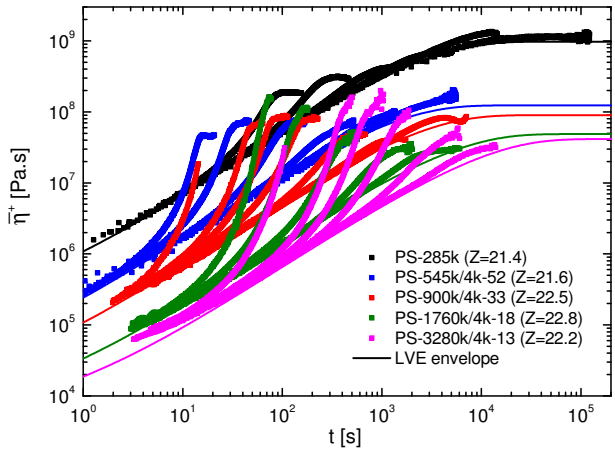

Figure 2.3: The measured extensional stress growth coefficient as a function of the time for the PS solutions at 130 °C. Data for PS-285k is taken from Ref. Huang *et al.* (2013a). Strain rate (from left to right) for PS-545k/4k-52: 0.2, 0.1, 0.03, 0.01, 0.003, 0.001s^{-1}; for PS-900k/4k-33: 0.2, 0.07, 0.04, 0.02, 0.007, 0.002, 0.0007s^{-1}; for PS-1760k/4k-18: 0.06, 0.03, 0.01, 0.003, 0.001s^{-1}; for PS-3280k/4k-13: 0.03, 0.01, 0.006, 0.003, 0.001, 0.0003s^{-1}

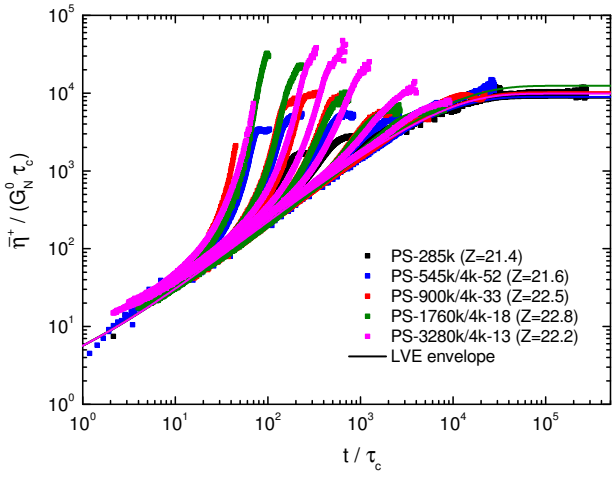

Figure 2.4: The normalized extensional stress growth coefficient as a function of the normalized time for the PS solutions. Data for PS-285k is taken from Ref. Huang *et al.* (2013a); data for PS-545k/4k-52 is taken from Ref. Huang *et al.* (2013b).

33%, a short period of stretch rate thickening is seen, and quickly followed by stretch rate constant and thinning. Finally, when the concentration is lower than 20%, the steady-state viscosity shows stretch rate thickening, which agrees with the observations reported by Bhattacharjee *et al.* (2002) and Sridhar *et al.* (2014) where the highest concentration of PS is 20%.

Since the solutions are compared under normalized parameters in Figure 2.5, the only parameter that cannot be normalized in the figure seems to be the number of Kuhn segments between entanglements, N_e, which is proportional to the entanglement molecular weight M_e. In non-dimensional terms, N_e equals the square of the maximum stretch ratio $\lambda_{\max}$ as shown in Table 2.3. It seems reasonable that with the increased flexibility associated with a larger value of N_e the solution at a lower concentration can reach a higher steady-state viscosity. However, it is not clear if the rather dramatic effect on the extensional viscosity is associated with this parameter change alone.

Yaoita *et al.* (2012) and Ianniruberto *et al.* (2012) suggest that the monomeric friction is reduced by stretching and orientating the polymer chains during extension. For solutions the average anisotropy is governed by the solvent and remains small, so the friction does not change significantly. But for melts the friction decreases significantly under fast elongation and suppresses the chain stretch, which leads to lower viscosity

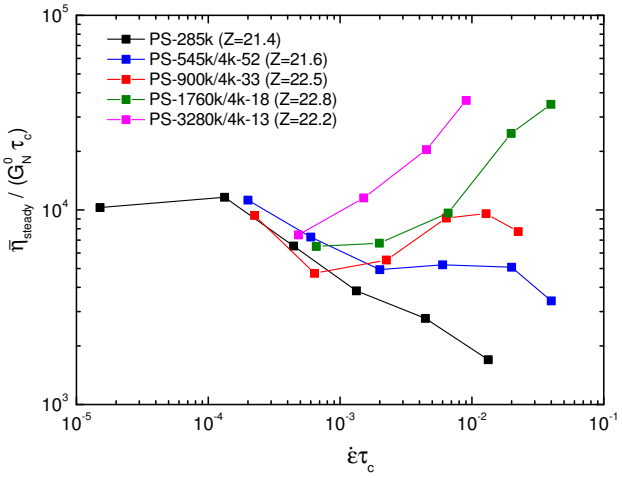

Figure 2.5: The normalized steady-state viscosity as a function of the normalized stretch rate for the PS solutions. Data for PS-285k is taken from Ref. Huang *et al.* (2013a); data for PS-545k/4k-52 is taken from Ref. Huang *et al.* (2013b).

than expected. According to Yaoita et al., the reduction of friction is less with lower concentration of the polymer, which seems to agree with our observations in this work.

Moreover, in our previous work [Huang *et al.* (2013b)] we have shown that when the same PS is diluted to the same concentration with a range of solvents, the qualitative behavior of the normalized steady-state viscosity is different from one solvent to another. In this case, since λ_{max} is the same, it seems that the only explanation is the reduction of friction due the nematic interactions between both polymer-polymer and polymer-solvent. The solvents used by Bhattacharjee *et al.* (2002) and Sridhar *et al.* (2014) to dilute PS are not oligomeric styrene as we used. But at the PS concentra-tion lower than 20%, the steady-state viscosity has the same trend, which indicates the interaction between polymer-solvent is weaker at low concentration. Furthermore, in the recent work of Masubuchi (2014), the authors suggest that the magnitude of orientation/stretch-induced reduction of friction is not universal but changes with the chemical structure of polymers. This may explain why some other polymer melts do not show stretch rate thinning behavior as PS melts, but show stretch rate thickening as PS solutions.

2.4 Conclusions

We have shown that the PS solutions which have identical linear rheology behave differently in extensional nonlinear rheology. In fact, we observed a systematic change of the extensional steady-state viscosity from stretch rate thinning to stretch rate thickening by decreasing the PS concentration. It is suggested that the parameter which dominates the nonlinear behavior is the orientation/stretch-induced reduction of friction reported by Yaoita *et al.* (2012) and Iannirubertо *et al.* (2012). But more work will be needed for a full understanding.

2.5 Appendix

The LVE properties of the PS solutions and the styrene oligomer OS-4k were obtained from small amplitude oscillatory shear (SAOS) measurements. An 8mm plate–plate geometry was used on an ARES–G2 rheometer from TA instruments. The measurements were performed at a range of temperatures under nitrogen. For each sample, the data was shifted to a single master curve at the reference temperature $T_r = 130\,^{\circ}\mathrm{C}$ using the time–temperature superposition procedure. The temperature shift factor a_T is reported in Table 2.4 for each PS solution. Steady shear flow measurement was also performed for OS-4k at 130 °C using the 8mm plate–plate geometry on the ARES–G2 rheometer. The zero-shear-rate viscosity for OS-4k is $\eta_s = 248$Pa.s.

Figure 2.6 shows the result of SAOS measurement for the solvent OS-4k. At a wide frequency range up to $\omega \approx 1 \times 10^4$ rad/s, OS-4k behaves like a Newtonian fluid and the loss modulus G'' matches $\eta_s\omega$ where η_s is obtained from steady shear flow measurement. The relaxation time of OS-4k is in the order of 10^{-5}s at 130 °C.

Table 2.4: The shift factor a_T from different temperatures to $T_r = 130\,^{\circ}\mathrm{C}$ for the polystyrene solutions. a_{Tg} is the shift factor calculated by Eq. 2.3. For the melts $a_{Tg} = 1$

Sample Name	120 °C	150 °C	170 °C	190 °C	a_{Tg}
PS-545k/4k-52	–	0.035	0.0031	–	0.145
PS-900k/4k-33	–	0.042	0.0042	–	0.0408
PS-1760k/4k-18	7.59	0.050	0.0052	0.0011	0.0237
PS-3280k/4k-13	–	0.054	0.0071	0.0013	0.0214

The temperature shift factor a_T for PS melts can be described by the Williams-Landel-

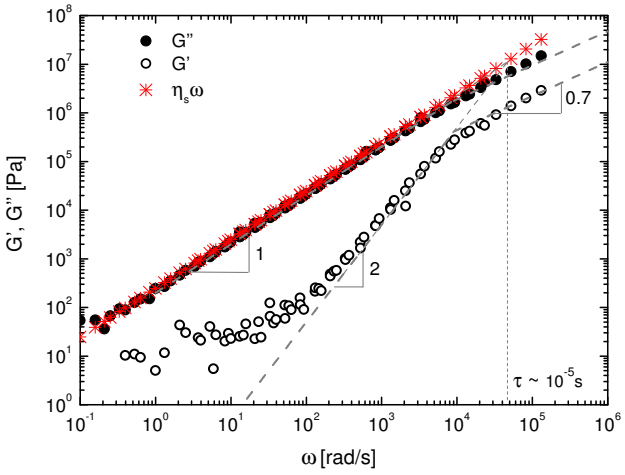

Figure 2.6: Storage modulus and loss modulus of OS-4k as a function of angular frequency at 130 °C.

Ferry (WLF) equation

$$\log_{10} a_T = \frac{-c_1^0 (T - T_r)}{c_2^0 + (T - T_r)}, \tag{2.2}$$

where $c_1^0 = 8.99$, $c_2^0 = 81.53$K, $T_r = 130$ °C, and T is temperature in °C [Huang (2013)]. However, with the same reference temperature $T_r = 130$ °C, Eq. 2.2 can not describe the PS solutions. This is because the melts and solutions have different values of T_g and therefore $T_r - T_g$ is different. The effect of different T_g can be corrected by a shift factor $a_{T\,g}$ which can also be obtained from a WLF equation as reported by Ref. Wagner (2014):

$$\log_{10} a_{Tg} = \frac{-c_1^0 \Delta T_g}{c_2^0 + \Delta T_g}, \tag{2.3}$$

where c_1^0 and c_2^0 have the same values as in Eq.2.2 and ΔT_g is the difference of T_g between PS melts and solutions. Figure 2.7 plots the corrected shift factor $a_T a_{Tg}$ as a function of $T - T_g$. A mater curve is obtained for all the PS solutions and melts, which

agrees with the observations reported in Ref. Wagner (2014). Values of a_{Tg} for the solutions are listed in Table 2.4.

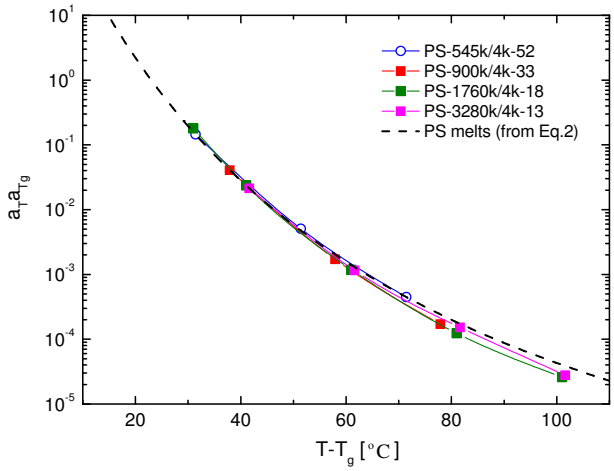

Figure 2.7: Corrected temperature shift factor $a_T a_{Tg}$ as a function of $T - T_g$. For PS melts $a_{Tg} = 1$ at the reference temperature $T_r = 130\,^{\circ}\mathrm{C}$.

The relationship between the solution plateau modulus, $G_N^0(\phi)$, and the melt plateau modulus, $G_N^0(1)$, is given by

$$G_N^0(\phi) = G_N^0(1)\,\phi^{1+\alpha}, \tag{2.4}$$

where α is the dilution exponent. It has been reported by Huang *et al.* (2013a) that $\alpha = 1$ for highly concentrated PS solutions with $\phi > 0.4$. Figure 2.8 plots G_N^0 as a function of ϕ for all the samples listed in Table 2.3. It seems that $\alpha = 1$ also works for the PS solutions with lower concentrations at least down to $\phi = 0.18$. There is a deviation from $\alpha = 1$ for PS-3280k/4k-13 which has the lowest concentration of $\phi = 0.13$. However, considering the higher polydispersity of the sample and the less satisfactory BSW fitting as shown in Figure 2.1, this deviation might be an artifact. In addition to the samples listed in Table 2.3, we have also diluted PS-545k in OS-4k with different concentrations down to $\phi = 0.17$. LVE measurements and BSW fittings were also performed for these samples. The plateau modulus G_N^0 as a function of ϕ for the additional samples PS-545k/4k is also shown in Figure 2.8 as open symbols. All of them follow $\alpha = 1$.

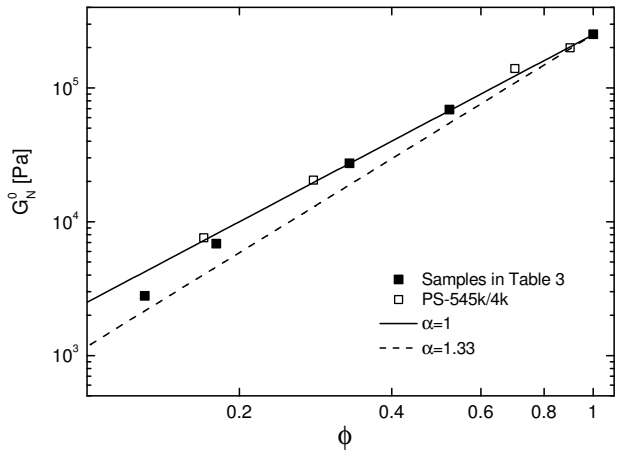

Figure 2.8: Plateau modulus G_N^0 as a function of the polymer volume fraction ϕ. The slope of the solid line in the figure is 2 ($\alpha = 1$), and the slope of the dashed line is 2.33 ($\alpha = 4/3$).

CHAPTER 3

Steady-state Extensional Viscosity of Solutions with Fixed Concentration of the Same Long Chain Component

3.1 Introduction

From an industrial point of view, in processing operations such as film blowing, injection molding or fiber spinning, where a strong elongational component is present, the focus is usually on the strain hardening behaviour that arises in the elongational flow. This phenomenon is observed when the stress growth coefficient $\bar{\eta}^+(t)$ rise above the linear viscoelastic envelope entering the non-linear regime. It turned out to have a positive repercussion on the homogeneity of the processing of the material. Therefore, over the past fifty years, reasonable effort have been put into improving well-controlled elongational stress measurements especially in start up [Cogswell (1969), Meissner (1971), Meissner (1971), Münstedt (1979), Sridhar *et al.* (1991), McKinley and Sridhar (2002)]. In extensional experiments it is easier to access the time-dependent value $\bar{\eta}^+(t)$ which is the transient elongational viscosity or stress growth coefficient than its asymptotic value $\bar{\eta}_s$. The latter one, also called steady elongational viscosity is difficult to measure because to reach Hencky strain of $\varepsilon = 7$ requires an elongation of circa 1100 times the initial dimension of the sample. The steady-state values of the exten-

sional viscosity reported in the past are often the maximum values of $\bar{\eta}^{+}(t)$ reached at a certain strain rate at the maximum experimentally accessible Hencky strain ε.

From the scientific side, in comparing model predictions with experimental data the steady-state conditions are preferable since the time-dependence disappears. The target of the experimentalists in more recent years has been directed at providing accurate data of uniaxial extensional measurements that could reach also high deformations and eventually steady-state stresses values [Bhattacharjee *et al.* (2002), Bhattacharjee *et al.* (2003) and Sridhar *et al.* (2014) (diluted entangled polymer solutions of polystyrene (PS)); Ye *et al.* (2003) (monodisperse and bi-disperse polystyrene solutions); Bach *et al.* (2003a) and Luap *et al.* (2005) (narrow molar mass distribution polystyrene (PS) melts); Münstedt *et al.* (1978), Bach *et al.* (2003b), Rasmussen *et al.* (2005) and Huang *et al.* (2012) (low density polyethylene (LDPE) melts); Nielsen *et al.* (2006)(bi-disperse PS melts); Nielsen *et al.* (2008) (stress relaxation after steady extensional flow of a linear PS melt); Nielsen *et al.* (2006b) (entangled branched PS melts of known architecture: asymmetric stars and symmetric pom-poms) ; Auhl *et al.* (2011) (melts of highly branched polymers long chain branching(LCB)), for which is difficult to reach steady-state values due to non-homogeneous deformations); Tirtaatmadja and Sridhar (1993) (polyisobutylene (PBI) dilute and semi-dilute polymer solutions); Huang *et al.* (2013a) and Huang *et al.* (2013b) (PS melts and concentrated solutions)].

Subsequently constitutive models have brought at the formulation of constitutive equations that could theoretically predict the time-dependent as well as the steady-state extensional viscosity. Good match was found from comparisons with some of the experimental data sets mentioned before [Marrucci and Ianniruberto (2004), Marrucci and Ianniruberto (2005), Wagner *et al.* (2005), Nielsen *et al.* (2008), Wagner and Rolón-Garrido (2008), Auhl *et al.* (2011), Wagner (2014), Ianniruberto and Marrucci (2013)].

In the last years many efforts have been made in order to understand the different trends experimentally observed of the steady-state elongational viscosity as a function of the Hencky strain rate for different polymer systems, i. e. diluted, semi-diluted and concen-trated solutions of linear molecules, well-entangled and few-entangled linear polymer melts, polydisperse melts and entangled branched melts.

Also explanations from the aspect of the molecular conformations of the chains have been attempted. Constant stress conditions imply that molecules are no longer stretching out and have reached a fixed configuration. The most reliable scenario once steady-state is reached assumes that the strain completely unfolds the randomly coiled chain which will be fully stretched. On the other hand is also possible that entanglements prevent the chains from being completely extended [Tirtaatmadja and Sridhar (1993)].

So far it has not yet understood what is the factor that determines the elongational stress level in steady-state conditions. A very recent paper of Huang *et al.* (2016) on highly polydisperse and branched LDPE industrial samples has shown that control-

ling the branches grew in the polymerization process is possible to predict the final steady-state stress level after elongational flow of different samples, i . e . to obtain the desired value. The purpose of the following work is to further investigate the time-independent stress level by means of well-controlled uniaxial extensional experiments on well-characterized polymer solutions and blends. A linear narrow molar mass distribution polystyrene PS-545k, which is the long chain component, is diluted in four different matrix of short molecules (OS-10k, PS-25k, PS-56k and PS-95k) in the same amount of 10 % weight fraction. The first two systems PS-545k/10k and PS-545k/25k are solutions since the low molecular weight chains are not entangled with each other. The oligomer 10k is below the critical value of the entanglement molecular weight M_e = 13.3k for PS reported by Bach *et al.* (2003a). The PS-25k, despite above the value M_e = 13.3k, it has been observed from linear viscoelastic (LVE) measurements that does not show the typical shape of an entangled system. We have observed that even when the PS-545k is blended with the OS-10k and the PS-25k no signature of entanglements is shown in LVE data. Probably, despite the high molecular weight of the long molecules, the dilution is such that the chains do not overlap each other. The latter two samples are instead entangled since both, PS-60k and PS-95k, are well above the value of M_e, hence they can be considered as bi-disperse blends. The glass tran-sition temperatures T_g of the solvents (OS-10k, PS-25k, PS-56k and PS-95k) is lower than the T_g of the melt PS-545k. The difference in the T_g of the components leads to a different T_g of the mixtures, which also implies a change in the friction and con-sequently a dissimilar chain mobility if samples are compared at the same reference temperature. Therefore measurements are performed and compared not at the same temperature but at the same distance relative to the T_g of the blended samples allowing a fair comparison under the same conditions of chains mobility and same relaxation time-scale.

3.2 Experimental Details

3.2.1 Materials

The PS-545k, which is the same material used in the previous works of Huang *et al.* (2013a) and Huang *et al.* (2013b) (and the work presented in chapter 2 and 4), was diluted in four different molecular weight polystyrenes, PS-95k, PS-60k, PS-25k and PS-10k, to prepare four mixtures with the same concentration. The samples therefore have the same long chain component (PS-545k) present in the same amount 10% but different short chain component. The PS-95k is identical to the material employed to prepare the bi-disperse blend used in the work of Hengeller *et al.* (2016). The PS-10k, PS-25k and PS-60k were bought from Polymer Standard Service (PSS). All materials have narrow molecular weight distribution, their weight average molecular (M_w)

and polydispersity index (PDI) have been checked by size exclusion chromatography (SEC) to confirm the values reported by the supplier. Table 3.1 includes the weight average molecular weights and the PDI obtained from our SEC analysis as well as the ones provided from PSS. The glass transition temperature T_g of the samples was found by mean of differential scanning calorimetry (DSC) technique. Values are also reported in Table 3.1.

Table 3.1: The molecular characteristics of the polystyrenes and the styrene oligomers.

Sample Name	M_w[g/mol] (from suppliers)	PDI (from suppliers)	M_w[g/mol]	PDI	T_g[°C]
PS-545k	–	–	545000	1.12	106.5
PS-95k	–	–	95100	1.07	105
PS-60k	58900	1.09	60325	1.12	103.5
PS-25k	25700	1.03	24528	1.07	101.9
PS-10k	9880	1.04	9454	1.08	89.3

3.2.2 Methods: Samples Preparation

The procedure used to prepare the mixtures is described in the Appendix 1. Size exclusion chromatography (SEC) was used as a medium to characterize the samples prepared, to check their composition and to ensure that no thermal degradation took place during/after mechanical characterization. We assume that the polystyrene density does not change with the M_w hence the volume fraction is the same as the weight fraction. In Table 3.2 are listed the four samples with the corresponding components and the relative glass transition temperature T_g.

Table 3.2: The components and the glass transition temperatures of the polystyrene mixtures with ϕ = 10wt% of $PS-545k$. Data for PS-545k is taken from Ref. Huang *et al.* (2013a).

Sample Name	Components	T_g[°C]
PS-545k	545k	106.5
PS-545k/95k	545k+95k	–
PS-545k/60k	545k+60k	105.9
PS-545k/25k	545k+25k	104.2
PS-545k/10k	545k+10k	98.4

3.2.3 Mechanical Spectroscopy

The linear viscoelastic response of the samples has been measured on an ARES-G2 rheometer from TA Instruments, with an 8 mm plate-plate geometry. Small amplitude oscillatory shear (SAOS) experiments were performed both on the PS mixtures and the pure components. Frequency sweep tests were conducted at least at three different temperatures in nitrogen atmosphere for each sample. The data were subsequently shifted to obtain a single master curve at a reference temperature T_{ref}, applying the principle of time-temperature superposition (TTS). The time-temperature shift factors a_T for the polystyrene solutions and melts are decribed by the Williams-Landel-Ferry (WLF) equation:

$$\log_{10} a_T = \frac{-c_1^0 \left(T - T_{ref}\right)}{c_2^0 + \left(T - T_{ref}\right)}, \tag{3.1}$$

where c_1^0 and c_2^0 are material constants (dependent from the T_{ref}), T_{ref} and T are respectively the reference temperature and the generic temperature expressed in °C.

However, with the same reference temperature T_{ref}, Eq. 3.1 can not describe the PS samples. This is because the melts, the blends and the solutions have different values of the glass transition temperature T_g and therefore $T_{ref} - T_g$ would be different.

Hence, due to the difference in T_g, data of the mixtures have been shifted at the same distance $T_{ref} - T_g$ from the T_g. The PS-545k/95k was measured at $T = 130\,^{\circ}\mathrm{C}$ since it was originally prepared for the work presented in Chapter 4.

Conversely to the procedure of Chapter 2, where the effect of different glass transition temperature was corrected with a shift factor $a_{T\,g}$ according to the WLF equation reported by Wagner (2014), we have decided to apply the WLF-equation under the condition that $T_{ref} - T_g$ is the same for the all the mixtures. We have also shifted the pure melts (short molecular weight components of the solutions) at the same T_{ref} of the corresponding mixture.

In Tables 3.3, 3.4, 3.5, 3.6 the time-temperature shift factors a_T and b_T are reported for the mixtures. The shift factors of the low molecular weight melts are listed in table 3.7 to table 3.10 .

Table 3.3: The time-temperature shift factors a_T and b_T from different temperatures to T_{ref} = 128.4 °C for the PS-545k/10k.

Shift Factors	108.4 °C	160 °C
a_T	99.86	0.006
b_T	0.55	1.075

Table 3.4: The time-temperature shift factors a_T and b_T from different temperatures to T_{ref} = 134.2 °C for the PS-545k/25k.

Shift Factors	114.2 °C	160 °C
a_T	657.81	0.016
b_T	1.83	1.086

Table 3.5: The time-temperature shift factors a_T and b_T from different temperatures to T_{ref} = 135.9 °C for the PS-545k/60k.

Shift Factors	150 °C	170 °C
a_T	0.087	0.006
b_T	0.678	0.619

Table 3.6: The time-temperature shift factors a_T from different temperatures to T_{ref} = 130 °C for the PS-545k/95k.

Shift Factors	150 °C	170 °C
a_T	0.02	0.001

Table 3.7: The time-temperature shift factors a_T and b_T from different temperatures to T_{ref} = 128.4 °C for the PS-10k.

Shift Factors	105 °C	119.4 °C	160 °C
a_T	348.17	9.05	0.023
b_T	0.78	1.32	2.12

Table 3.8: The time-temperature shift factors a_T and b_T from different temperatures to $T_{ref} = 134.2\,°C$ for the PS-25k.

Shift Factors	114.2 °C	132 °C	160 °C
a_T	491	1.62	0.015
b_T	1.67	1.004	0.86

Table 3.9: The time-temperature shift factors a_T and b_T from different temperatures to $T_{ref} = 135.9\,°C$ for the PS-60k.

Shift Factors	130 °C	150 °C	170 °C
a_T	4.846	0.092	0.006
b_T	0.839	0.687	0.616

Table 3.10: The time-temperature shift factors a_T and b_T from different temperatures to $T_{ref} = 130\,°C$ for the PS-95k.

Shift Factors	150 °C	170 °C
a_T	0.02	0.0014

3.2.4 Extensional Experiments

Uniaxial extensional experiments were performed using the FSR described in section 1.4. Before measurements the samples were molded under vacuum into cylindrical specimens with a diameter of $5.4mm$ and a height ranging between $1.5 - 2.5mm$. They were annealed and pressed during the molding at approximately $T = 120\,°C$. The experimental temperature has been chosen to be the same as the one used in shear measurements. Therefore all the experiments were performed at the same distance $T_{ref} - T_g$ from T_g (according to their different T_g) and at constant strain rate $\dot{\varepsilon}$. Only the experiments of PS-545k/95k have been conducted at $T = 130\,°C$ and subsequently data were shifted to $T_{ref} = 135\,°C$ using the shift factor $a_T = 0.3199$ to allow direct comparisons with the others systems at the same conditions. Each solution was tested at least at four different stretch rates. To ensure reproducibility of the data experiments were repeated for minimum two strain rates for each sample (as an example we show in Figure 3.6(a) the blue dots which are a repetition of the experiment at $\dot{\varepsilon} = 0.03s^{-1}$ for the PS-545k/25k).

The average difference between the axial and the radial stress is calculated with the

following equation [Szabo (1997)]:

$$\langle \sigma_{zz} - \sigma_{rr} \rangle = \frac{F(t) - \frac{1}{2}mg}{\pi R(t)^2} \tag{3.2}$$

where $F(t)$ and $R(t)$ are respectively the force detected from the weight cell and the radius at the mid-filament measured from the laser, and m_g is the mass of the sample. Figures 3.5(b), 3.6(b), 3.7(b), 3.8(b) show the measured stress difference of the mixtures (corrected with a correction factor defined in Rasmussen *et al.* (2010)). The extensional stress growth coefficient is obtained normalizing respect to the strain rate:

$$\bar{\eta}^+ = \frac{\langle \sigma_{zz} - \sigma_{rr} \rangle_{corr}}{\dot{\varepsilon}} \tag{3.3}$$

where the strain rate is defined as $\dot{\varepsilon} = d\varepsilon/dt$, with Hencky strain ε. In Figures 3.5(a), 3.6(a), 3.7(a), 3.8(a) are presented the stress growth coefficient data for the mixtures.

3.3 Results

3.3.1 Linear Viscoelasticity

LVE data are shown by plotting the storage modulus G' and the loss modulus G'' as a function of the angular frequency ω. Plots on the left hand side (Figures 3.1(a), 3.2(a), 3.3(a), 3.4(a)) present the data for the mixtures, while on the right hand side (Figures 3.1(b), 3.2(b), 3.3(b), 3.4(b)) data of the corresponding pure short component (NMMD melt) of the mixture are shown. The two black solid lines reported in each plot represent the typical slopes of 1 and 2 respectively for the loss and the storage modulus in the terminal region. Table 3.11 summarizes the reference temperature at which the master curve of each sample has been created.

From figures 3.1(a) and 3.2(a) corresponding to the LVE of the two solutions PS-545k/10k and PS-545k/25k, the moduli seem to suggest that no entanglements are present in these systems. In fact the loss modulus G'' is always higher than the corresponding storage modulus G' over a range of frequencies of eight order of magnitude. They cross each other in the glassy region where the inverse of the frequency corresponding to this crossover point is known to be an indication of the relaxation time τ_k of a Kuhn segment. At low frequencies G' and G'' eventually approach the viscous regime where the characteristic slopes are 2 and 1.

Table 3.11: The reference temperatures T_{ref} for each sample.

Sample Name	T_{ref}[°C]
PS-545k/10k	128.4
PS-10k	128.4
PS-545k/25k	134.2
PS-25k	134.2
PS-545k/60k	135.9
PS-60k	135.9
PS-545k/95k	130
PS-95k	130

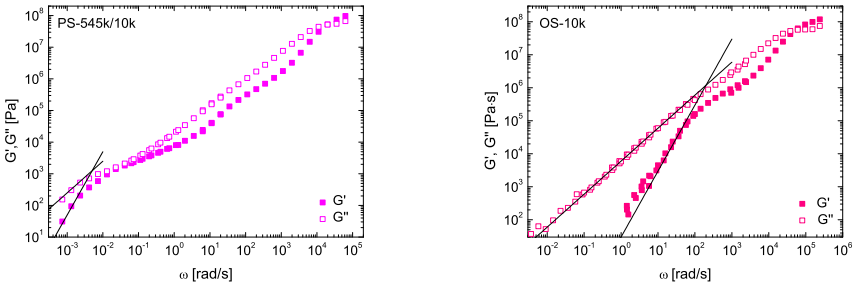

(a) (b)

Figure 3.1: (a) LVE data for PS-545k/10k at T_{ref} = 128.4 °C. (b) LVE data for PS-10k at T_{ref} = 128.4 °C.

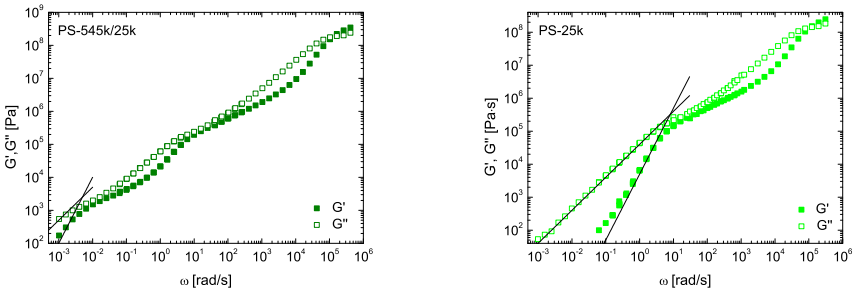

(a) (b)

Figure 3.2: (a) LVE data for PS-545k/25k at T_{ref} = 134.2 °C. (b) LVE data for PS-25k at T_{ref} = 134.2 °C.

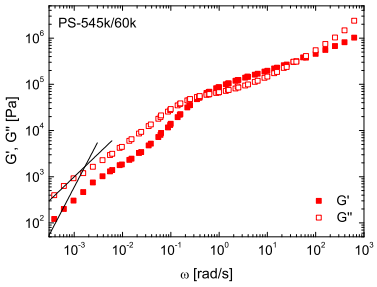

(a)

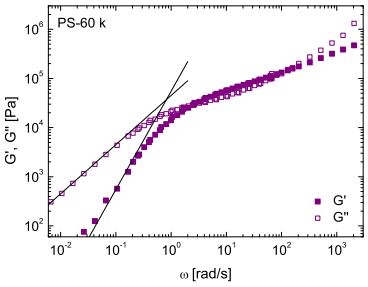

(b)

Figure 3.3: (a) LVE data for PS-545k/60k at $T_{ref} = 135.9\,^{\circ}\mathrm{C}$. (b) LVE data for PS-60k at $T_{ref} = 135.9\,^{\circ}\mathrm{C}$.

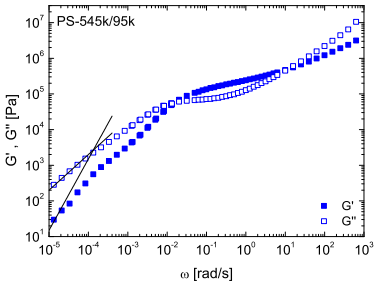

(a)

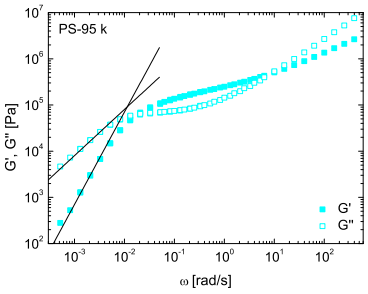

(b)

Figure 3.4: (a) LVE data for PS-545k/95k at $T_{ref} = 130\,^{\circ}\mathrm{C}$. (b) LVE data for PS-95k at $T_{ref} = 130\,^{\circ}\mathrm{C}$.

Figures 3.1(b) and 3.2(b) show the LVE of the two solvents, OS-10k and PS-25k, of the above mentioned solutions. Data are spanned over a frequency range of nine order of magnitude and also here the cross over at high frequencies was captured. In the terminal regime the moduli have the characteristic slopes of a Maxwellian liquid.

Conversely from the two solutions, the LVE data of the PS-545k/60k and the PS-545k/60k shown in figures 3.3(a) and 3.4(a) present the typical shapes of entangled systems. Here the data do not cover as wide range of ω as in the previous plots, hence the third crossover point is not shown.

The G' and G'' of the PS-545k/60k show a signature of few entanglements. In the terminal region, approximately from $\sim 10^{-3}$ to $\sim 10^{-1}$, the presence of two components are clear in the unusual trend of the moduli. At even lower frequencies they eventually start approaching the characteristic slopes.

Similar observations can be done regarding the LVE data of the PS-545k/95k with the difference that the newtonian regime is reached at approximately $\sim 10^{-5}$ and the intermediate frequencies regime, between the two crossover points, is slightly wider than the one of PS-545k/60k.

Figures 3.3(b) and 3.4(b) show respectively the LVE of the two NMMD melts PS-60k and PS-95k.

3.3.2 Start up and Steady-state Extensional Flow

Start up of Extensional Flow: $\bar{\eta}^+$ and $\langle \sigma_{zz} - \sigma_{rr} \rangle_{corr}$

Figures 3.5(a), 3.6(a), 3.7(a), 3.8(a) show the stress growth coefficient $\bar{\eta}^+$ as a function of time at a temperature 30 °C higher than their T_g. Only the PS-545k/95k was not measured at the same distance from its glass transition temperature since the experiments were performed at $T = 130$ °C much earlier than the planning of the present work. For direct comparisons with the other samples the steady-state elongational viscosity data have been shifted to $T_{ref} = 135$ °C (30 °C higher than the corresponding T_g) using the shift factor $a_T = 0.3199$ and plotted as a function of the strain rate (3.10(b)). The black solid lines in the plots are the predictions from the LVE shear measurements.

The extensional data of the PS-545k/10k and PS-545k/25k, figure 3.5(a) and figure 3.6(a) respectively, always show a large amount of strain hardening, even at the lowest strain rate $\dot{\varepsilon} = 0.003 s^{-1}$ presented. At lower strains they follow the LVE predictions but then they deviate abruptly towards an elongational steady-state viscosity level circa two order of magnitude higher than the linear viscoelastic values, the deviation happens earlier at higher strain rate and later at lower strain rate. Data are a bit scattered,

especially at the two lowest strain rates, due to the low forces induced from the material on the weight cell, which did not have enough resolution for such small values. Both the PS solutions present a big strain hardening in agreement with the observations of Huang *et al.* (2013a).

In figures 3.7(a) and 3.8(a) data of the two blends, PS-545k/60k and PS-545k/95k, are presented. For the PS-545k/60k experiments were performed at six different strain rates and for all of them, after an initial match with the LVE prediction trend, strain hardening is observed. However there is a vertical shift between the linear viscoelastic line and the extensional data that might be attributed to the presence of residual solvent in the sample used for the shear measurements. Also here data are quite scattered due to the low resolution of the weight cell in relation with weak stresses. More scattering is observed since the cross section area of the filament at the end of the experiment becomes very small and also problems with laser detection arise.

Only four strain rate experiments are shown for the PS-545k/95k in figure 3.8(a). The lowest strain rate experiment, $\dot{\epsilon} = 0.0003 s^{-1}$ was originally performed at $T = 160\,^{\circ}\mathrm{C}$ and then shifted to $T = 130\,^{\circ}\mathrm{C}$ with the calculated shift factors $a_T = 0.00463$ and $b_T = 0.91$. This measurement closely follow the LVE predictions and shows a slight deviation just at the end. Data are very smooth and much less scattered than the other cases due to the higher molar mass of the short component of the sample (PS-95k).

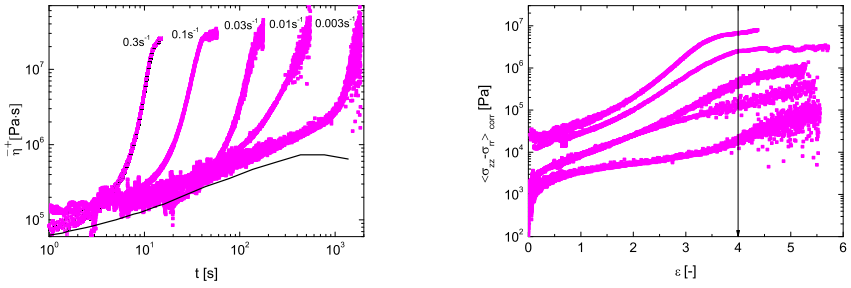

(a) (b)

Figure 3.5: (a) The extensional stress growth coefficient as a function of time for PS-545k/10k at $T_{ref} = 128.4\,^{\circ}\mathrm{C}$ ($T_{ref} - T_g$). (b) The extensional stress as a function of Hencky strain for PS-545k/10k at $T_{ref} = 128.4\,^{\circ}\mathrm{C}$ ($T_{ref} - T_g = 30\,^{\circ}\mathrm{C}$).

Figures 3.5(b), 3.6(b), 3.7(b), 3.8(b) show the measurements of the four samples above in the form of stress average difference $\langle \sigma_{zz} - \sigma_{rr} \rangle_{corr}$ as a function of the Hencky strain ε to better visualize the elongational steady-state viscosity. Figure 3.5(b) shows that all the samples of PS-545k/10k were stretched above hencky strain $\varepsilon = 5$ (less the one at

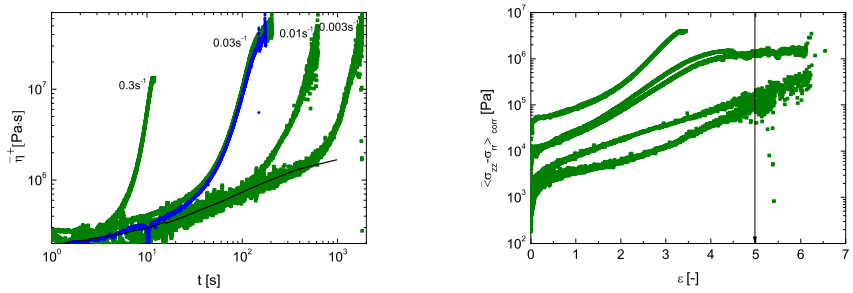

(a) (b)

Figure 3.6: (a) The extensional stress growth coefficient as a function of time for PS-545k/25k at $T_{ref} = 134.2\,°C$ ($T_{ref} - T_g$). (b) The extensional stress as a function of Hencky strain for PS-545k/10k at $T_{ref} = 134.2\,°C$ ($T_{ref} - T_g = 30\,°C$).

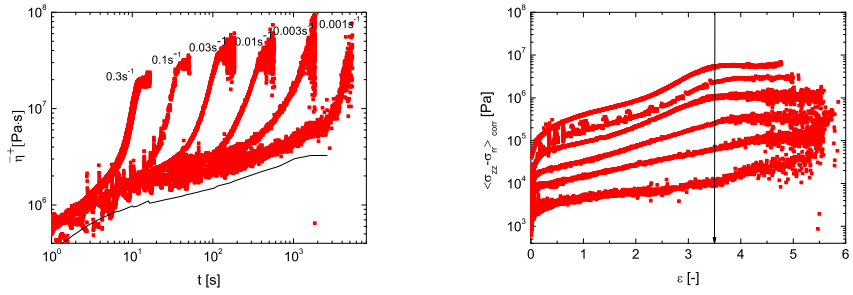

(a) (b)

Figure 3.7: (a) The extensional stress growth coefficient as a function of time for PS-545k/60k at $T_{ref} = 135.9\,°C$ ($T_{ref} - T_g$). (b) The extensional stress as a function of Hencky strain for PS-545k/60k at $T_{ref} = 135.9\,°C$ ($T_{ref} - T_g = 30\,°C$).

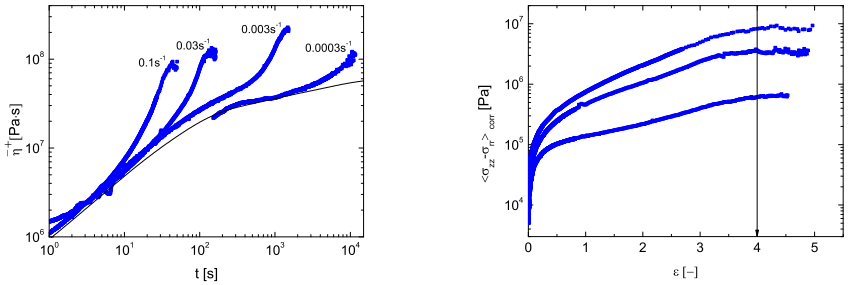

(a) (b)

Figure 3.8: (a) The extensional stress growth coefficient as a function of time for PS-545k/95k at T_{ref} = 130 °C. (b) The extensional stress as a function of Hencky strain for PS-545k/95k at T_{ref} = 130 °C.

higher strain rate) and they reached a steady-state value after hencky strain $\varepsilon = 4$. Also all measurements for the PS-545k/10k in figure 3.6(b) approach a steady-state value. The data at $\dot{\epsilon} = 0.0003 s^{-1}$ do not reach hencky strains higher than 3.5 due to breaking of the filament. Steady-state viscosity is reached after a Hencky strain of 3.5 for the PS-545k/60k at all the stretch rates. In figure 3.8(b) just the three higher strain rates measurements are reported since those are the relevant ones for the comparison with the other samples. Up to Hencky strain 4 the extensional stress values are constant in time.

Extensional Steady-state Viscosity $\bar{\eta}_s$

The extensional steady-state viscosity $\bar{\eta}_s$ has been plotted as a function of the Hencky strain rate $\dot{\varepsilon}$ for all the samples. Figures 3.9(a), 3.9(b), 3.10(a) and 3.10(b) show that in each plot steady-state viscosity values are almost constant at different strain rates. A plateau region is observed in all the cases. In the case of the PS-545k-95k and the PS-545k-60k an extensional rate thinning is observed since the $\bar{\eta}_s$ is slightly lower at the fastest strain rates. This time the data for all the systems are shown at the same distance (30 °C higher) from their own T_g. The data of PS-545k/95k have been shifted to T = 135 °C.

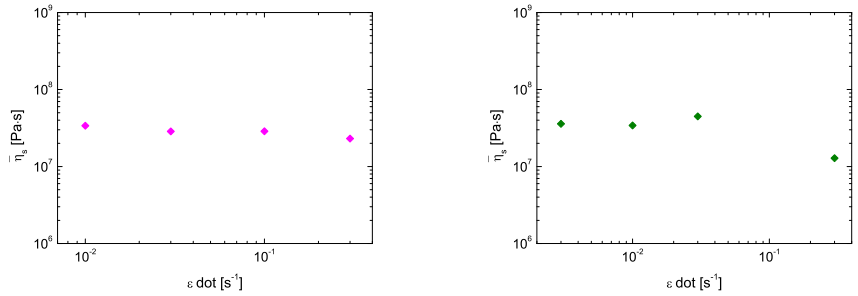

(a) (b)

Figure 3.9: (a) The steady-state extensional viscosity as a function of of the strain rate for PS-545k/10k at T_{ref} = 128.4 °C. (b) The steady-state extensional viscosity as a function of of the strain rate for PS-545k/25k at T_{ref} = 134.2 °C.

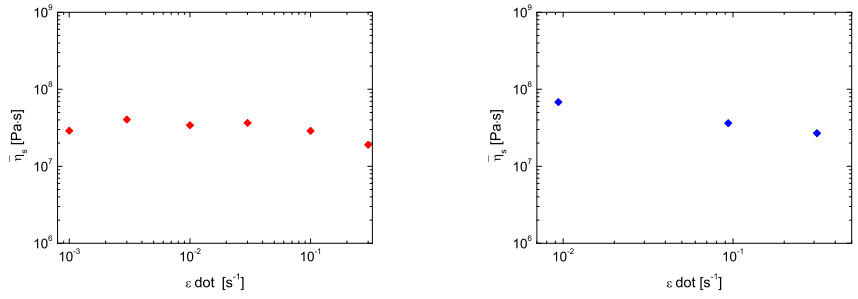

(a) (b)

Figure 3.10: (a) The steady-state extensional viscosity as a function of of the strain rate for PS-545k/60k at T_{ref} = 135.9 °C. (b) The steady-state extensional viscosity as a function of of the strain rate for PS-545k/95k at T_{ref} = 135 °C.

3.4 Discussion

The interesting result is found plotting all the experimental data of all the systems at the same $T_{ref} - T_g$. They reach the same level of steady-state viscosity and a good match is observed for all the samples at the same Hencky strain rates. It is observed that more strain hardening is manifested for the solutions, PS-545k/10k and PS-545k/25k, than for the blends, PS-545k/60k and PS-545k/95k, as it is shown in figure 3.11. This evidence is in agreement with the work of Huang *et al.* (2013a), where was suggested that dilution increases the degree of strain hardening of the polymers due to either a higher value of the molecular weight of the segment between two entanglements M_e (which translates in a higher degree of chain stretching, i. e. more flexibility) or to a lower decrease of the friction coefficient in strong elongational flow Huang *et al.* (2013b).

To have a better overview, with respect to the previous plot that appears a bit crowded, we also plot on the same figure 3.12 the extensional steady-state viscosity as a function of the strain rate for all the samples.

The choice of compare the experimental data at the same distance from T_g is due to the will of being coherent in having the different systems under the same conditions of molecules flexibility. It is well-known that polymer chain mobility changes with temperature. At temperatures lower than the glass transition temperature polymer molecules are frozen in a particular configuration. As the temperature is increased above the T_g the polymer chains start to have a certain freedom to move around. The higher the $T - T_g$ the bigger is the chain mobility.

To further support our experimental results we also plot some data taken from Nielsen *et al.* (2006) in Figure 3.13. [1] Two blends, called from the authors Blend 2 and Blend 3, which have the same monodisperse long molecular weight component, linear PS of 390k, diluted in a matrix of monodisperse low molecular weight component either PS-50k (in Blend 2) or PS-100k (in Blend 3) were measured in extensional flow at different strain rates at the same $T_{ref} = 130\,^{\circ}\mathrm{C}$. The composition is almost the same for the two systems, respectively 14.3% and 14.02% weight fraction of the PS-390k. In this case all the linear PS presents in the blends have the same glass transition temperature since their molar mass is above the critical molecular weight over which T_g is constant. Here the values of the steady-state extensional viscosity of the two blends (see Figure 3.13) taken at the same stretch rate completely overlap each other confirming what we have observed in our systems.

[1] This work has been inspired from a Poster entitled: 'Modeling the extensional rheology of model entangled linear chains'. Taisir Shahid, Christian Clasen, Filip Oosterlinck, Evelyne van Ruymbeke. The work was presented at the SUPOLEN Summer School in Capri 2015.

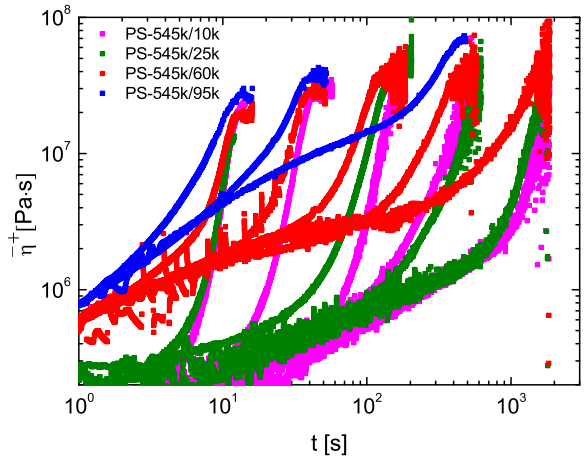

Figure 3.11: The extensional stress growth coefficient as a function of the time for all the solutions plotted at $T_{ref} = T_g + 30\,^{\circ}\mathrm{C}$.

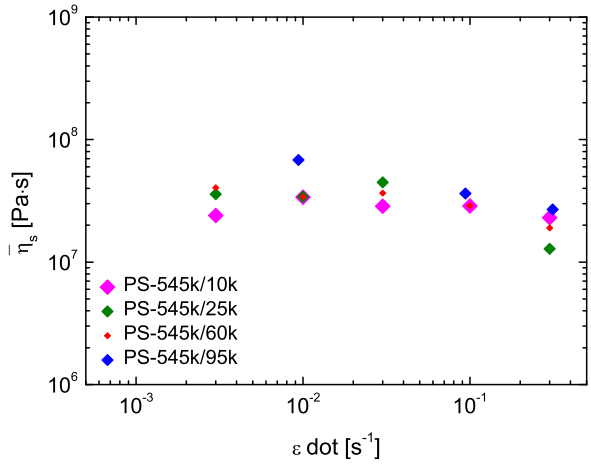

Figure 3.12: The steady-state extensional viscosity as a function of the strain rate for all the solutions at $T_{ref} = T_g + 30\,^{\circ}\mathrm{C}$.

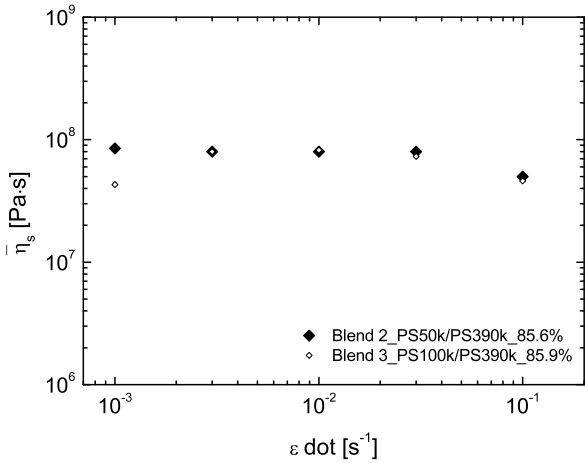

Figure 3.13: Steady elongational viscosity as a function of the elongational rate for Blend 2 and Blend 3 at T_{ref} = 130 °C (data are taken from Nielsen *et al.* (2006)).

3.5 Conclusions

We have investigated the extensional steady-state stress level by means of well-controlled uniaxial extensional experiments of a series of samples constituted by long linear polystyrene chains blended in the same proportion with four different low molecular weight linear polystyrenes. We have shown that comparing experimental data at the same distance from the glass transition temperature T_g a match of the steady-state elongational stress is observed for all the samples. This finding suggests that the stress level is not affected by the short chain components present in the sample but is determined solely by the high molecular weight molecules.

CHAPTER 4

Stress Relaxation of Bidisperse Polystyrene Melts: Exploring the Interactions between Long and Short Chains in Non-linear Rheology

We present start-up of uniaxial extension followed by stress relaxation experiments of a bi-disperse 50% by weight blend of 95k and 545k molecular weight polystyrene. We also show, for comparison, stress relaxation measurements of the polystyrene melts with molecular weight 95k and 545k, which are the components of the bi-disperse melt. The measurements show three separated relaxation regimes: a fast regime, a transition regime and a slow regime. In the fast regime the orientation of the long chains is frozen and the stress relaxation is due to stretch relaxation of the short chains primarily. Conversely in the slow regime the long chains have retracted and undergo relaxation of orientation in fully relaxed short chains.

4.1 Introduction

Industrial polymers are largely polydisperse systems. One step towards understanding polydisperse polymers is the experimental characterization and modelling of bi-

disperse blends. In fact the prediction of bi-disperse systems is a strong way to probe the validity of theoretical models.

The motion of entangled polymer chains has been described by the reptation theory of Doi and Edwards (1986), which in its original form assumes that each polymer chain slithers through a tube made of other polymer chains with a friction coefficient that is independent of the other chains. In this frame the mutual influence of reptating chains was not considered and each chain moves out of its own tube assuming an equilibrium configuration irrespective of the state of the other chains. The tube through which the polymer diffuses is assumed to be fixed in time.

Over the years many attempts were made to develop blending laws based on the Doi–Edwards model [Lee *et al.* (2005), Khaliullin and Schieber (2010), Read *et al.* (2012), van Ruymbeke *et al.* (2012) and van Ruymbeke *et al.* (2014)]. Two main boosts in the tube motion were proposed: a constraint released (CR) mechanism de Gennes (1975) and a dynamic tube dilation (DTD) mechanism by Marrucci (1985). The first mechanism is activated by the slow tube dynamic in which some of the entaglements' constraints along the chain are released allowing more freedom in the lateral movements of the test chain. The DTD mechanism says that the tube renewal due to the faster motion and relaxation of the surrounding short chains results in a widening of the tube diameter speeding up the reptation of the longer chains. The fraction of the relaxed molecules acts like a solvent on the unrelaxed molecules.

The first development in the description of the CR of the double reptation mixing rule was introduced by Tsenoglou C. (1987) and des Cloizeaux (1988), which attempt to de-scribe the terminal relaxation region, more sensitive to the bi-modal molecular weight distribution. In this approach the entanglement between two different M_w chains is a random event proportional to the volume fraction of the components and as soon as one of the two polymers diffuses away, the coupling point formed by the entanglement will instantaneously relax. That holds just if the longest relaxation times of the two com-ponents are sufficiently apart from each other. Validation was found with experimental viscoelastic data combined with dielectric spectroscopy on entangled binary blends of linear cis-polyisoprenes [Watanabe *et al.* (2004a), Watanabe *et al.* (2004b)].

Struglinski and Graessley [Struglinski and Graessley (1985), Struglinski and Graessley (1986)] investigated the linear viscoelasticity of five series of well entangled binary melts of linear polybutadiene, each with a wide range of concentrations. The ratio between the molecular weight of the long and the short molecules M_L/M_S ranged between 2.5 and 10.7. Besides the experimental work they suggested some molecular theories, earlier based just on the tube and reptation model and later adding mechanisms such as path length fluctuations and constraint release. They introduced the existence of two different relaxation behaviours determined by a relevant parameter defined as $Gr = M_L M_e^2 \big/ M_S^3$, where M_L and M_S are respectively the molecular weight

of the long and the short component, and M_e is the molecular weight of a strand between two entanglements. The critical value of the parameter defines the limit of the two cases. Picturing the long polymer component constraints in a tube made up of entanglements with short and long chains if $Gr << Gr_c$, the entanglements with short chains are long-lived hence the high M_w chain relaxes in a region constrained by both components, called thin tube, and the reptation time of the long chains is independent of blend composition. Conversely if $Gr >> Gr_c$ short chains constraints are not anymore active to define the long chain path and tube dilation takes place i . e . the long molecules diffuse in the wider tube where the only active constraints are within long polymers.

The exact value of Gr_c is not universally recognised. The original one proposed by Struglinski and Graessley was 1, whereas in a later work of Park and Larson (2004), was empirically fixed at 0.064, which gave a better estimate to delimit the two regimes of the skinny and dilated tube. The authors proposed an extended version of the Milner-McLeish model [Milner and McLeish (1998)] from linear monodisperse polymers to linear bi-disperse melts incorporating dynamic tube dilation (DTD) and Rouse constraint release mechanism (CRR). The time scale is divided into three regimes: the first one until the reptation time of the short chains, an intermediate one that lasts up to the reptation of the long chains and the terminal one after the terminal relaxation of the long chains. Predictions showed good agreement with a wide series of linear viscoelastic data of bidisperse 1,4 polybutadienes and polyisoprenes linear melts spanned on a large range of Gr values.

Some relaxation experiments from states close to equilibrium have shown that a cooperative effect exists between chains. In particular, Kornfield *et al.* (1989) used a rheo-optical technique to measure the dynamic infrared dichroism in the relaxation phase following step shear for each component in bi-disperse entangled polymer melts of hydrogenated and deuterated polyisoprenes containing from 10 to 75 % vol. of long chains. They found that polydispersity can strongly affect the relaxation process of the components, decreasing the longest relaxation time of the high molecular weight polymer and delaying the longest relaxation time of the short component regardless the M_w of the long chain matrix. They explained that the observed slower relaxation of the shorter molecules is due to a combined effect of anisotropy in the orientation of the Rouse segments and a nematic orientation induced by the neighbouring long chains.

More recently, Ianniruberto *et al.* (2012) suggested a reduction of the monomeric friction coefficient caused by alignment of the Kuhn segments of polymer chains. The stretch-orientation induced reduction of the friction ζ is based on the molecular concept that aligned objects generate an anisotropic and reduced friction when parallel to each other in contrast to the random configuration. Based on the same concept, Yaoita *et al.* (2012) further investigated the molecular origin of the different behavior between polymer melts and solutions with primitive chain simulations. In a more recent study on solvent effects in monodisperse concentrated polymer solutions, Huang *et al.* (2013b)

also addressed to the existence of nematic interactions between solvent-polymer and polymer-polymer molecules to explain an observed dependence on solvent nature in non-linear extensional flow.

Compared to monodisperse polymer melts and solutions, the situation is more challenging for bi-disperse entangled melts because they emphasize complex interactions between long and short chains especially in non-linear relaxation process. Non-linear viscoelastic properties in elongational flow have not been investigated as intensely. Extensional data of polystyrene blends of super high M_w dissolved, with small volumetric fraction, in a matrix of shorter polydisperse chains were modeled by Wagner *et al.* (2005). The prediction showed that increasing the amount of the long component in the blends resulted in more strain hardening.

Nielsen *et al.* (2006) characterized three bi-disperse poly-styrene melts in non-linear extensional flow, which are the only measurements that reached steady state for bi-disperse systems to our knowledge. They mixed PS-390k with PS-50k in two different concentrations to investigate the effect of dilution, as well as PS-390k with PS-100k in the same concentration of the previous one to test the effect of short molecules length. A maximum, relative to the $3\eta_0$, in the steady state elongational viscosity vs. elongational rate was observed for all the samples. Conversely to the observations of Wagner *et al.* (2005), the amount of strain hardening increases as the long chains are more diluted. Relying on the few available extensional data several mixing laws have been developed for predicting the non–linear viscoelastic behaviour of bi-disperse linear melts [van Ruymbeke *et al.* (2010), Wagner (2011), Rasmussen (2014)].

A more recent work by Auhl *et al.* (2009) focuses on the onset of chain stretch of long chains when diluted by shorter ones. Start up elongational data of two series of binary blends of polyisoprene with broad concentration range are fitted with a model that confirms their prediction: long chain stretch appears at lower Hencky strain when the long chains are diluted by the short ones than in the pure melt. They explain this behaviour by a proposed novel mechanism, the effective stretch relaxation time, which implies the stretch relaxation of the fat tube through the motion of the chain in the thin tube.

However, data of stress relaxation following steady extensional flow, which are more relevant for the understanding of relaxation mechanisms of bi-disperse systems, are still missing.

In the present work we measured a bi-disperse 50% by weight blend of 95k and 545k molecular weight polystyrene (for which the estimated Struglinsky-Graessley parameter is $Gr = 0.112$), referred to Blend 50L-50S, in both uniaxial extensional flow and stress relaxation. The purpose is to investigate cooperative interactions between polymer chains and measure how the mechanism of the short chains is affected in presence of the long chains. Data for the blend are compared to data for the pure components.

4.2 Experimental

4.2.1 Synthesis and Chromatography

The polystyrene PS-545k melt used in this work has been previously described and characterized in both shear and extensional rheology by Huang *et al.* (2013a). The polystyrene PS-95k has been synthesized by the means of living anionic polymerization according to the standard procedure by Ndoni *et al.* (1995). The reaction was carried out for 4 hours at 35 °C in freshly distilled cyclohexane, with the use of the titrated solution of sec-butyllithium in hexane as the initiator. The molar mass of PS-95k was determined with size exclusion chromatography (SEC) with non-stabilized tetrahydrofuran (THF) as the eluent and with the use of a column set consisting of a $5\mu m$ guard column and two $300 \times 8mm^2$ columns (PLgel Mixed C and Mixed D). The system was equipped with a triple detector system including a combined Viscotek model 200 differential refractive index (DRI), a differential viscosity detector and a Viscotek model LD 600 right angle laser light scattering detector (RALLS). On the basis of calibration with narrow molar mass polystyrene standards and flow rate signal adjusting according to Irganox signals, the values of the weight-average molecular weight $\bar{M}_w$ and the polydispersity index PDI, defined as the ratio of the $\bar{M}_w$ over the number-average molecular weight $\bar{M}_n$, were determined. Table 4.1 summarizes the weight-average molecular weight $\bar{M}_w$ and the polydispersity index PDI of the two polystyrenes.

Table 4.1: Molecular properties of the two monodisperse polystyrene components (the values for PS-545k are taken from Huang *et al.* (2013a)). The reptation (τ_m) and the Rouse (τ_R) times are measured at 130 °C.

Sample	$\bar{M}_w$[g/mol]	PDI	$\tau_m\,[s]$	$\tau_R\,[s]$	Z
PS-545k	545000	1.12	58750	705	41.0
PS-95k	95100	1.07	169.3	20.4	7.14

4.2.2 Blend Preparation

The polystyrene blend was prepared using the two monodisperse melts described above. PS-95k and PS-545k were dissolved together in THF and the solution was stirred at room temperature for 24 hours. Once both components were well dissolved and mixed homogeneously, the THF solution was poured into methanol drop by drop, which precipitated out the blend. The precipitated blend was recovered by filtration. The wet powder was then dried for more than eight hours in open air and later dried in a vacuum oven at 70 °C for 2 weeks to ensure the complete evaporation of the residual solvent. To

check concentration homogeneity two samples at different locations of the blend were tested in SEC. The concentration analysis was conducted by integral estimation of the peak areas of the bimodal curve in SEC to make sure that the desired concentration was obtained.

Table 4.2 summarizes the corresponding weight fraction of the components in the bidisperse blend 50L-50S. The weight-average molecular weight $\bar{M}_w$ has also been calculated for the blend and the value is reported in the same table.

Table 4.2: The weight fractions of PS-95k and PS-545k and the weight average molecular weight $\bar{M}_w$ of the Blend 50L-50S.

Sample	$wt\%PS-545k$	$wt\%PS-95k$	$\bar{M}_w$[g/mol]
Blend 50L-50S	49.8	50.2	319000

4.2.3 Mechanical Spectroscopy

The linear viscoelasticity of the pure monodisperse polystyrene melts and the Blend 50L-50S have been measured on an ARES-G2 rheometer from TA Instruments, with an 8 mm parallel plate geometry. Small amplitude oscillatory shear flow measurements were performed for all three samples at 130, 150 and 170 °C in nitrogen atmosphere. The data were shifted to a single master curve at 130 °C, using the principle of time temperature superposition (TTS). The time-temperature shift factors for PS-95k, PS-545k and the Blend 50L-50S were found to be in agreement with a single Williams-Landel-Ferry (WLF) equation of the form,

$$\log_{10} a_T = \frac{-c_1^0 (T - T_0)}{c_2^0 + (T - T_0)}, \tag{4.1}$$

where $c_1^0 = 8.99$ and $c_2^0 = 81.53K$, $T_0 = 403K$ and T is the temperature in K.

4.2.4 Extensional Flow

The extensional stress measurements were performed with a filament stretching rheometer (FSR) [Bach *et al.* (2003b), Román Marín *et al.* (2013)]. The FSR has been recently modified with the introduction of two independent motors, one connected to the top

plate and the other one connected to the laser. Before starting an experiment, the samples of Blend 50L-50S were molded into cylindrical shaped pillars with a fixed radius R_0 of 2.7 mm and a thickness of L_0 between 1.32 and 1.45 mm, giving an aspect ratio $\Lambda_0 = L_0/R_0$ ranging between 0.49 and 0.54. The same procedure was followed for the monodisperse PS-95k samples, except that the radius R_0 was 4 mm and the thickness L_0 was around 2 mm for all the samples. To make sure that no air bubbles were trapped in the samples, the dried polymer powder was molded at approximately 150 °C for 20 minutes and then pressed and annealed at the same temperature under vacuum for an additional 20 minutes, to ensure the complete relaxation of the polymer chains. Before each experiment the sample was allowed to fully relax after pre-stretching to a radius R_p. The Hencky strain is calculated from on line measurement of the mid–filament radius $R(t)$ as

$$\varepsilon = -2 \ln \left[R(t) \Big/ R_p \right] \tag{4.2}$$

while the strain rate is defined as $\dot{\varepsilon} = d\varepsilon/dt$. The mean value of the difference between the axial and the radial stress in the mid-filament is obtained from the measured values of $F(t)$ and $R(t)$, with a force balance that neglects surface tension and inertial effects as reported by Szabo (1997) and Szabo and McKinley (2003) as

$$\langle \sigma_{zz} - \sigma_{rr} \rangle = \frac{F(t) - m_f g \Big/ 2}{\pi R(t)^2}, \tag{4.3}$$

where $F(t)$ is the axial force, g is the gravitational acceleration and m_f is the weight of the filament. At small strains, during the start up of the extensional flow, there is a contribution in the stress difference that arises from the shear components in the deformation field. This effect is caused by the no-slip boundary condition at the end plates, and is more prominent at small aspect ratios [Nielsen *et al.* (2006)]. This effect may be compensated by a correction factor as mentioned in Rasmussen *et al.* (2010) that ensures less than 3% deviation from the corrected initial stress. For large strains the correction vanishes and the radial variation of the stress in the symmetry plane becomes negligible [Kolte *et al.* (1997)]. Finally, the extensional stress growth coefficient is calculated as

$$\bar{\eta}^+ = \frac{\langle \sigma_{zz} - \sigma_{rr} \rangle_{corr}}{\dot{\varepsilon}}. \tag{4.4}$$

Stress relaxation measurements present a special challenge, since merely halting the plates does not produce a true stress relaxation experiment, because typically the filament will be subjected to a progressive thinning on its own [Wang *et al.* (2007); Lyhne

et al. (2009)]. A technique to perform a direct stress relaxation experiment follow-ing steady uniaxial extension on polymer melts has been introduced by Nielsen *et al.* (2008) on the above-mentioned FSR. The novelty consists in the use of a closed loop controller that monitors the mid-filament diameter; in this way the necking is avoided by adjusting the position of the top plate. In a stress relaxation experiment, at the start-up of the elongation, a constant strain rate is applied on the sample. As soon as the stress relaxation starts at an arbitrarily given Hencky strain ε_0, the mid-filament radius is kept constant by the active control loop, giving $\dot{\varepsilon} = 0$. The extensional stress decay coefficient during the stress relaxation is defined as

$$\overline{\eta^-} = \frac{\langle \sigma_{zz} - \sigma_{rr} \rangle}{\dot{\varepsilon}}, \tag{4.5}$$

where $\dot{\varepsilon}$ is the strain rate in the start-up of the uniaxial extensional flow. The extra shear contribution, mentioned before for the start-up of the extension flow, is negligible during the stress relaxation process [Nielsen *et al.* (2008)].

4.3 Results and Analysis

4.3.1 Linear Viscoelasticity

The storage modulus G' and loss modulus G'', plotted as a function of the angular frequency ω, are shown in Figure 4.1 for PS-95k and PS-545k, and in Figure 4.2 for the Blend 50L-50S. The LVE data for the two monodisperse melts have been fitted with a continuous Baumgaertel-Schausberger-Winter (BSW) relaxation spectrum [Baumgaertel *et al.* (1990)]. The choice of using this model is due to its success in describing linear monodispese solutions and melts [Huang *et al.* (2013a), Huang *et al.* (2013b)]. The stress relaxation modulus $G(t)$ is defined in terms of the continuous spectrum $H(\tau)$ of relaxation times τ as follows,

$$G(t) = \int_0^\infty \frac{H(\tau)}{\tau} \exp(-t/\tau)\, d\tau, \tag{4.6}$$

$$H(\tau) = H_e(\tau) + H_g(\tau). \tag{4.7}$$

The spectrum $H(\tau)$ is composed of two contributions due to two different behaviours: the entanglement or viscoelastic one, defined as $H_e(\tau)$; and the glassy one, defined as

$H_g(\tau)$, expressed as

$$H_e(\tau) = n_e G_N^0 \left(\frac{\tau}{\tau_m}\right)^{n_e} h(1-\tau/\tau_m), \tag{4.8}$$

$$H_g(\tau) = n_e G_N^0 \left(\frac{\tau}{\tau_c}\right)^{-n_g} h(1-\tau/\tau_m). \tag{4.9}$$

Here G_N^0 is the plateau modulus, τ_c is the characteristic time of the glassy mode, τ_m is the longest relaxation time, n_e and n_g are the slopes, respectively, of the viscoelastic and the glassy spectra in a log-log plot. $h(x)$ is the Heaviside step function determining the cut-off of the two spectra. The values of n_e and n_g, which are material specific constants, were fixed to 0.23 and 0.70, respectively, in the case of nearly monodisperse polystyrene melts [Huang *et al.* (2013a), Huang *et al.* (2013b)], while the other three parameters G_N^0, τ_c and τ_m were optimized by the fitting. A detailed explanation of the meaning of BSW-parameters can be found in Huang *et al.* (2013a). For convenience we reproduce here the asymptotic result in the glassy regime

$$G''(\omega)/(G_N^0 n_e) \sim \frac{\pi}{2\cos\left(n_g\pi/2\right)}(\tau_c\omega)^{n_g} \text{ for } \omega \to \infty, \tag{4.10}$$

$$\tan\delta = G''/G' = \tan(n_g\pi/2). \tag{4.11}$$

Correspondingly it may be shown that the relaxation modulus in the glassy regime ($t \ll \tau_m$) has the power law behaviour

$$G(t)/(G_N^0 n_e) = \Gamma(n_g)(t/\tau_c)^{-n_g}, \tag{4.12}$$

where $\Gamma()$ is the Gamma function.

The material properties of the two PS mono-disperse melts obtained from the BSW-fitting of the master curve at 130 °C are listed in Table 4.3, together with the value of the zero-shear-rate viscosity η_0 and an average relaxation time τ_w [Nielsen *et al.*(2006)] calculated as

$$\eta_0 = \int_0^\infty G(s)ds \doteq n_e G_N^0 \tau_m, \tag{4.13}$$

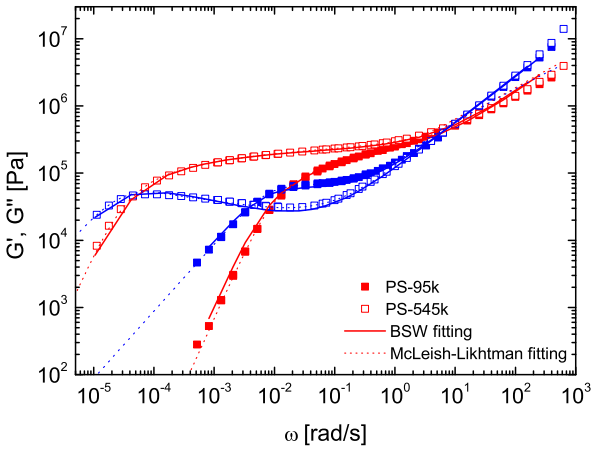

Figure 4.1: LVE data fitted with the BSW spectrum and the McLeish-Likhtman theory for PS-545k and PS-95k at 130 °C.

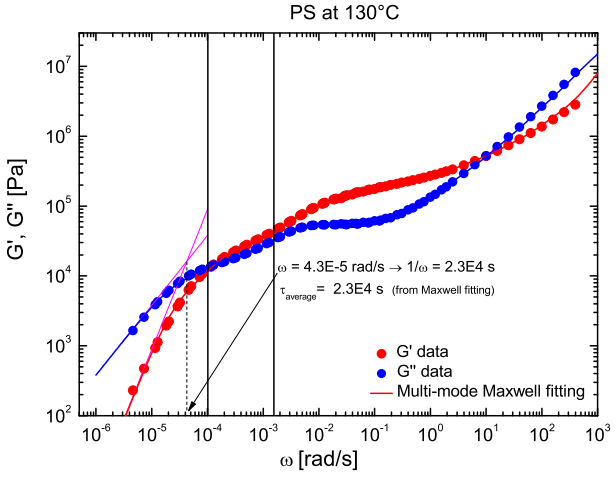

Figure 4.2: LVE data fitted with the Multi-mode Maxwell spectrum for Blend 50L-50S at 130 °C.

$$\tau_w = \frac{\int_0^\infty G(s)sds}{\int_0^\infty G(s)ds} \doteq \frac{1+n_e}{2+n_e}\tau_m. \tag{4.14}$$

Table 4.3: Material properties of PS-95k and PS-545k obtained from the BSW-fitting ($T = 130\,^\circ$C). [Values for PS-545k are taken from Huang *et al.* (2013a).]

Parameters	PS-545k	PS-95k
n_e	0.23	0.23
n_g	0.7	0.7
G_N^0[Pa]	256700	258080
τ_c[s]	0.419	0.400
τ_m[s]	58750	169.3
τ_w[s]	32400	93.38
η_0[Pa · s]	$2.823 \cdot 10^9$	$8.827 \cdot 10^6$

In both equations the dot indicates that the glassy contributions have been neglected. Note the value of the parameter $n_g = 0.70$ (corresponding to $\tan\delta \approx 2$) as the best fit to the data. It reflects the slope of $G''(\omega)$ for large frequency. This regime, commonly referred to as the Rouse regime has been extensively analysed [Likhtman and McLeish (2002)] in terms of constrained and unconstrained Rouse motion. We include therefore in Figure 4.1 the McLeish-Likhtman (ML) theory predictions (see Table 4.4). The prediction is almost identical with the BSW fitting except in the limit of large frequencies, where the ML-theory shows $G'(\omega) \sim G''(\omega)$ in contrast to the data.

Table 4.4: Material parameters of PS-95k and PS-545k obtained from the ML-theory ($T = 130\,^\circ$C).

ML Parameters	PS-545k	PS-95k
$\bar{M}_e$[Kg/mol]	17.1	16.8
G_e[Pa]	$3.41 \cdot 10^5$	$3.44 \cdot 10^5$
τ_e[s]	0.41	0.67
c_ν[s]	0.1	0.1

For the blend we use the Multi-mode Maxwell spectrum in the form

$$G(t) = \sum_k g_k e^{-t/\lambda_k}. \tag{4.15}$$

The Maxwell fitting parameters g_k and λ_k for the Blend 50L-50S are reported in Table 4.5. The value of the zero-shear-rate viscosity and average relaxation time computed from the definitions in Eqs. 4.13 and 4.14 become respectively $\eta_0 = \sum \lambda_k g_k = 3.82 \cdot 10^8$ Pa s and $\tau_w = \sum \lambda_k^2 g_k / \sum \lambda_k g_k = 2.3 \cdot 10^4 s$.

Table 4.5: Maxwell fitting parameters g_k and λ_k for the Blend 50L-50S.

k	g_k (Pa)	λ_k (s)
1	$6.76 \cdot 10^3$	$3.43 \cdot 10^4$
2	$1.83 \cdot 10^4$	$6.31 \cdot 10^3$
3	$1.52 \cdot 10^4$	$1.16 \cdot 10^3$
4	$6.67 \cdot 10^4$	$2.14 \cdot 10^2$
5	$5.70 \cdot 10^4$	$3.93 \cdot 10^1$
6	$5.28 \cdot 10^4$	7.22
7	$7.08 \cdot 10^4$	1.33
8	$1.84 \cdot 10^5$	$2.44 \cdot 10^{-1}$
9	$4.06 \cdot 10^5$	$4.50 \cdot 10^{-2}$
10	$1.15 \cdot 10^6$	$8.27 \cdot 10^{-3}$
11	$3.23 \cdot 10^6$	$1.52 \cdot 10^{-3}$
12	$5.14 \cdot 10^7$	$2.80 \cdot 10^{-4}$

Comparing the average relaxation time $\tau_w = 23000s$ for the Blend 50L-50S with the one obtained from the BSW fitting of the LVE data of the pure 545k (long c omponent)$\tau_w =$ $32400s$, both computed with Eq. 4.14, we can affirm that the terminal relaxation of the long chains in the blend is somewhat faster than in the pure melt. We take this to mean that the long chains are relaxing in a fat tube where the short chains are not imposing significant constraints. In the frame of the Struglinsky-Graessley criterion we are consequently in the limit of $Gr >> Gr_c$. Our system ($Gr = 0.112$) therefore seems to agree with the value of 0.064 reported by Park and Larson (2004) rather than the value $Gr_c = 1$ reported by Struglinski and Graessley (1985), Struglinski and Graessley (1986).

4.3.2 Start up of Extensional Flow

The molecular weight M_w of the two monodisperse components in Blend 50L-50S is selected such that their respective longest relaxation times are well separated from each other. We expect therefore that different mechanisms can be activated for each component independently. The Rouse time τ_R, which indicates the stretch relaxation time, is defined as $\tau_R = Z^2 \tau_e$, where τ_e is the relaxation time of the strand between two entanglements with molecular weight M_e, and $Z = M_w/M_e$ is the number of entanglements

per chain. We use M_e = 13300g/mol [Bach *et al.* (2003a)] to determine the value of Z for our monodisperse melts. The reptation time τ_m, which indicates the maximum relaxation time of a whole chain, can be obtained from LVE measurements. The values of τ_m, τ_R and Z for the two monodisperse polystyrenes are listed in Table 4.1.

To identify the regimes, we wish to interpret the dynamics in terms of time constants for the components. We estimate the Rouse times of the short and long constituents in the blend to be identical to those in the pure melts given in Table 4.1. Moreover since the long chains are essentially frozen at the relaxation time of the short component, we may roughly estimate the terminal relaxation time of the short chain to be approximately equal to that of the pure melt. However, the terminal relaxation of the blend will be reptation of the long chains in a sea of fully relaxed short chains. As an estimate for this time we use the relaxation time τ_w obtained from the Maxwell spectrum. Hence we arrive at the relaxation times in Table 4.6.

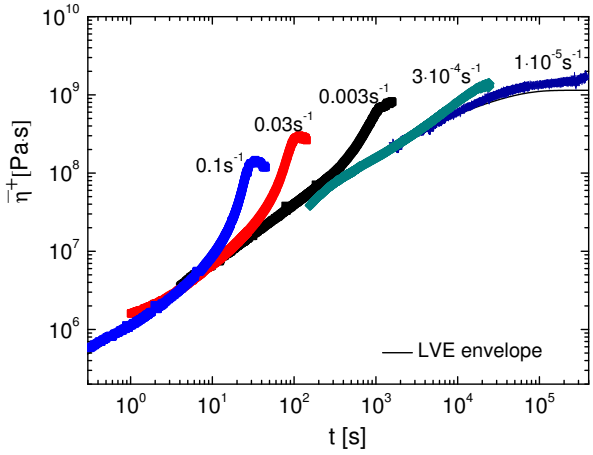

Figure 4.3: Stress growth coefficient as a function of time for the Blend 50L-50S measured at 130 °C. Except for the two longest stretch rates measured at 160 °C and then shifted to 130 °C with the horizontal shift factor a_T = 0.0038 and the vertical shift factor b_T = 0.91, according to the TTS superposition principle. The solid line is the LVE prediction based on the parameters listed in Table 4.5.

To relate the relaxation in terms of the molecular parameters of the two components, we discuss the strain rates in terms of their time constants. Based on the relaxation times from Table 4.6 we define non-dimensional stretch rates in terms of the Weissenberg number $Wi = \dot{\varepsilon}\tau$ for the short and long chains as reported in Table 4.7, where the superscripts S and L refer to short and long chains, respectively.

Table 4.6: Estimation of the time constants for short and long components in the blend.

Blend 50L-50S	Rouse time	Terminal time
Short component	$\tau_R^S = 20.4$s	$\tau_m^S = 169$s
Long component	$\tau_R^L = 705$s	$\tau_w^L = 23000$s

Table 4.7: Weissenberg numbers based on Rouse time and terminal time for short and long chains.

$\dot{\epsilon}\left[s^{-1}\right]$	Wi_R^S	Wi_d^S	Wi_R^L	Wi_d^L
$1 \cdot 10^{-5}$	$2.04 \cdot 10^{-4}$	$1.69 \cdot 10^{-3}$	$7.05 \cdot 10^{-3}$	0.23
$3 \cdot 10^{-4}$	$6.12 \cdot 10^{-3}$	0.012	0.21	6.9
0.003	0.061	0.51	2.1	69
0.03	0.61	5.1	21	690
0.1	2.0	17	71	2300

Figure 4.3 shows the measured corrected extensional stress growth coefficient $\overline{\eta}^+$ plotted as a function of time at 130 °C for the Blend 50L-50S. The sample was stretched at 5 different rates $\dot{\epsilon}$, which correspond to 5 different flow regions separated by the reptation time and Rouse time of the long and short chains. All the measurements were conducted at 130 °C, except the ones at the slowest stretch rates $\dot{\epsilon} = 1 \cdot 10^{-5} s^{-1}$ and $\dot{\epsilon} = 3 \cdot 10^{-4} s^{-1}$. These two were performed at 160 °C and shifted to 130 °C according to the Time Temperature Superposition principle, with shift factors $a_T = 0.0038$ and $b_T = 0.91$. The solid line in the plot is the LVE prediction calculated from the parameters listed in Table 4.5. The elongational measurements show good agreement with the LVE at small strains. The measurement at $\dot{\epsilon} = 1 \cdot 10^{-5} s^{-1}$ closely follows the LVE, except at high Hencky strains where the stress is slightly higher. At this strain rate we expect the system to be still close to the equilibrium configuration, since $\dot{\epsilon} < 1/\tau_d^L$ which means that the flow is not fast enough to orient the polymer chains. As the $\dot{\epsilon}$ increases, more and more deviation from the LVE envelope of the experimental curves is observed, meaning that the chains experience higher degree of stretching, which results in more strain hardening. Even at $\dot{\epsilon} = 3 \cdot 10^{-4}\, s^{-1}$, corresponding to a Wi_R^L of 0.2, light strain hardening is observed. This is in fact in agreement with the work of Auhl *et al.* (2009) who predict an increase in the stretch relaxation time of the pure long chains when diluted by shorter chains. From Table 4.7 it can be seen that only for the highest stretch rate ($\dot{\epsilon} = 0.1 s^{-1}$) $Wi_R^S > 1$, indicating the short chains are stretched by the flow.

In Figure 4.4 we show the same corrected extensional stress difference $\langle \sigma_{zz} - \sigma_{rr} \rangle$ plotted as a function of Hencky strain at 130 °C for the Blend 50L-50S. From this plot it is clear that $\langle \sigma_{zz} - \sigma_{rr} \rangle$ reaches a steady-state value above $\varepsilon = 3$ for each stretch rate.

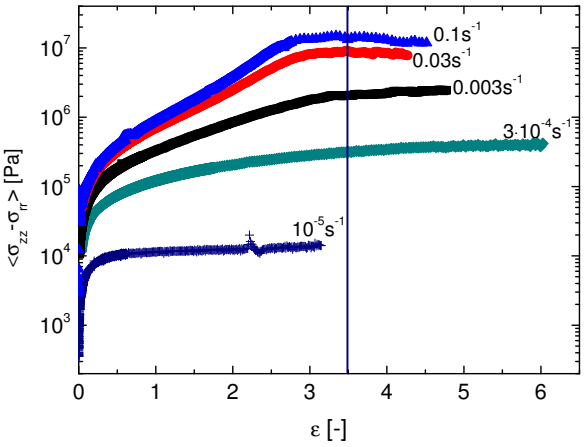

Figure 4.4: The measured stress for the Blend 50L-50S at 130 °C as a function of Hecky strain. The two slowest stretch rate measurements were performed at 160 °C and then shifted to 130 °C.

That allows the determination of a steady-state viscosity $\overline{\eta}_s$.

4.3.3 Relaxation after Fixed Flow Time

The uniaxial extensional flow was stopped in the start-up after a fixed flow time of $t_0 = 35s$ and then stress relaxation was performed. Figure 4.5 shows the measurements at 130 °C at $\dot{\varepsilon} = 0.003, 0.03$ and $0.1s^{-1}$. The Weissenberg numbers corresponding to the three strain rates $Wi_R^S = 0.061, 0.61$ and 2 and $Wi_R^L = 2.1, 21$ and 71, meaning that the long chains are in all experiments stretched by the flow while the short components are near to equilibrium at the slowest rate, oriented at $0.03s^{-1}$ and stretched at the highest strain rate.

To analyze the data let us initially recall the LVE analysis for the Maxwell spectrum of the form in Eq. 4.15. If we shift the time axis such that the flow is from $t = -t_0$ where $t_0 = \varepsilon_0/\dot{\varepsilon}$ to $t = 0$, the stress decay for $t > 0$ is given in the linear viscoelastic limit by

$$\sigma_E^-(t) = \dot{\varepsilon} \sum_j g_j \lambda_j \left(1 - e^{-t_0/\lambda_j}\right) e^{-t/\lambda_j} \tag{4.16}$$

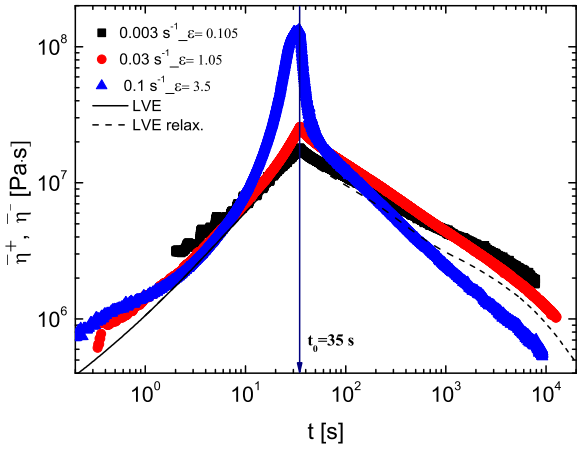

Figure 4.5: Stress relaxation measurements of the Blend 50L-50S after a fixed flow time $t_0 = 35s$ of uniaxial extension. The experiments were performed at $\dot{\varepsilon}$ of 0.003, 0.03 and 0.1 s^{-1} at 130 °C. The solid line is the LVE prediction and the dashed line is the LVE relaxation prediction for $\dot{\varepsilon} = 0.003s^{-1}$, both are based on the parameters listed in Table 4.5.

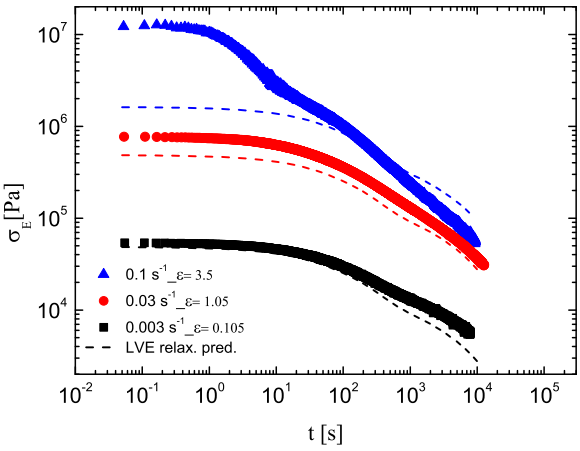

Figure 4.6: The stress decay data after a fixed elongational flow time $t_0 = 35s$ for the Blend 50L-50S. The data are originally from Figure 4.5 plotted according to Eq. 4.16.

It is illustrative to consider the two limits $t_0 \to 0$ (relaxation after step strain), with $t_0 \cdot \dot{\varepsilon} = \varepsilon$ fixed, and $t_0 \to \infty$ (relaxation after steady flow):

$$\text{step strain for } t_0 \to 0: \quad \sigma_E^-(t) = \varepsilon \sum_j g_j e^{-t/\lambda_j} \tag{4.17}$$

$$\text{steady flow for } t_0 \to \infty: \quad \sigma_E^-(t) = \dot{\varepsilon} \sum_j g_j \lambda_j e^{-t/\lambda_j} \tag{4.18}$$

By $t_0 \to \infty$ and $t_0 \to 0$ we mean t_0 larger than the longest relaxation time and smaller than the shortest relaxation time respectively. Thus for $t_0 < t_{min}$ the relaxation modes are weighted according to the individual moduli irrespective of the time constants. Conversely for relaxation after $t_0 > t_{max}$ the contributions from the individual modes are weighted by the products of the moduli and the time constants. Hence the fast modes from the small time constants contribute only a negligible amount compared to the longest time constants for relaxation after steady flow. Moreover the LVE prediction of stress decay depends on the strain rate applied in the uniaxial flow according to Eq. 4.18. In order to show the relaxation process at earlier times we take the stress decay data from Figure 4.5 and plot them according to Eq. 4.16 in Figure 4.6. For $\dot{\varepsilon} = 0.003 s^{-1}$ and $\dot{\varepsilon} = 0.03 s^{-1}$, at short times (first 10 s approximately) the stress for Blend 50L-50S is almost constant. At the same early times, the corresponding relaxation after the experiment at $\dot{\varepsilon} = 0.1 s^{-1}$ is much faster.

4.3.4 Stress Relaxation following Steady Extensional flow

We performed stress relaxation measurements after a fixed Hencky strain of 3.5, where steady-state was reached. The three strain rates are the same as the experiments at fixed flow time.

Figure 4.7 and 4.8 show the results for the Blend 50L-50S and PS-95k, respectively. In Figure 4.7 we plot the extensional stress growth coefficient $\overline{\eta}^+(t)$ followed by the stress decay coefficient $\overline{\eta}^-(t)$ as a function of time for the Blend 50L-50S. All the measurements were performed at 130 °C. We expected steady extensional flow to be established at $\varepsilon_0 = 3$, see Fig. 4.4. To confirm this hypothesis one additional experiment was performed with $\dot{\epsilon} = 0.1 s^{-1}$ and $\varepsilon_0 = 4$. Indeed it appears that the relaxation process is independent of ε_0 provided $\varepsilon_0 > 3$, confirming that once steady flow is reached, the following relaxation process is unaffected by the flow time. Also in the plot we show an experiment made at $\dot{\varepsilon} = 0.003 s^{-1}$ and stopped at $\varepsilon_0 = 0.3$, so that the relaxation spectrum is in the linear regime. This measurement agrees completely with the LVE predictions shown by the yellow solid line in figure 4.7. The black solid line in the

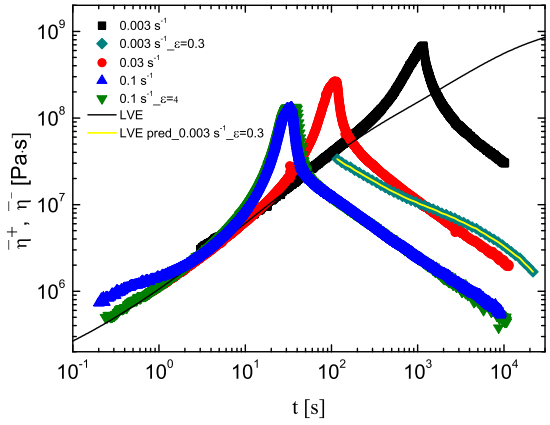

Figure 4.7: Stress relaxation measurements of the Blend 50L-50S after fixed Hencky strain of $\varepsilon_0 = 3.5$. The experiments were performed at $\dot{\varepsilon}$ of 0.003, 0.03 and 0.1 s^{-1} at 130 °C. Two extra measurements were done. One at $\dot{\varepsilon} = 0.1s^{-1}$ where the flow has been stopped at $\epsilon = 4$ and one at $\dot{\varepsilon} = 0.003s^{-1}$ stopped at $\varepsilon_0 = 0.3$, before entering the non linear regime.

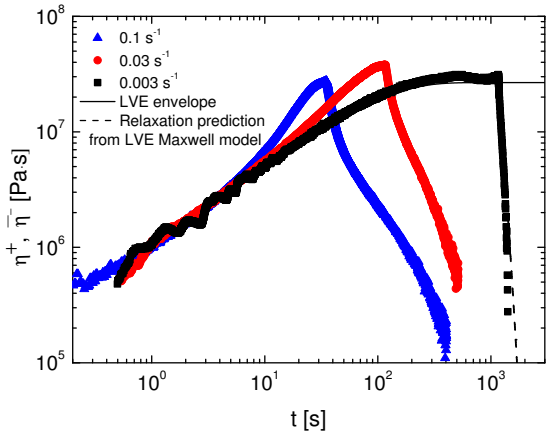

Figure 4.8: Stress relaxation measurements of the pure PS-95k after fixed Hencky strain of $\varepsilon_0 = 3.5$. The experiments were performed at $\dot{\varepsilon}$ of 0.003, 0.03 and 0.1 s^{-1} at 130 °C. In all cases the flow was stopped at $\varepsilon_0 = 3.5$ and allowed to relax until the force detected from the weight cell was almost zero.

figure 4.7 is the LVE envelope for start-up. Figure 4.8 shows the analogous results for the monodisperse melt PS-95k. At the stretch rate of $\dot{\varepsilon} = 0.003s^{-1}$ ($Wi_d^S = 0.51$), the measured data follow the LVE envelope and the relaxation prediction (dashed line) even at Hencky strain of 3.5.

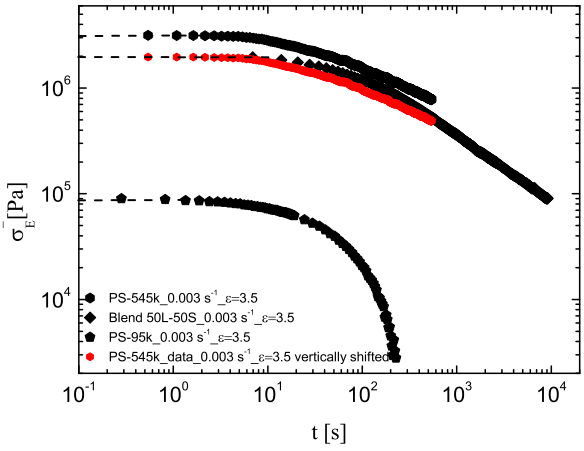

Figure 4.9: Comparison of the stress decay data of the Blend 50L-50S, the pure PS-95k and the pure PS-545k at 130 °C after cessation of elongational flow (up to $\varepsilon_0 = 3.5$) at the same strain rate $\dot{\varepsilon} = 0.003s^{-1}$. The dashed lines are guidelines meant to show the stress level right when relaxation starts.The red data are the one of the long chains PS-545k vertically shifted.

Figures 4.9, 4.10 and 4.11 compare the stress relaxation process of the Blend 50L-50S with the pure short chain PS-95k at the same three strain rates and the same imposed macroscopic Hencky strain. In Figure 4.9 concurrently with the stress decay data of the Blend 50L-50S and the PS-95k we also show the measurement of the pure long component in the blend, PS-545k. Data points for $t > 600s$ have not been reported because their reproducibility ends up at that time (Figure 4.9). The very high M_w of the sample prevented measurements at higher strain rates. Although the short components represent 50% in weight of the blend it is seen from Figure 4.9 that the stress in the Blend 50L-50S is much closer to the stress in the pure long component than the stress in the pure short component. It means that the short chains do not contribute significantly to the stress level (depicted by the dashed lines in the plot) in the bi-disperse melt. The stress reduction in the Blend 50L-50S relative to the pure long component is about a factor of 2. Also in figure 4.9 we have shifted the pure long component stress vertically to compare with the blend. It appears that the initial relaxation for the blend is somewhat slower than for the pure component. This may be related to the increase

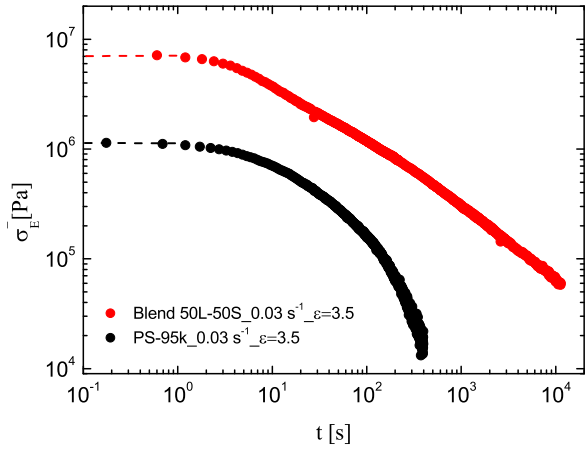

Figure 4.10: Comparison of the stress decay data of the Blend 50L-50S and the pure PS-95k at 130 °C after cessation of elongational flow (up to $\varepsilon_0 = 3.5$) at the same strain rate $\dot{\varepsilon} = 0.03s^{-1}$. The dashed lines are guidelines meant to show the stress level right when relaxation starts.

in the relaxation time due to dilution with short chains predicted by Auhl *et al.* (2009).

Figures 4.10 and 4.11 show comparisons of the stress decay data of the Blend 50L-50S and the PS-95k after cessation of steady elongational flow at the strain rate respectively of $\dot{\varepsilon} = 0.03s^{-1}$ and $\dot{\varepsilon} = 0.1s^{-1}$. Also here the low molecular weight component in the blend does not seem to have a significant contribution in the stress of the blend. It would be interesting to compare the orientation of the short chains in the blend and in the pure short chain melt on the molecular level. The purpose of this comparison would be to determine if the short polymers are independent from the long ones or there is some kind of interaction, e.g. that the presence of the long chains in the blend might activate a higher degree of stretching of the short molecules. The right tool that can cast light on this question is neutron scattering on quenched PS samples [Hayes *et al.* (1996)].

Concerning the measurements of the Blend 50L-50S at different strain rates we refer to Figure 4.12. The stress relaxation curves can be approximately divided into three regimes: a fast dynamic regime covering time from start of relaxation to about $20s$, a transition regime from $20s$ to about $700s$ and a slow dynamics regime from $700s$ to the end of the experiments which is well before the terminal time of the long chains. Initially we concentrate on the relaxation for time up to 20 s. This number corresponds

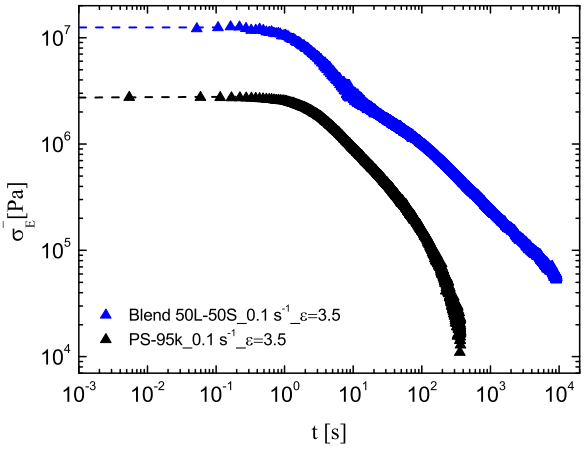

Figure 4.11: Comparison of the stress decay data of the Blend 50L-50S and the pure PS-95k at 130 °C after cessation of elongational flow (up to $\varepsilon_0 = 3.5$) at the same strain rate $\dot{\varepsilon} = 0.1s^{-1}$. The dashed lines are guidelines meant to show the stress level right when relaxation starts.

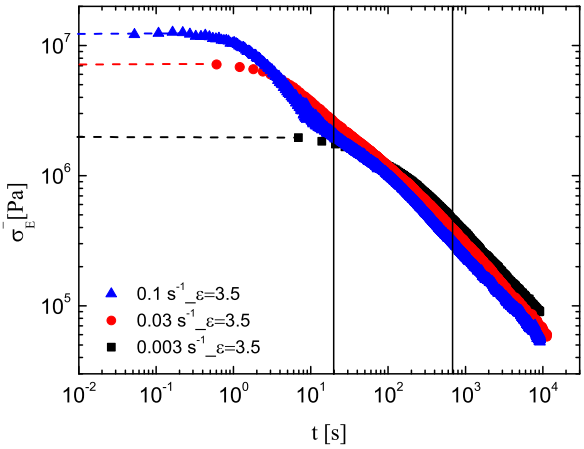

Figure 4.12: The stress decay for the Blend 50L-50S. The data are originally from Figure 4.7. The dashed lines are guidelines meant to show the stress level right when relaxation starts.

closely to the Rouse time of the short chains. Hence we suggest that the molecular relaxation is dominated by fast stretch relaxation of both the long and the short components. The large slope in this region and the knee at $20s$ supports this expectation. The transition regime from about $20s$ to $700s$ would then be retraction of the long chains in a sea of reptating short chains. The relaxation up to $20s$ is faster after extension at the highest stretch rate as observed also by Nielsen *et al.* (2008). This seems natural since more modes are presumably excited at the highest stretch rates. Keep in mind however, that for fixed ε_0, the flow time decreases with increasing extension rate. According to Eqs. 4.16–4.17 a decrease in the flow time would in itself result in faster relaxation even in the LVE limit. The long time dynamics for $t \sim 700s$, is dominated by a power law behaviour over two decades. In this regime we expect relaxation of the long chains in a sea of essentially equilibrated short chains. Moreover there is a slight vertical shift here, which can be attributed to the disentanglement of the long chains by the steady flow prior to relaxation. The trend is in the right way, higher strain rates give rise to more disentanglement, up to order 50% as predicted by Andreev *et al.* (2013). To speculate on the origin of the power law behaviour, we note that the short chains are completely relaxed, and the long chains have completely retracted, only anisotropic orientation of the long chains remains. The long chains begin therefore to undergo their usual, equilibrium relaxation processes, as characterized by the LVE data in Figure 4.2. Indeed we note from Figure 4.2 a Rouse like power law behaviour up to frequencies around $2 \cdot 10^{-3}$ corresponding in time roughly to the power law stress relaxation for $t \sim 700s$.

4.4 Conclusions

Results are given for a fixed flow time prior to relaxation and for relaxation after steady flow. In both situations we observe that the rate of stress relaxation increases as the stretch rate in the prior flow is increased.

The measurements are analyzed in terms of three separated relaxation regimes: a fast regime, a transition regime and a slow regime. In the fast regime we expect the orientation of the long chains to be essentially frozen and the stress relaxation to be due to stretch relaxation of the short chains primarily. Conversely in the slow regime we expect the long chains to have retracted and to be undergoing relaxation of orientation in a sea of essentially fully relaxed short chains that act as a solvent. The latter relaxation has a distinct power law behaviour that extends in one situation over more than two decades in time. It is noted that the power law corresponds to a similar relaxation in the low frequency part of the linear viscoelastic spectrum, although this correspondence may be fortuitous. Comparison with the pure long and short components seems to indicate that the stress in the blend is carried primarily by the long component even though it represents only 50% by weight.

CHAPTER 5

Nematic effects and strain coupling in entangled polymer melts under strong flow

We combine Filament Stretching Rheometry (FSR) with small-angle neutron scattering (SANS) to perform single chain structural studies after uniaxial elongation with high deformation ratios and stress relaxation from steady state flow conditions. We study two entangled systems: a short chain melt and a bidisperse melt composed of a 50/50 wt mixture of short and long chains. By labeling the short chains we show a pronounced nematic effect of the long chains which increases the initial short chain stretch by ~13% and delays their relaxation by a factor of ~4. We fit the 2D data with a modified Warner-Edwards model accounting for relaxing ends and confirm that the non-affine mean-field result $\nu = 0.5$ for the strain coupling is still valid for very fast flows. The SANS data provides a structural explanation for the two first regimes of the non-linear relaxation, particularly a transition regime where the long chains are relaxing in a sea of reptating short chains maintained by the nematic field of the long chains.

5.1 Introduction

Filament stretching rheometry allow elongation rates higher than the inverse Rouse time and therefore open up for new investigations in fast flows of polymer melts and

solutions, in particular reaching steady-state flow [Bach *et al.* (2003a); McKinley and Sridhar (2002)]. Despite the recognized success of the classical Doi-Edwards (DE) tube model [Doi and Edwards (1986)] and its later modified manifestations [McLeish (2002)], the non-linear viscoelastic behaviour of entangled polymer chains in fast flows still possesses a challenge and there is currently no full theoretical description of the underlying physics in such systems. Recently it was proposed by some of us that not only chain orientation but also direct nematic interactions contribute to the non-linear rheological response in strong extensional flow [Huang *et al.* (2013b)]. In Huang *et al.*(2013b) three concentrated solutions of polystyrene (PS) with different PS oligomers acting as solvent are shown to behave identical in linear flow but pronouncedly dif-ferent in non-linear flow in direct violation of current tube theory predictions (apart from the latest modifications presented in direct response to these experiments [Wag-ner (2015); Ianniruberto (2015)]). Here we push the idea of an entangled polymer system diluted by shorter chains into the regime of a bidisperse melt of long and short entangled chains and flip the viewpoint by focusing on the short chain behaviour and how these are influenced by the presence of a highly entangled and stretched surround-ing environment of longer chains. We exploit the power of FSR to perform true stress relaxation experiments after steady state flow and combine these with small-angle neu-tron scattering experiments to obtain unique structural information on the short chain conformations during relaxation with and without the influence of the stretched long chain environment.

5.2 Experimental

Samples Description

We investigate two systems: a pure melt of short polystyrene (95 kg/mol) chains and a bidisperse melt composed of a 50/50 wt mixture of short and long (545 kg/mol) polystyrene chains. Note that both chain populations are entangled with the number of entanglements per chain $Z_L \approx 41$ and $Z_S \approx 7$ for the long and short chains respectively [Hengeller *et al.* (2016)]. In both systems a fraction of the short chains are deuterated (86 kg/mol) and thus allows for direct comparison of the short chain relaxation in these two scenarios. We label these two sample series Short-in-Short (SiS) and Short-in-Long (SiL) respectively. Synthesis and chromatography of the monodisperse polystyrene melts, PS-545k and PS-95k employed in this work have already been described along with characterisations of both shear and extensional rheology [Hengeller *et al.* (2016); Huang *et al.* (2013a)]. The main characteristics of the sample constituents are summarised in Table 5.1.

Table 5.1: The weight-average molecular weight $\bar{M}_w$, the polydispersity index *PDI* and the weight fractions of the PS-545k Huang *et al.* (2013a), PS-95k Hengeller *et al.* (2016) and D-PS-86k in the samples SiL (Short in Long) and SiS (Short in Short).

Components	PS-545k	PS-95k	D-PS-86k
M_w[g/mol]	545000	95100	86300
PDI	1.12	1.07	1.02
Sample SiL (*wt%*)	50	40	10
Sample SiS (*wt%*)	0	90	10

SANS Samples Preparation

As shown in Hengeller *et al.* (2016) extensional steady state flow conditions are established at Hencky strain $\varepsilon_0 = 3$, and here we focus our attention to this value and to the highest strain rate investigated, $\dot{\varepsilon} = 0.1\ s^{-1}$. The details of the quenching and stretch-ing experiments are given in Hengeller *et al.* (2016) (and in Appendix B). However, for the SANS experiments it is vital to quench the samples fast enough to trap the rel-evant molecular configurations. To quench the PS melt cylinder as rapidly as possible we blow Nitrogen gas perpendicular to the cylinders. To get a rough estimate of the cooling rate we assume that the cylinders are of uniform temperature T. Based on correlations for heat transfer [Churchill and Bernstein (1977)] we estimate the quenching rate to be given by

$$\frac{dT}{dt} = -(0.3 + 0.48\mathrm{Re}^{1/2})\frac{4k_g}{d^2\rho_s C_p}\Delta T \tag{5.1}$$

Here ΔT is the temperature difference typically of order 100K, and the Reynolds number for the Nitrogen flow is $\mathrm{Re} = vd\rho/\mu$ where v is the gas velocity and d the diameter. The physical properties of Nitrogen are estimated to be roughly $\rho = 1.0\ \mathrm{kg/m^3}$, $\mu = 0.02\ 10^{-3}$ Pa s and $k_g = 2.7\ 10^{-2}$ W/m K. The physical properties of polystyrene are density $\rho_s = 1.05\ 10^3\ \mathrm{kg/m^3}$ and heat capacity $C_p = 1.21\ 10^3$J/kg K [van Krevelen (1990)]. As an example we take a cylinder of diameter $d = 1$mm. Then even at a relatively low flow rate $v = 0.1$ m/s we obtain a quenching rate of about -10K/s which brings the melt temperature below the glass transition much faster than the Rouse time (≈ 20 s), so we are confident that the initial molecular configuration survives. This is confirmed by scattering experiments on samples quenched at a lower temperature (125°C, but at the same Weissenberg number) which within experimental error are identical to the 130°C results.

Rheological Experiments

Figure 5.1 shows the stress relaxation data for the two samples normalized by the first value of the stress decay $\sigma(t = 0)$ plotted against the relaxation time. The red arrows highlight the times at which a quenching was performed and thus six different stages

of the relaxation process have been investigated. In the figure the Rouse and reptation time of the monodisperse linear short components are also reported. The first red arrow on the left side in Figure 5.1 shows the quench in the steady state, which correspond to zero relaxation time (in practice ~0.05 s). In Hengeller *et al.* (2016) the rheology data are separated into 3 domains approximately defined in the following time intervals: a fast regime (0-20s), a transition regime (20-700s) and a slow regime for longer times than 700s (log(700) ~ 2.85). Here we focus on the short chain structural behavior as revealed by SANS during the two first regimes.

SANS Experiments

SANS results originate from two different beam times. First experiments were performed at the SANS-1 instrument at the Swiss Spallation Neutron Source (SINQ) and the second at the Quokka beamline at ANSTO, Australia. In both cases 3 overlapping settings covered a full q-range from $5 \cdot 10^{-3}$ Å^{-1} to 0.25 Å^{-1}. We use the low q data for fits to extract principal axis radii of gyration but focus on the central setting for 2D fitting since the relevant length scales are best represented here. We followed standard data reduction procedures, i.e. correcting for detector efficiency using incoherent water scattering, and subtracting background scattering which is dominated by the incoherent scattering from polystyrene and measured in a polystyrene sample with no deuterated chains.

5.3 Results and Analysis

Our initial analysis follows Hassager *et al.* (2012) and extracts values for the radius of gyration parallel and perpendicular to the stretch direction respectively by fitting a modified Debye model directly to the full 2D data set. The scattering function is

$$S(\mathbf{q}) = \frac{2}{x^4}(\exp(-x^2) + x^2 - 1) \tag{5.2}$$

with $x^2 = (q_{\|}R_{g\|})^2 + (q_{\perp}R_{g\perp})^2$ and $\mathbf{q} = (q_{\perp}, q_{\|})$. The evolution of the principal axes parameters are shown in Figure 5.1(b) and it is clear that the short chain relaxation is affected by the presence of the long chains immediately indicating a nematic effect of the long chains. It has previously been demonstrated with infrared dichroism and NMR in similar systems of long/short blends that the local orientational order of the two chains is identical [Hayes *et al.* (1996); Chapellier *et al.* (1993)] and thus we can ascribe any difference in the parallel principal axis parameters as originating directly from a difference of the short chain stretching. In Figure 5.1(c) we plot the excess stretch evaluated as the ratio $R_{g\|}^{\mathrm{SiL}}/R_{g\|}^{\mathrm{SiS}}$ and at $t = 0$ we find that the short chains are

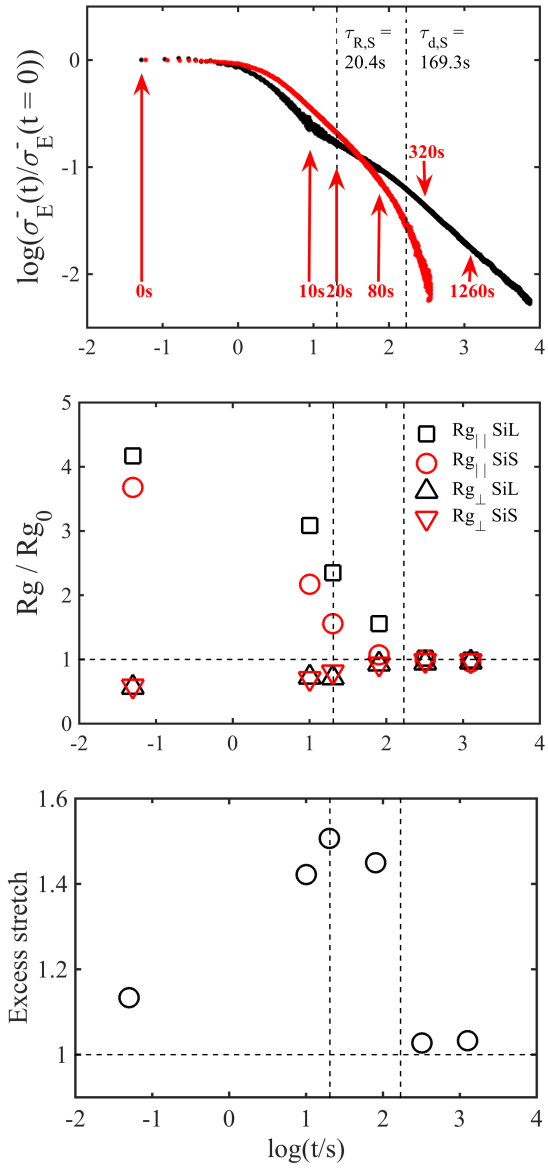

Figure 5.1: (a) Tensile stress σ_E^- of the SiL (black) and SiS (red) samples at 130°C after cessation of fast uniaxial elongational flow at Hencky strain $\varepsilon = 3$ and strain rate $\dot{\varepsilon} = 0.1s^{-1}$. Dashed vertical lines indicate the short chain Rouse and reptation time. Red arrows indicate times where a quenched samples was produced for scattering studies. (b) Evolution of the parallel and perpendicular radii of gyration during the relaxation as determined by the modified Debye model. (c) Excess stretch ratio $R_{g||}^{SiL}/R_{g||}^{SiS}$.

stretched ca. 13% more in the long chain blend. As the relaxation progresses we find an extremum in the excess stretch since the SiS chains relax faster than the SiL short chains. From 5.1(b) this relaxation delay can be visually estimated to ca. a factor 4 from where the two datasets reach the relaxed state ($R_{g\|}/R_{g0} = 1$). Even though the trend is clear from these fits, the numbers can not be completely accurate since the 2D patterns from the SiL sample show lozenge like scattering patterns which are incompatible with the simple 2D Debye model which produce only elliptical patterns. The lozenges originate from partially relaxed chains and thus the R_g values for the SiL sample for $t > 0$ are lower bounds on the true numbers as any isotropic material will artificially add to the low q signal effectively lowering the R_g. This also means that for $t > 0$ the excess stretch is a lower bound.

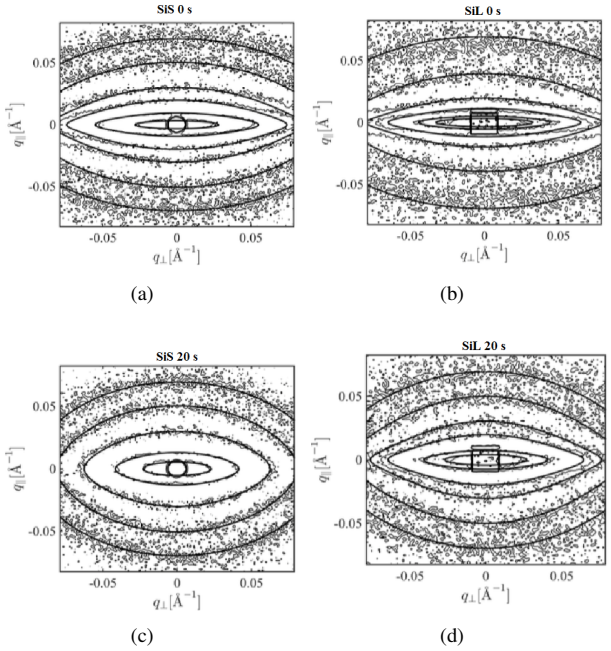

Figure 5.2: Examples of two-dimensional scattering data and accompanying 2D fits for both sample series: (a) SiS 0 s. (b) SiL 0 s. (c) SiS 20 s. (d) SiL 20s.

Our anisotropic SANS data can be modelled using the Warner-Edwards (WE) model [Warner and Edwards (1978)] for the SiS sample and the modified WE-model with dangling ends (DE-model) [Read and McLeish (1997a)] which we find to be directly applicable for the SiL system without the complications arising from chain scission etc. present in a cross-linked system [Read and McLeish (1997b); Westermann *et al.* (1998); Read and McLeish (1998)]. In the DE-model each chain is described as hav-

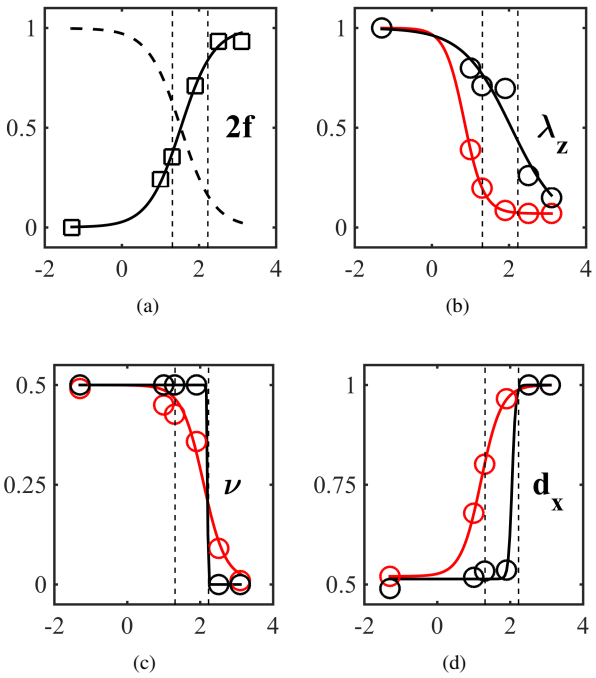

Figure 5.3: Evolution of normalized fit parameters from the DE- and WE-models as a function of logarithmic time: The total dangling end fraction ($2f$) and the amount of stretched material $1-2f$ (dashed line), the strain ratio relative to the initial value ($\lambda_z/\lambda_z(t=0)$), the strain coupling parameter (ν) and the derived transverse tube diameter (d_x/d_0). Dashed lines indicate the Rouse time ($\tau_{R,S}$) and reptation time ($\tau_{d,S}$) of the short chains, see Figure 5.1. Black data is SiL, red data is SiS. Sigmoidal fits are meant as a guide for the eye.

Table 5.2: Parameters from the WE/DE-model fits. The transverse tube diameter is derived via $d_x = d_0\lambda_x^\nu$ where $\lambda_x = 1/\sqrt{\lambda_z}$ and $d_0 = 7.51$ nm.

	SiS			SiL			
Time [s]	λ_z	ν	d_x [nm]	f	λ_z	ν	d_x [nm]
0	14.33	0.49	3.91	0	17.37	0.5	3.68
10	5.59	0.45	5.09	0.12	13.89	0.5	3.89
20	2.82	0.43	6.02	0.18	12.35	0.5	4.01
80	1.22	0.36	7.25	0.36	12.1	0.5	4.03
320	1	0.09	7.51	0.47	4.51	0	7.51
1260	1	0.01	7.51	0.47	2.59	0	7.51

ing two dangling ends each a fraction f of the total chain. The total scattering function is a combination of terms from the isotropic dangling ends described by Gaussian chain statistics and the central stretched portion described by the WE model. Thus, the DE model reduces to the WE model for $f = 0$. In both models the tube diameter is given by $d_\mu = d_0 \lambda_\mu^\nu$ with λ_μ being the microscopic (or local) strain ratio in direction μ ($\mu = x, y, z$) where z is the stretch direction, d_0 the tube diameter of the relaxed melt and the ν parameter allowing for anisotropic strain coupling of the tube potential. Assuming incompressibility, the perpendicular strain ratios are related to λ_z as $\lambda_x = \lambda_y = 1/\sqrt{\lambda_z}$. The value of the strain coupling has been a topic of discussion for some time [Straube (1995); Pyckhout-Hintzen *et al.* (2013); Read and McLeish (1997a)] and for moderate strain ratios has been clearly demonstrated experimentally to be non-affine with $\nu = 0.5$ [Pyckhout-Hintzen *et al.* (2013)] so that the tube diameter scales as $d_\mu = d_0 \sqrt{\lambda_\mu}$ confirming various theoretical predictions Heinrich *et al.* (1988); Rubinstein and Panyukov (1997). However, it is unclear if this scaling also applies for the much higher strain ratio described here and further, it is not clear how ν and (the effective microscopic) λ_z behaves as the system relaxes. It is important to recognise that the microscopic and macroscopic strain ratios are not necessary the same [Heinrich and Straube *et al.* (1987)] and a number of models have attempted to relate the two theoretically [Ott *et al.* (2014)]. Nevertheless, if it was possible to quench the samples infinitely fast, the macroscopic strain ratio experienced in the filament plane of observation at $t = 0$ for the employed Hencky strain would be $\lambda_z = \exp(3) \approx 20$. Notice that this is considerably higher than any previously reported elongation ratio in SANS based structural studies of fully labeled chains - to our knowledge a factor of 4-5 higher. In our analysis we fix $R_g = 7.82$ nm, the value obtained from an isotropic Debye fit to the fully relaxed sample and $d_0 = 7.51$ nm, calculated from $R_g^2 = d_0^2 Z_S/6$. We present fits where we allow both ν and λ_z to vary, but impose constraints by the following strategy: We start the fitting from $t = 0$ s with the initial parameter set constrained by the 2D Debye fits, i.e. setting the effective microscopic strain ratio λ_z^ν equal to $R_{g\|}/R_{g0}$. Each consecutive fit uses the fit of the previous time point as lower/upper bounds with the following assumptions: the fraction of dangling ends is monotonically increasing in time and approaches $f = 0.5$ for long times, the strain coupling will be isotropic in the long time limit ($\nu = 0$) and finally that the effective strain felt by the short chains will be monotonically decreasing as the system relaxes.

We note that we find it impossible to fit the $t = 0$ data assuming affine or isotropic microscopic deformations ($\nu = 1$ or $\nu = 0$) with reasonable physical parameters. The fits are done using home-written Matlab code minimising the residuals in a least-square sense. The fitting gives the presented evolution of the main fit parameters shown in Figure 5.3 with suitable normalizations. The actual fit parameters are listed in Table 5.2 and examples of the 2D fits are shown in Figure 5.2.

In the DE model, the most robust fit parameter is the dangling end fraction which effectively weighs the scattering contributions of isotropic and stretched material. In Fig. 5.3(a) the evolution of f shows again that the relaxation of the short chains are

delayed in the presence of the long chains corroborating the result from the principal axis parameters from Fig. 5.1(b-c): the fit predicts that at $\tau_{R,S}$ only around 36% of the short chains have relaxed and that a population of the chains remain stretched until after $\tau_{d,S}$ and very close to the 700s found to indicate the transition to a pure long chain relaxation in Hengeller *et al.* (2016). The collective output from the model fits tells the same story, namely that the effective strain is felt over a prolonged time scale in the SiL sample, but the individual fit parameters provide a much more detailed picture of how the relaxation progresses. First, we note that for both samples the fits for $t = 0$ predict the non-affine strain coupling $\nu = 0.5$ confirming the results from Pyckhout-Hintzen *et al.* (2013) even for the much stronger flow conditions employed here. For $t > 0$ the fits to the SiS data predicts that the strain coupling relaxes with an onset around the Rouse time while the coupling is maintained for much longer times in the SiL sample. The effective strain felt by the short chains also show markedly different behavior. In the SiS sample the strain relaxation is almost done after a Rouse time, while in the SiL sample the strain persist to times again very close to the 700s mentioned above. Fig. 5.1 shows that the initial relaxation is faster in the blend than in the pure melt and in Hengeller *et al.* (2016) it is suggested that the initial fast relaxation is from primarily longitudinal stretch relaxation of both short and long chains. For the short chains we can now attribute this to the increased stretch which effectively will excite more higher relaxation modes at the high strain rate and it also fits well with the derived transverse tube diameter d_x which in the SiL sample remains at a value of roughly $d_0/2$ indicating that little transverse relaxation takes place initially. Thus, the overall structural picture that emerges is that the rheological transition regime is caused by a cooperative nematic effect where the short chain stretch is maintained by the long chains and relaxes primarily longitudinal, i.e. by reptation as already suggested in Hengeller *et al.* (2016). The long chains relax in this sea of reptating short chains until around $t = 700$s after which they relax in a solvent of relaxed short chains.

5.4 Conclusions

In conclusion, we confirm the ruling out of both non-deformed and affinely deformed tubes in entangled melts akin to crosslinked networks [Pyckhout-Hintzen *et al.* (2013)]. We confirm the non-affine mean-field result $\nu = 0.5$ for the strain coupling, even sub-jecting the sample to a significantly increased stretch and strain rate than previously documented. We propose a non-affine strain coupling relaxation with onset around the Rouse time of the short chains. In the blend we demonstrate a nematic field effect on the short chains from the aligned and stretched long chains showing an initial increased stretch of the short chains of ca. 13% and a clear nematic effect influencing the short chain relaxation causing a delay of roughly a factor of 4 under the present conditions. The cooperative nematic effect explains the rheological signature from a structural per-spective, particularly in the intermediate transition regime appearing

after an initial fast stretch dominated relaxation. Our structural data will provide input for ongoing theoretical efforts implementing direct nematic interactions at the fundamental level.

CHAPTER 6

Summarizing Chapter

6.1 Work Overview

In this Ph.D. project, anionically synthesized linear polystyrenes have been used to design well-defined model polymer systems, i. e. diluted and concentrated solutions, melts and bi-disperse blends, to experimentally investigate the observed differences in their rheological behaviour, with a particular focus on the extensional properties. The main target of the work has been to carry on the research of the missing physics that could explain the many different trends observed in the steady-state elongational viscosity as a function of the strain rate (i. e. in the non-linear regime).

Linear viscoelastic properties of the samples have been characterized with small amplitude oscillatory experiments (ARES-G2 from TA-Instruments) while non-linear features have been investigated in strong uniaxial extensional deformations (Filament Stretching Rheometer (FSR) at DTU and VADER1000 from RheoFilament). We have utilized the unique features of the extensional rheometer to reach steady flow conditions after constant strain rate flow and to perform stress relaxation from different stages of an extensional experiment. Moreover we have shown how the techniques may be used in combination with small-angle neutron scattering (SANS) experiments to perform single chain structural studies after uniaxial elongation both after steady extensional flow and at several times during stress relaxation. The work that has been carried out in the Ph.D. project can be summarized as follows:

***Chapter 2**: Further Investigation of the Flexibility of a Polymer Chain - Probing the Influence of Dilution in Polymer Solutions*

To further test the hypothesis introduced in the works of Huang *et al.* (2013a) and Huang *et al.* (2013b), we have considered the influence of solvent volume fractions on the non-linear rheological responses of polymer solutions in extensional flow. We have prepared five polystyrene (PS) solutions with different concentrations of the same PS polymer (with the molecular weight M_w = 545k), diluted with the same oligomeric styrene (with M_w = 4k). We have tested the influence of nematic interactions as a function of solvent volume fraction. The steady-state extensional viscosity data of the solutions present different behaviours, from a strain rate extensional thinning trend to a strain rate extensional thickening trend by increasing the degree of dilution. The different concentration of the polymer in the solutions corresponds to a different chain flexibility. It has been shown that the non-linear rheological responses of polymer solutions are close to the predictions of the current tube model at a critical solvent volume fraction. That finally shed light on the differences observed between the data of Huang *et al.* (2013a) and Sridhar *et al.* (2014), Bhattacharjee *et al.* (2002).

***Chapter 3**: Bi-disperse Polymer Systems - Testing the Influence of the Long Chain Component on the Steady-state Elongational Stress Level*

In the work of Huang *et al.* (2013b), the same high M_w polymer PS-545k was diluted in three different low M_w molecules to test the solvent effect in extensional flow. Here, following the same method as they used but with a different purpose, a series of polymeric systems, where the concentration and the M_w of the long chains have been fixed and the diluting matrix changes, have been experimentally analyzed. Here we have investigated the influence of the long molecular weight components on the non-linear steady-state stress level of polymer solutions and bi-disperse blends in extensional flow. We have prepared four polystyrene (PS) mixtures, two solutions and two blends, with same concentrations of the same PS polymer (with the molecular weight M_w= 545k), diluted in different short chains matrices (oligomeric styrene OS-10k, and three polystyrenes with M_w of PS-25k, PS-60k and PS-95k). Comparisons of the extensional data of the systems at the same distance from the glass transition temperature of each sample, have shown that the steady-state level of the systems analyzed is governed by the long molecular weight components although they represent just the 10% in volume of the overall mixture. Moreover, the steady-state viscosity of all of the systems seems to have a constant value as the strain rate is increased.

***Chapter 4**: Bi-disperse Melts - Investigating the influence of the Long Chains on the Short Chains in Fast Elongational Flows*

One step towards understanding polydisperse polymers is the characterization of bi-disperse blends. Even though linear viscoelastic properties of bi-disperse polystyrene blends have been investigated thoroughly both theoretically and experimentally in re-

cent years [Nielsen *et al.* (2006)], both non-linear shear and extensional flow properties are lacking. The purpose of the present study has been to investigate cooperative interactions between long-short polymers, in strong elongational flow using a bi-disperse polystyrene blend of 95k and 545k M_w with 50% weight ratio. We have carried out both uniaxial extension and stress relaxation experiments (following steady extensional flow and after a fixed flow time) to determine if orientation and extension of long PS chains may induce orientation and extension in shorter chains. Stress relaxation data, which are more relevant for the understanding of relaxation mechanisms, have shown three separated regimes: in the first regime, at short times, the conformation of the long chains is frozen and the stress decrease is mainly due to stretch relaxation of the short chains; in the transition regime also the long chains begin retracting; finally in the slow regime, the long chains have relaxed their stretching and keep losing orientation in a matrix of totally relaxed short chains. The data of the blend have been compared with the data of the pure components and was observed that the stress in the blend is carried primarily by the high M_w component. The extensional viscosity of systems investigated, provides only indirect evidence about the extent to which the molecules have been unraveled and stretched by the flow field. More directed information has been obtained by neutron scattering experiments on quenched liquid bridges of polystyrene presented in the follow up work.

***Chapter 5**: Small Angle Neutron Scattering - Chain Structure Measurements*

Small-angle neutron scattering technique (SANS) has been employed to perform single chain structural studies after both uniaxial elongation and stress relaxation following steady-extensional flow. The two entangled systems investigated are a pure melt of short chains and a bi-disperse melt composed of a 50/50 % wt mixture of short and long chains. By labelling the short chains (10 % wt in each sample) we can observe the molecular configuration reached in the two cases, in the blend and in the pure melt, under the same flow conditions. It is found that, at the same experimental flow conditions, the long chains induce a higher degree of stretching in the short chains and delays their relaxation process compared with the case in which they are pure. 2D-data have been fitted with a modified Warner-Edwards model accounting for relaxing ends. Finally, we have proposed a non-affine strain coupling relaxation with onset around the Rouse and reptation time without and with the presence of a nematic field respectively.

6.2 Future Work

A possibility for a future project would be to provide new insight by producing presently unavailable experimental results on the extensional rheology of polymers of well-defined branched molecular architectures. Indeed well-characterized branched polymers are considered as model polymers for the validation of the developing theoretical models on branched structures. The specific target will be to measure the molecular architecture depicted in Figure 6.1(a) (POM-POM architecture) and compare it with a linear chain [see Figure 6.1(d)] in two types of extensional flow experiments: extensional flow at constant elongation rate and extensional flow at constant elongation rate followed by stress relaxation. The target molecules should be synthesized in 2 or 3 versions [see figures 6.1(a), 6.1(b) and 6.1(c)]. Here green symbolizes deuterium labelled strands, and black normal strands (with hydrogen rather than deuterium). Unlabeled is either completely black or completely green and labelled is as shown in the Figure 6.1(b) and Figure 6.1(c). By mixing small amounts of the molecules in the Figures with unlabelled (either completely green or completely black) counterparts it is possible to study the conformation of the central part or the extremity of the molecules with neutron scattering. The simultaneous tests of the ability of a models to generate mechanical and structural predictions will constitute a rigorous test of the validity of the model.

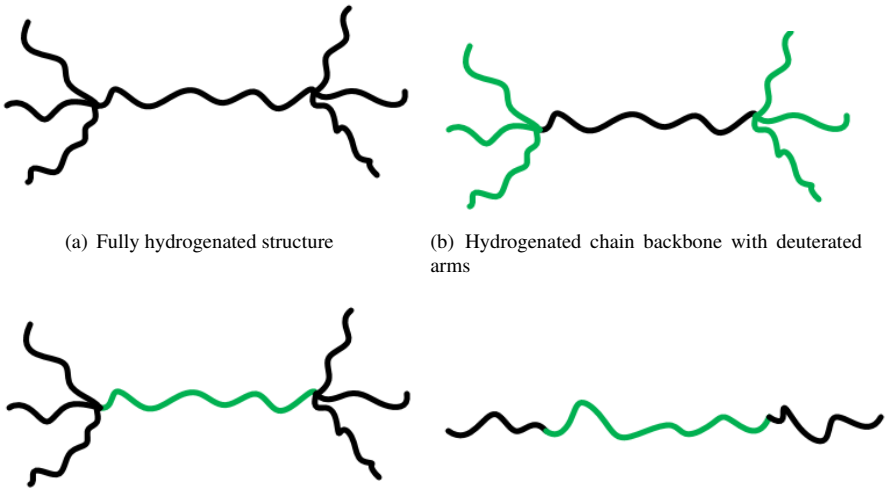

(a) Fully hydrogenated structure

(b) Hydrogenated chain backbone with deuterated arms

(c) Deuterated chain backbone with hydrogenated arms

(d) Linear chain with deuterated central backbone and hydrogenated chain-ends

Figure 6.1: Pom-Pom and linear architectures with different labelling of the chain segments.

APPENDIX A

Supporting Information

A.1 Material: Polystyrene

The synthetic polymer used in this work is polystyrene, which consist of long flexible chains of high molecular weight randomly coiled without any order. This results in a physical solid state called amorphous. In this state the chains assume their unperturbed dimensions as they do in solution under θ conditions. In the melt, thermal energy is sufficiently high for long segments of each polymer chain to move in a random micro-Brownian motions. Cooling down below the glass transition temperature T_g long-range interactions along individual chains cannot occur while short-range interactions between contiguous groups along the backbone chain or substituent groups are still allowed. Those are called secondary-relaxation processes. The more flexible the chain the lower the T_g (that is why the same polymer molecule is more flexible in solution than in a melt, and if it is more flexible is also more stretchable). The flexibility of a polymer chain also influences the so-called critical molecular weight M_c upon which we have the formation of entanglements. Relatively flexible polymers, as PS, have high M_c, while more rigid chain polymer have lower M_c so they became entangled at lower M_w. This feature makes the polystyrene a well-suitable polymer for investigating properties for moderately entangled polymers, but not for highly entangled polymers with more than 100 entanglements, since the M_w would be too high and the stresses induced into the material would make experiments difficult to perform.

Usually in experimental study polystyrene is preferred to others polymers since it is possible to synthesize model polymer systems throughout anionic polymerization under high vacuum. This technique is a very favorable method because the obtained polymers have narrow molar mass distribution, and it is relatively easy to reach the desired molecular weight. An additional reason for using polystyrene is its high glass transition temperature that is much above room temperature (for monodisperse linear polymers with $M_w > 50k$ the T_g is around 107 °C). Figure A.1 shows the trend of the T_g, experimentally measured with size exclusion chromatography, as a function of the molecular weight M_w of the polystyrenes employed in this PhD work.

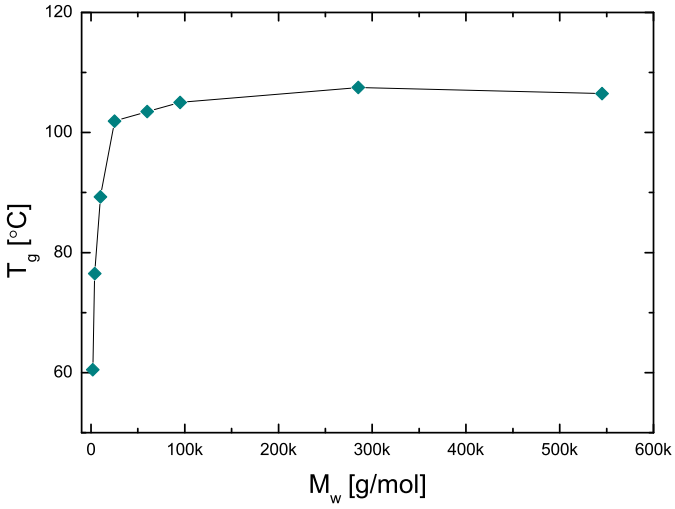

Figure A.1: The glass transition temperature T_g, experimentally measured with size exclusion chromatography, as a function of the molecular weight M_w of the polystyrenes employed in this PhD work.

Most of the extensional experiments with the FSR have been carried out at $T = 130\,°C$, which is just 25 °C above the T_g of the material. By measuring so close to the T_g the extensional properties can be determined over a wide range of Hencky strain rates varying up to a factor of 10^5 using the empirical rule of Time-Temperature Superposition. According to this criterion a change in the temperature corresponds to a variation in the time-scale of observation. This imply therefore that the rheological response and behaviour of a polymer in a specific frequency range and at a fixed temperature is equivalent to the rheological response and behaviour in an another frequency range at

a different temperature. In the contest non-isothermal linear viscoelasticity is the horizontal time-shift factor a_T that describes the way the molecular relaxation varies with the temperature. It can be determined from experimental data measured at a series of temperatures by shifting the data horizontally and vertically. However it is convenient to have a functional equation for a_T (and for b_T) for both data-fitting and for predictions. For this purpose it has been used the semi empirical WLF equation (Williams, Landel and Ferry). The time-temperature shift factors a_T of polystyrene are strongly dependent on the temperature, especially in the region close to the T_g, which implies that a very accurate temperature control during the experiments is critical to obtain correct measurements. Generally speaking polymer melts are more sensitive to temperature changes than polymer solutions, nonetheless the solutions employed in our studies have been obtained blending high molecular weight PS melts with olygomeric styrenes, hence they also show a significant temperature dependence. The main reason for choosing a styrene oligomer as solvent is because polystyrene and styrene oligomer have the same solubility parameters, and the interaction parameter χ for the system is thus minimized and phase separation should not occur.

A.2 Methods

A.2.1 Procedure for Making Polymer Blends through Precipitation

Dissolving the Components

We start weighting the two polystyrenes (PS) of different molecular weight according to the desired weight fraction. Then the two components are placed in a beaker and tetrahydrofuran (THF) is added. The overall concentration of polystyrene in THF should be approximately equal to the overlap concentration. For PS with molecular weight between 200k and 550k, a concentration of circa $10 \sim 15$ *mg/ml* has been used. Once that the solution, with the right amount of THF is ready, a magnetic stirring bar is put in the mixture and a piece of aluminium foil is used to cover the beaker to avoid contamination and solvent evaporation. The beaker is then placed on a stirring plate, under a fume hood, and the solution is shuffled overnight.

Precipitation

The day after all the components are well-dissolved and blended so it is possible to precipitate the product. We use methanol as a non-solvent for the polystyrene. A volume of methanol, about 10 times the volume of THF used to dissolve the components, is poured into a big beaker and while stirring it the THF solution is poured into the tank

drop by drop. For the purpose a glass dropper or a glass pipette can be used. After that all the THF solution has been poured into methanol, the stirring is stopped and the big beaker is covered with a piece of aluminium foil. We wait until the product precipitates and sets down at the bottom of the beaker.

Filtration

Once the precipitate has deposited on the bottom of the container and we can carefully remove the upper clean liquid (which is a mixture of THF and methanol) pouring it into another beaker. A funnel covered with a filter paper is placed on a conical flask. Normally a filter paper with the particle retention size of $40\mu m$ can be used. This size allows for a fast filtration rate (The lower concentration of polystyrene in THF in the first step of the procedure would give a smaller particle size after the precipitation step. In this case, smaller particle retention size of the filter paper should be employed in the filtration procedure). The remaining liquid, which still contains the precipitate, is poured into the funnel with the filter paper. The mixture of solvents (THF and methanol) will pass across the filter paper and fill up the conical flask while the precipitate will be trap on the filter paper.

Drying

The precipitate is collected from the filter paper and is placed in a petri dish covered with a holey aluminium foil. The petri dish is first placed under the fume hood for several hours, so that the solvent in excess can evaporate, and later is put into a vacuum oven at 70 °C for $2 \sim 3$ days. If the estimated glass transition temperature T_g of the polystyrene blend is lower than 70 °C (e.g. PS blended with a styrene oligomer), the drying temperature is setted to be lower than the estimated T_g, and the product is dried for a longer time (up to one week).

A.2.2 Filament Quenching

During a uniaxial extension experiment at constant strain rate, where the polymer sample is stretched to some desired Hencky strain, or during a stress relaxation experiment, where the polymer chains will have different configuration at some specific time, it has been possible to rapidly quench filament samples (containing deuterium) with the newly developed filament stretching rheometer, VADER-1000.

The conduction oven of this device is mounted on a slide system to allow for fast removal from the sample surroundings and is equipped with a safety switch, which automatically shuts off the nitrogen flow when the oven is in the up position. Both features ensure for a quickly drop of the filament temperature. In addition, as soon as the oven was lifted up, a flow of nitrogen gas at $T \sim 20$ °C was injected perpendicular

to the middle part of the filament. Due to the atactic nature of the polystyrene, the material does not crystallize but goes from the experimental T of $130°C$ to below its glass transition temperature T_g, allowing for freezing of the flow structure for post analysis with small angle neutron scattering (SANS) experiments. In the following sections we estimate the quenching rate to give an idea on how fast is the cooling process:

Cooling of Cylinder in Cross-flow

We consider the cooling of a cylinder under cross-flow. As an example we take a polystyrene cylinder of diameter $2R = 1mm$. The physical properties of polystyrene given by Bach *et al.* (2003a) are density $\rho_s = 1.05 \cdot 10^3 Kg\, m^3$, heat capacity $C_p = 1.21 \cdot 10^3 J/KgK$, and thermal conductivity $k_s = 0.14 J/smK$. The cylinder has an initial temperature of $T = 403K = 130\,°\mathrm{C}$. The cross flow is Nitrogen gas of temperature $T = 303K = 30\,°\mathrm{C}$ so that $\Delta T = 100K$. The flow velocity is expected to be in the range $v_0 \in [0.1; 1]\, m/s$ corresponding to Reynolds numbers $\mathrm{Re} \in [5; 50]$. The object is to find the rate of cooling of the cylinder.

Analysis based on Correlations for Nusselt Number

The physical properties of Nitrogen are estimated to be roughly $\rho = 1.0 Kg/m^3$, $\mu = 0.02 \cdot 10^{-3} Pa \cdot s$ and $k = 2.7 \cdot 10^{-2} W/mK$. In addition we use the Prandtl number $\mathrm{Pr} = 0.7$, which is a good approximation for most gasses. We use as reference a plot reported by Churchill and Bernstein (1977), which shows a correlation for Nusselt number of a large number of data sets. The Nusselt number is defined as $Nu = 2Rh/k$ where h is the heat transfer coefficient. Specifically for $\mathrm{Pr} = 0.7$ the data are we approximated by the equation:

$$Nu = 0.3 + 0.48\mathrm{Re}^{1/2} \tag{A.1}$$

For the given flow velocities we arrive at the estimate for the Biot numbers reported in Table A.1.

Table A.1: Summary of Biot number results for cross flow.

v_0	Re	Nu	h	Bi
$[m/s]$	–	–	$\left[W/m^2K\right]$	–
0.1	5	1.4	37	0.13
1.0	50	3.7	100	0.36

The boundary condition on the surface of the cylinder is formulated as:

$$-k_s \frac{dT_s}{dr} = h\left(T_s - T_g\right) \tag{A.2}$$

where T_s is the solid temperature (polystyrene) and T_g is the gas temperature (Nitrogen) at the surface. We introduce the non-dimensional radial coordinate $\tilde{r} = r/R$ to rewrite the condition in the form:

$$\frac{d\left(T_s - T_g\right)}{d\tilde{r}} = -\frac{hR}{k_s}\left(T_s - T_g\right) = Bi\left(T_s - T_g\right) \tag{A.3}$$

where Bi is the Biot number. As shown in Table A.1 the Biot number in the relevant range of velocities are smaller than unity indicating that the main resistance to heat transport is outside the cylinder. To get a rough estimate of the cooling rate we therefore take the cylinder of uniform temperature T_s corresponding to $Bi = 0$:

$$\pi R^2 L \rho_s C_p \frac{dT_s}{dt} = -2\pi RLh\Delta T \tag{A.4}$$

if we combine equation A.4 with equation A.1 we get:

$$\frac{dT}{dt} = -\left(0.3 + 0.48\mathrm{Re}^{1/2}\right)\frac{k_g}{R^2 \rho_s C_p}\Delta T \tag{A.5}$$

The results for the quenching rates are shown in Table A.2. Note from the equation, that faster quenching may be obtained in two ways. Either by increasing the velocity or by decreasing the radius of the cylinder.

Table A.2: Summary of results including quenching rates for $Bi = 0$ model.

v_0	Re	Nu	h	Bi	dT/dt
$[m/s]$	–	–	$\left[W/m^2K\right]$	–	$[K/s]$
0.1	5	1.4	37	0.13	-12
1.0	50	3.7	100	0.36	-37

A.3 Experimental Errors

A.3.1 Residual Solvent/Moisture and Air Bubbles

The presence of bubbles in the samples before performing an experiment [see the two cylindrical specimens on the left hand side of Figure A.2(a)] or after stretching [see the two quenched filaments in Figure A.2(a) and Figure A.2(b)] is usually caused from the presence of residual solvents and/or water absorbed from the air humidity.

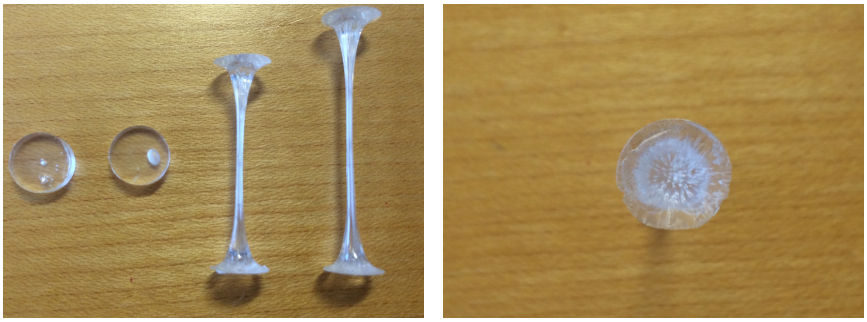

(a) (b)

Figure A.2: (a) PS samples with bubbles trapped inside: On the left hand side two PS pellets before stretching; on the right hand side two PS filaments after stretching. (b) Top view of a stretched PS filament with bubbles.

Undried samples, before moulding, can sometimes be recognised from their appearance. Their morphology can be fiber-like or foam-like (as shown in Figure A.3). In these cases a second precipitation is needed (following the procedure described in Section A.2.1) to obtain a product with powder-like morphology and higher surface area, which is more easy to dry.

Bubbles made of solvents, water or air can dramatically affect rheological as well as neutron scattering measurements. The samples will present a lower T_g (which is very critical factor in PS samples as discussed in Section A.1) and a lower viscosity compared to well dried samples (see Figure A.4). In rheological experiments, these two factors will cause an horizontal as well as a vertical shift in the LVE data and a vertical shift in the extensional data (which will be lower than the case of a dried sample). Moreover, bubbles in the mid-filament plane cause an error in the calculation of the cross-section area (which is actually smaller than expected) resulting in a wrong estimation of the stress.

Figure A.3: Examples of undried samples. On the left hand side the PS has foam-like morphology while on the right hand side has fiber-like morphology.

Figure A.4: Well-dried samples before and after stretching.

In small angle neutron scattering experiments the presence of bubbles in the sample may alter the 2D patterns, since other materials (such as solvent or air) will scatter in a different way the neutron beam than the material of interest.

A.3.2 Temperature Control

Accurate and reliable rheology measurements depend upon precise temperature control. As mentioned in Section A.1 PS is very sensitive to temperature changes and even 1 °C of difference can result in a 10% deviation of the elongational steady-state viscosity level [Huang (2013)]. The most of the extensional experiments reported in this thesis have been carried out on the VADER 1000. This device is equipped with a cylindrical conduction oven (with a heated bottom plate) insulated with aerospace

grade ceramic to ensure temperature stability and uniformity along the entire chamber length. The oven can reach temperatures between 20 °C and 250 °C with 0.1 °C accuracy which ensures the accuracy of our measurements.

A.3.3 Material Degradation

UV radiation

Polystyrene is susceptible to degradation by the action of sunlight. The main effect is due to UV radiations in the wavelength band of $300 - 400nm$ (within the visible light spectrum). The action of the UV radiation is accompanied by the oxidation so that the overall degradation reaction is a photo-oxidation (caused from the combined exposure to oxygen and light). The extent of degradation varies from location to location owing to the differences in the intensity of the radiation. This is of considerable importance in rheological characterization because the degradation is reflected in a yellowing effect and generally in a loss of mechanical properties such as a lower elongation at break and a reduced impact strength. To avoid exposition of the material to the sunlight, samples have always been preserved in containers and bottles made of dark glass and stored in drawers and cupboards.

Thermal and Mechano-Degradation

Long exposure of PS samples at temperatures higher than their T_g, for example during extensional experiments (where the pre-stretching phase is usually performed at 160 °C for 2-3 hours) or also at lower temperatures than the T_g but for longer time (for example when the samples are kept in the oven for several weeks) can result in material degradation. Also in other situations such as moulding process (not under vacuum) and multiple use of the same material for experiments cause material degeneration. On top of that the mechanical stress induced into the material during stretching or high shear deformation can further contribute to degradation and it is particularly severe for high-molecular weight polymers that exist in a highly entangled state. Even a fast stirring rate in the first step of the precipitation procedure described in Section A.2.1 can induce bonds breakage. Size exclusion chromatography analysis as been used as a mean to check that no degradation occurred (in the drying process, during sample preparation and after experiments). Each sample was tested and compared with the fresh one.

APPENDIX B

Neutron Scattering Sample Preparation

B.1 Materials and Samples Preparation

Synthesis and chromatography of the monodisperse polystyrene melts, PS-545k and PS-95k employed in this work have already been described in Huang *et al.* (2013a) and Hengeller *et al.* (2016). The two samples have also been characterized in both shear and extensional rheology by the authors. The deuterated polystyrene D-PS-86k was purchased from Polymer Standard Service (PSS). The final sample, called Short in Long (SiL), used in the scattering experiments contains 50% weight of the long chains and 50% of the short chains. For clarity of description, we nominate the PS-545k as long chains, while the PS-95k and the D-PS-86k represent the short chains in the system. Table B.1 summarizes the weight-average molecular weight $\bar{M}_w$, the polydispersity index PDI and the weight fractions of the three components in the SiL sample. No significant difference of glass transition temperature T_g of the SiL with respect to the monodisperse polystyrenes has been detected.

The deuterated polystyrene blend (SiL) was prepared by dissolving the three components, weighted in the desired amount, in tetrahydrofuran (THF). The solution was stirred at room temperature overnight to ensure that all the components were mixed homogeneously. Precipitation of the mixture was then performed by pouring it drop by drop into methanol, followed by filtration to recover the mixture. Finally the residual

solvent in the powder was first evaporated at room temperature in the fume hood and then in a vacuum oven at 70 °C for 2 weeks.

Table B.1: The weight-average molecular weight $\bar{M}_w$, the polydispersity index *PDI* and the weight fractions of the PS-545k Huang *et al.* (2013a), PS-95k Hengeller *et al.* (2016) and D-PS-86k in the SiL. Values reported for the deuterated component are the ones provided by the supplier.

Components	Long Chains	Short Chains	Deuterated Short Chains
wt%	50	40	10
Sample name	PS-545k	PS-95k	D-PS-86k
M_w[g/mol]	545000	95100	86300
PDI	1.12	1.07	1.02

In order to compare the experimental results obtained from the neutron scattering analysis regarding the molecular orientation of short polymer molecules blended together with longer ones we have prepared the corresponding sample of purely short molecules, with 10% deuterium, named Short in Short SiS. The matrix is represented by the same protonated PS used in the blend 50L-50S (same batch) PS-95k while the deuterated sample D-PS-80k was purchased by Polymer Standards Service (PSS). The procedure employed to prepare the final sample (SiS) in the same as the one described of the sample SiL.

B.2 Mechanical Spectroscopy

Small amplitude oscillatory shear measurements were performed to determine the linear viscoelastic (LVE) properties of both SiL and SiS samples. An 8 mm plate-plate geometry was used on an ARES-G2 rheometer from TA Instruments. The experiments were done at different temperatures, ranging from 130 to 190 °C in nitrogen atmosphere. Data were shifted to a single master curve at 130 °C, according to the Time Temperature Superposition (TTS) principle. In table B.2 are reported the shift factors a_T at different temperatures.

Table B.2: Temperature shift factors for the SiL

Sample name	150 to 130 °C	170 to 130 °C	190 to 130 °C
SiL	0.0158	$9.96 \cdot 10^{-4}$	$1.5 \cdot 10^{-4}$

In Figure B.1 the LVE data of the SiL and the Blend 50L-50S (taken from Hengeller *et al.* (2016)) are compared at the same reference temperature (130 °C). It can be seen

that the LVE properties of the two blends are close to each other. Figure B.2 shows the overlay of the LVE data of the hydrogenated PS-95k melt (from Hengeller *et al.* (2016)) and the LVE of the sample SiS.

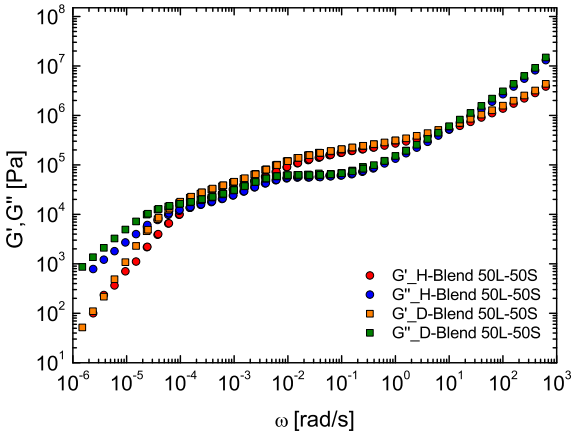

Figure B.1: Comparison of the LVE data of the Blend 50L-50S used in the work of Hengeller *et al.* (2016) and the SiL sample.

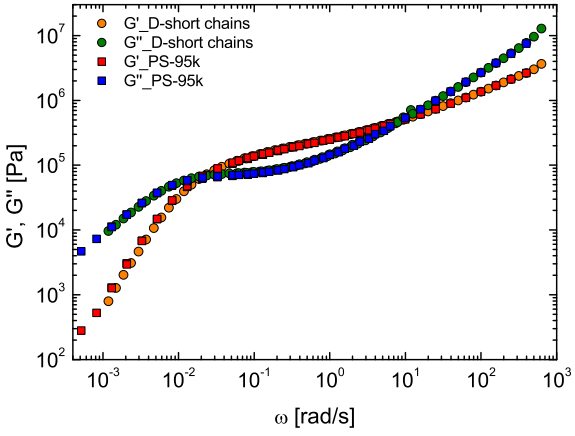

Figure B.2: Comparison of the LVE data of the PS-95k used in the work of Hengeller *et al.* (2016) and the SiS sample.

B.3 Filament Stretching and Quenching

B.3.1 Quenching at Steady-state Extensional Flow

The extensional stress measurements of the Blend 50L-50S, have been described by Hengeller *et al.* (2016). Figure B.3 shows the measured corrected extensional stress difference $\langle \sigma_{zz} - \sigma_{rr} \rangle$ plotted as a function of Hencky strain. The experimental data correspond to three stretch rates $\dot{\varepsilon} = 0.003 s^{-1}$, $\dot{\varepsilon} = 0.03 s^{-1}$, $\dot{\varepsilon} = 0.1 s^{-1}$ and were performed at 130 °C. From the plot, it can be seen that the extensional steady flow conditions are established at around an Hencky strain of 3.

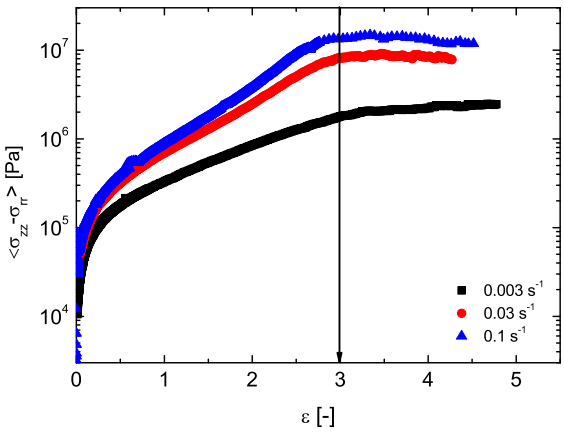

Figure B.3: Extensional tress data as a function of Hencky strain for the Blend 50L-50S (Hengeller *et al.* (2016)).

In order to investigate the dynamics of the short molecules in the blend in steady-state flow we perform uniaxial extension measurements on the SiL under the same experimental conditions of the Blend 50L-50S, and quench the sample at Hencky strain 3, where the steady-state is reached. The extensional stress measurements followed by the quenching have been performed on the newly developed filament stretching device, VADER-1000, designed to measure polymer melts in extensional flow. The samples were molded into cylindrical shaped pellets with a diameter D_0 of 8 mm. The choice of a bigger diameter, respect to the 5.4 mm used in Hengeller *et al.* (2016), is related with the necessity to have a thicker filament at the end of the experiments. In fact, in neutron scattering measurements a volume of circa $1 mm^3$ of sample is required to obtain a good statistic in a reasonable time. The final mid-diameter of the samples was always above

0.5*mm*. Pre-stretching procedure was performed at 160 °C, in nitrogen environment, to a diameter ranging from 5.8 mm and 2.38 mm, respectively for the lowest and the highest stretch rate. After pre-stretching the temperature was decreased to 130 °C, at which all the measurements were performed. Table B.3 reports the values of the diameter D_p at 130 °C before the experiments start. Prior to extension, the samples were allowed to relax to equilibrium. For $t > 0$ extensional flow started with a constant stretch rate $\dot{\varepsilon}$. When it reached Hencky strain of 3 at a time $t = \varepsilon/\dot{\varepsilon} = 3/\dot{\varepsilon}$, the cylindrical oven was lifted up, exposing the filament to the room temperature and a jet of Nitrogen gas was blown in correspondence of the mid-filament plane. At the same time the stretching experiment stops automatically. The mid-filament diameter after quenching D_q and the number of samples prepared for each stretch rate are reported in table B.3. In the table are also reported values of the fully relaxed sample, which corresponds to stretch rate $\dot{\varepsilon} = 0$. This sample has been obtained by pre-stretching the filament at 160°*C*, then the temperature was decreased at 130°*C* and before quenching, it was ensured that all the residual stresses were completely relaxed.

Table B.3: Summary of experimental quenching parameters.

$\dot{\varepsilon}\left[s^{-1}\right]$	$D_p\,(130°C)\,[mm]$	$D_q\,[mm]$	$\#Samples$
0	-	1.2	3
0.003	5.38	1.18	4
0.03	3.14	0.65	7
0.1	2.33	0.49	9

Due to sample shrinking during quenching the diameter after quenching D_q may be slightly smaller than the desired diameter which corresponds to Hencky strain 3. The difference is below 1.5%. The neutron scattering results rely on the assumption that the sample quenches before the polymer chains have the time to relax. To check that the cooling process was fast enough to do not allow the loss of the molecular configuration (reached right before the quenching) an extra experiment has been performed. The measurement has been designed to be at the same Weissemberg number of the one at $\dot{\varepsilon} = 0.1s^{-1}$ at 130°*C* but at 125°*C*. The corresponding strain rate ($\dot{\varepsilon} = 0.0245s^{-1}$) at this temperature has been obtained by applying the TTS with a shift factor $a_T = 4.07$. In this way the experimental temperature is closer to the T_g of PS, and the relaxation time of the chains is higher than at 130°*C*. Analysis of the SANS isointensity patterns of the two experiments (reported in Chapter 5) probed that the average conformation of the individual short chains is essentially the same. Figure B.4 shows the comparison between data of uniaxial experiments with $\dot{\varepsilon} = 0.1s^{-1}$ at 130°*C* for the Blend 50L-50S (performed with the FSR) and the SiL sample (performed with the VADER 1000). The measurement of Blend 50L-50S reaches a higher value of Hencky strain, while the two data sets of the D-Blend 50L-50S stop at Hencky strain 3, point at which the quenching was performed. A good matching between the curves is shown, which ensures the reproducibility of the data (whithin the same instrument and between the FSR and the VADER 1000) and the same behaviour of the two samples in extensional flow.

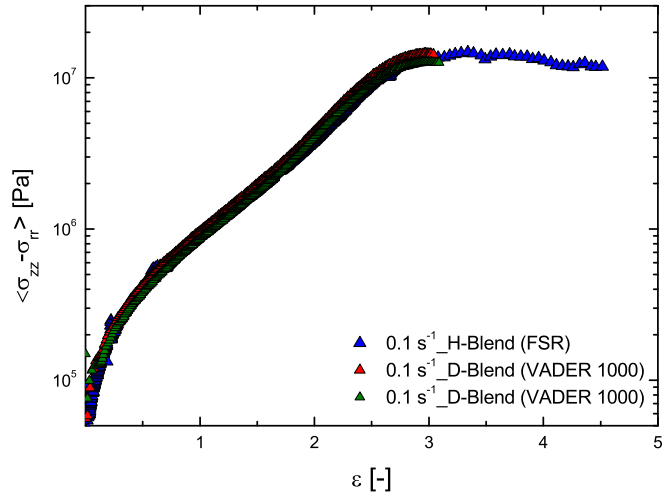

(a)

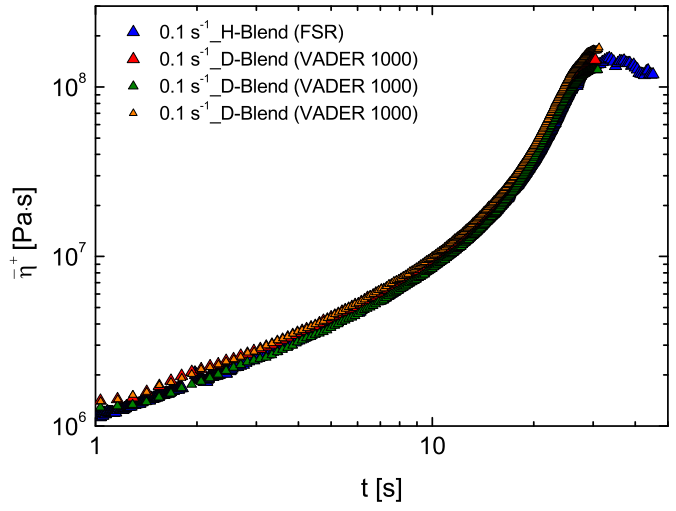

(b)

Figure B.4: (a) Comparison of the stress data as a function of Hencky strain of the Blend 50L-50S (measured with the FSR) and the SiL sample quenched at $\varepsilon = 3$ (measured with the VADER 1000). (b) Comparison of stress growth coefficient data as a function of time of the Blend 50L-50S (measured with the FSR) and the sample SiL quenched $\varepsilon = 3$(measured with the VADER 1000).

Figure B.5 shows the liquid bridges obtained after quenching of the sample SiL.

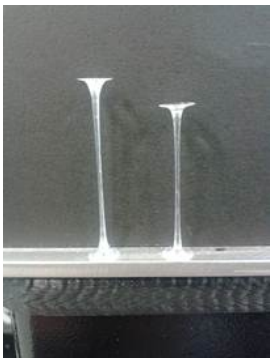

Figure B.5: Deuterated-PS filaments quenched.

Once that the samples for each stretch rate were prepared, they had to be arranged in a suitable way to perform neutron scattering experiments. All the liquid bridges were cut and deprived of the asymmetric extremities. The central rod-like part (almost homogeneous cylindrical shape) was then placed, together with the other rods obtained from the same kind of experiment, in a sample holder specifically designed for the purpose. Figure B.6 shows the 3-D design of the sample holder, while Figure B.7 shows how the PS rods (obtained for the experiment at $\varepsilon = 0.03 s^{-1}$) were organized in the sample holder. The sample holder is made of aluminium, which is almost transparent to neutrons; the inner circular window has a diameter of 9 mm, that allows the neutron beam (circa 6-7 mm) to cross just the central part of the samples.

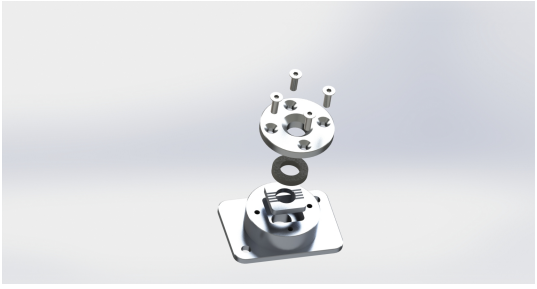

Figure B.6: Sample holder 3D design.

Figure B.7: Sample holder with the polystyrene rods.

B.3.2 Quenching during Stress Relaxation

In the work of Hengeller *et al.* (2016) stress relaxation experiments following startup of uniaxial elongation were also performed for the sample Blend 50L-50S at 130°C. The flow was stopped when the true steady-state value for the extensional stress growth coefficient was reached. It was observed that experimental data of the Blend 50L-50S at the highest deformation rate, $\dot{\varepsilon} = 0.1s^{-1}$, exhibited a pronounced bump in the stress decay curve. Figure B.8 shows the stress relaxation data (for the Blend 50L-50S and for the PS-95k) normalized by the first value of the stress decay $\sigma(t = 0)$ plotted against the relaxation time, where t=0 is the start of the relaxation part experiment. To further investigate the relaxation dynamics of the short molecules the SiL and the SiS samples were uniaxially stretched with $\dot{\varepsilon} = 0.1s^{-1}$ until steady-state conditions (up to Hencky strain 3), relaxed and quenched at different times during relaxation. In figure B.8 the red arrows highlight the corresponding times at which the quenching was performed. Sample SiL was quenched at six different stages of the relaxation process (see Figure B.9(a)), covering a wide spectrum (quenching parameters are listed in Table B.4). In the plot are also reported the reptation time and the Rouse time of the monodisperse linear long and short components as well as the reptation time of the bimodal melt, all taken from Hengeller *et al.* (2016).

Table B.4: Summary of the quenching parameters for the sample SiL: relaxation time, the mid-diameter value and the number of samples.

Relaxation time $[s]$	$Log_{10}(t)$	Mid-Diameter$[mm]$	$\#Samples$
10	1	~ 0.5	4
20	1.3	~ 0.5	8
80	1.9	~ 0.5	4
320	2.5	~ 0.5	4
1260	3.1	~ 0.5	4
13000	4.08	~ 0.5	3

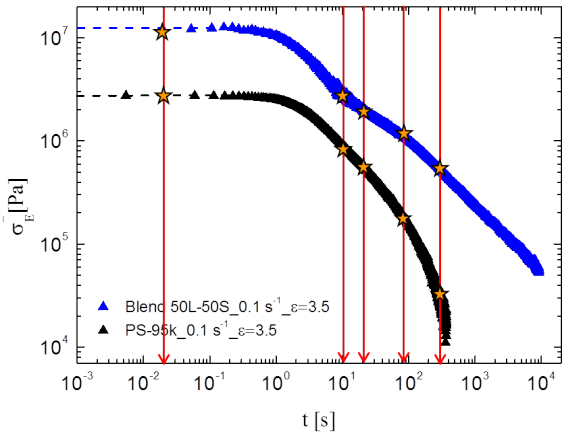

Figure B.8: Normalized stress decay σ_E^- for the Blend 50L-50S and for the PS-95k at 130°C after cessation of fast uniaxial elongational flow (up to $\varepsilon_0 = 3$ at strain rate $\dot{\varepsilon} = 0.1s^{-1}$). The red arrows indicate times where quenched filaments were produced for both the deuterated samples.

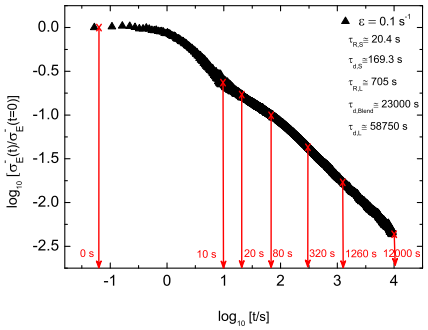

(a)

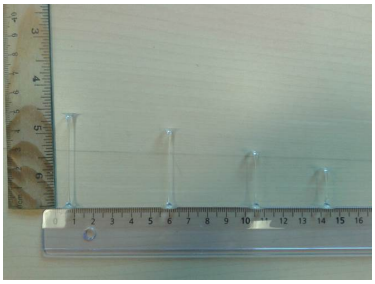

(b)

Figure B.9: (a) Normalized stress decay σ_E^- for the Blend 50L-50S at 130°C after cessation of fast uniaxial elongational flow (up to $\varepsilon_0 = 3$ at strain rate $\dot{\varepsilon} = 0.1s^{-1}$). The six red arrows indicate times where quenched filaments were produced.(b) Quenched samples at different relaxation times: the shorter filaments correspond to the longer relaxation time.

APPENDIX C

Joint Author Statements

Technical University of Denmark

Joint author statement

If a thesis contains articles (i.e. published journal and conference articles, unpublished manuscripts, chapters etc.) made in collaboration with other researchers, a joint-author statement verifying the PhD student's contribution to each article should be made by all authors. However, if an article has more than three authors the statement may be signed by a representative sample, cf. article 12, section 4 and 5 of the Ministerial Order No. 1039 27 August 2013 about the PhD degree. We refer to the Vancouver protocol's definition of authorship.

A representative sample of authors is comprised of

- Corresponding author and/or principal/first author (defined by the PhD student), and if there are more authors:
- 1-2 authors (preferably international/non-supervisor authors)

Titel of the article	Bridging the gap between polymer melts and solutions in extensional rheology
Author(s)	Huang Q., Hengeller L., Alvarez N. J., and Hassager O.
Journal/conference * If applicable	Macromolecules
Name of PhD student	Ludovica Hengeller
Date of Birth	23 January 1988

Description of the PhD student's contribution to the abovementioned article

Prepared part of the samples of the different solutions, both before and after experiments, for characterization with Size Exclusion Chromatography (SEC). Carried out the analysis of the peak areas to determine the samples composition.
Prepared the samples of the different solutions for determination of the glass transition temperature with Differential Scanning Calorimetry (DSC).
Engaged in discussions about the results and help with data analysis.
Provided feedback on the manuscript.

Signature of the PhD student Ludovica Hengeller Date 16/02/16

Signatures of co-authors

As a co-author I state that the description given above to the best of my knowledge corresponds to the process and I have no further comments.

Date (DD/MM/YY)	Name	Signature
16/02/16	Qian Huang	Qian Huang
16/02/16	Nicolas J. Alvarez	
16/02/16	Ole Hassager	

Joint author statements shall be delivered to the *PhD administration* along with the PhD thesis

Joint author statement

If a thesis contains articles (i.e. published journal and conference articles, unpublished manuscripts, chapters etc.) made in collaboration with other researchers, a joint-author statement verifying the PhD student's contribution to each article should be made by all authors. However, if an article has more than three authors the statement may be signed by a representative sample, cf. article 12, section 4 and 5 of the Ministerial Order No. 1039 27 August 2013 about the PhD degree. We refer to the Vancouver protocol's definition of authorship.

A representative sample of authors is comprised of
- Corresponding author and/or principal/first author (defined by the PhD student), and if there are more authors:
- 1-2 authors (preferably international/non-supervisor authors)

Titel of the article	Stress relaxation of bi-disperse polystyrene melts: Exploring the interactions between long and short chains in non-linear rheology
Author(s)	Hengeller L., Huang Q., Dorokhin A., Alvarez N. J., Almdal K., and Hassager O.
Journal/conference * if applicable	Rheologica Acta
Name of PhD student	Ludovica Hengeller
Date of Birth	23 January 1988

Description of the PhD student's contribution to the abovementioned article

Prepared the blend and performed all the experiments (oscillatory measurements, filament stretching experiments of start-up and stress relaxation).
Carried out post processing of data and data fitting.
Prepared the samples, both before and after experiments, for characterization with Size Exclusion Chromatography (SEC). Carried out the analysis of the peak areas to determine the samples composition.
Prepared the samples of the different solutions for determination of the glass transition temperature with Differential Scanning Calorimetry (DSC).
Wrote the first draft of the article manuscript.

Signature of the PhD student Ludovica Hengeller Date 16/02/16

Signatures of co-authors

As a co-author I state that the description given above to the best of my knowledge corresponds to the process and I have no further comments.

Date (DD/MM/YY)	Name	Signature
16/02/16	Qian Huang	Qian Huang
16/02/16	Andriy Dorokhin	Dorokhin
16/02/16	Nicolas J. Alvarez	Nicolas J. Alvarez

PhD and Continuing Education
February 2015 | page 2/2

Technical University of Denmark

DTU

Titel of the article	Stress relaxation of bi-disperse polystyrene melts: Exploring the interactions between long and short chains in non-linear rheology
Author(s)	Hengeller L., Huang Q., Dorokhin A., Alvarez N. J., Almdal K., and Hassager O.

16/02/16 Kristoffer Almdal

16/02/16 Ole Hassager

Joint author statements shall be delivered to the *PhD administration* along with the PhD thesis

Technical University of Denmark

Joint author statement

If a thesis contains articles (i.e. published journal and conference articles, unpublished manuscripts, chapters etc.) made in collaboration with other researchers, a joint-author statement verifying the PhD student's contribution to each article should be made by all authors. However, if an article has more than three authors the statement may be signed by a representative sample, cf. article 12, section 4 and 5 of the Ministerial Order No. 1039 27 August 2013 about the PhD degree. We refer to the Vancouver protocol's definition of authorship.

A representative sample of authors is comprised of

- Corresponding author and/or principal/first author (defined by the PhD student), and if there are more authors:
- 1-2 authors (preferably international/non-supervisor authors)

Titel of the article	Nematic effects and strain coupling in entangled polymer melts under strong flow
Author(s)	Kirkensgaard Jacob J.K., Hengeller L., Dorokhin A., Christopher J. Garvey, Almdal K., Mortensen K., Hassager O. , and Huang Q.
Journal/conference * if applicable	Macro Letters
Name of PhD student	Ludovica Hengeller
Date of Birth	23 January 1988

Description of the PhD student's contribution to the abovementioned article

Prepared the deuterated blend and the deuterated short molecular weight component melt. Performed all the experimental rheology and carried out post processing of rheology data. Prepared the samples for characterization with Size Exclusion Chromatography (SEC) and the samples for determination of the glass transition temperature with Differential Scanning Calorimetry (DSC).
Prepared the quenched samples to perform Small Angle Neutron Scattering measurements and helped in the experiments at the Paul Sherrer Institute.
Wrote the part of SANS samples preparation in the article manuscript.

Signature of the PhD student: Ludovica Hengeller Date 16/2/2016

Signatures of co-authors

As a co-author I state that the description given above to the best of my knowledge corresponds to the process and I have no further comments.

Date (DD/MM/YY)	Name	Signature
16/02/16	Jacob J.K. Kirkensgaard	
16/02/16	Andriy Dorokhin	Dorokhin

Technical University of Denmark

Titel of the article	Nematic effects and strain coupling in entangled polymer melts under strong flow
Author(s)	Kirkensgaard Jacob J.K., Hengeller L., Dorokhin A., Christopher J. Garvey, Almdal K., Mortensen K., Hassager O., and Huang Q.

16/02/16	Christopher J. Garvey	C. J. Garvey
16/02/16	Kristoffer Almdal	
16/02/16	Kell Mortensen	
16/02/16	Ole Hassager	
16/02/16	Qian Huang	Qian Huang

Joint author statements shall be delivered to the *PhD administration* along with the PhD thesis

Bibliography

Alvarez, N. J., J. M. Román Marín, Q. Huang, M. L. Michelsen, and O. Hassager, "Creep measurements confirm steady flow after stress maximum in extension of branched polymer melts", Phys. Rev. Lett. 110, 168301 (2013).

Andreev, M., R. N. Khaliullin, R. J. A. Steenbakkers , and J. D. Schieber, "Approximations of the discrete slip-link model and their effect on nonlinear rheology predictions". J Rheol 57(2),535–557 (2013).

Anna, S., C. Rogers, and G. H. McKinley, "Controlling the kinematics of a filament stretching rheometer using a real-time active control mechanism", J. Non-Newtonian Fluid Mech. 87, 307–335 (1999).

Auhl, D., P. Chambon, T. C. B. McLeish, and D. J. Read, "Elongational flow of blends of long and short polymers: effective stretch relaxation time", Phys. Rev. Lett. 103, 136001 (2009).

Auhl, D., D. M. Hoyle, D. Hassell, T. D. Lord, O. G. Harlen, M. R. Mackley, and T. C. B. McLeish, "Cross-slot extensional rheometry and the steady–state extensional response of long chain branched polymer melts", J. Rheol. 55(4), 875–900 (2011).

Bach, A., K. Almdal, H. K. Rasmussen, and O. Hassager, "Elongational viscosity of narrow molar mass distribution polystyrene", Macromolecules 36, 5174–5179 (2003a).

Bach, A., H. K. Rasmussen, and O. Hassager, "Extensional viscosity for polymer melts measured in the filament stretching rheometer", J. Rheol. 47(2), 429–441 (2003b).

Barnes, H. A.,"Handbook of Elementary Rheology", University of Wales, Institute of Non-Newtonian Fluid Mechanics, (2000).

Baumgaertel, M., A. Schausberger, and H. H. Winter, "The relaxation of polymers with linear flexible chains of uniform length", Rheol. Acta 29, 400–408 (1990).

Berry, G. C., and T. G. Fox, "The viscosity of polymers and their concentrated solutions", Advances in Polymer Science 5, 261–357 (1968).

Bhattacharjee, P. K., J. P. Oberhauser, G. H. McKinley, L. G. Leal, and T. Sridhar, "Extensional rheometry of entangled solutions", Macromolecules 35, 10131–10148 (2002).

Bhattacharjee, P. K., D. A. Nguyen, G. H. McKinley and T. Sridhar, "Extensional stress growth and stress relaxation in entangled polymer solutions", J. Rheol. 47, 269–290 (2003).

Bird, R. B., R. C. Armstrong, and O. Hassager, "Dynamics of Polymeric Liquids", Vol. 1 Wiley, New York (1987).

Chapellier, B., B. Deloche, and R. Oeser, "Segmental order in uniaxially strained bimodal polymer networks: a deuterium-NMR study", J. Phys. II France 3, 1619–1631 (1993).

Churchill, S. W., and M. Bernstein, "Transactions of the ASME", 99, 300 (1977).

Cogswell, F. N., "Tensile deformations in molten polymers", Rheol. Acta 8, 187–194 (1969).

Colby, R., L. J. Fetters, and W. Graessley, "Melt viscosity-molecular weight relationship for linear polymers", Macromolecules 20, 2226–2237 (1987).

Daoud, M.; de Gennes, P.G., "Some remarks on the dynamics of polymer melts", J. Polym. Sci.: Polym. Phys. 17, 1971–1981 (1979).

de Gennes, P. G., "Dynamics of entangled polymer solutions. II Inclusion of hydrodynamic interactions", Macromolecules 9, 594–598 (1975).

de Gennes, P. G., "Reptation of a polymer chain in the presence of fixed obstacles", J. of Chem. Phys. 55, 572–579, (1971).

des Cloizeaux, J., "Double reptation vs. simple reptation in polymer melts", J. Europhys. Lett. 5, 437–432 (1988).

Doi, M., "Explanation for the 3.4 power law of viscosity of polymeric liquids on the basis of the tube model", J. Polym. Sci.: Polym. Lett. Ed. 19, 265–273 (1981).

Doi, M., "Introduction to polymer physics", Clarendon Press, Oxford, (1996).

Doi, M. and S. F. Edwards, "Dynamics of concentrated polymer systems. III. Rheological properties", J. Chem. Soc., Faraday Trans. 2 74, 1818–1832 (1978).

Doi, M. and S. F. Edwards, “The theory of polymer dynamics”, Oxford Univ. Press, New York, (1986).

Edwards, S., “The statistical mechanics of polymerized material”, Proceedings of the Physical Society 92, 9–16 (1967).

Graessley, W., “Entangled linear, branched and network polymer systems- molecular theories”, Advances in Polymer Science 47, 69–117 (1982).

Hassager, O., K. Mortensen, A. Bach, K. Almdal, H. K. Rasmussen, and W. Pyckhout-Hintzen, “Stress and neutron scattering measurements on linear polymer melts undergoing steady elongational flow", Rheol. Acta 51, 385–394 (2012).

Hayes, C., L. Bokobza , F. Boué, E. Mendes , and L. Monnerie, “Relaxation dynamics in bimodal polystyrene melts: a Fourier-transform infrared dichroism and small-angle neutron scattering study”, Macromolecules 29, 5036–5041 (1996).

Heinrich, G and E. Straube, “Theoretical investigation of SANS from elastomeric networks with topological constraints”, Polymer Bulletin 17, 255–261 (1987).

Heinrich, G, E. Straube, and G. Helmis, “Rubber elasticity of polymer networks: Theories”, Adv. Polym. Sci. 85, 33–87 (1988).

Hengeller, L., Q. Huang, A. Dorokhin, K. Almdal, N. J. Alvarez, and O. Hassager, “Stress Relaxation of Bidisperse Polystyrene Melts: Exploring the Interactions between Long and Short Chains in Non-linear Rheology", Rheol. Acta, (2016).

Huang, Q., H. K. Rasmussen, A. L. Skov, and O. Hassager, “Stress relaxation and reversed flow of low-density polyethylene melts following uniaxial extension”, J. Rheol. 56(6), 1535–1554 (2012).

Huang, Q. Ph.D. thesis, Technical University of Denmark, (2013).

Huang, Q., O. Mednova, H. K. Rasmussen, N. J. Alvarez, A. L. Skov, K. Almdal, and O. Hassager, “Concentrated polymer solutions are different from melts: role of entanglement molecular weight”, Macromolecules 46, 5026–5035 (2013a).

Huang, Q., N. J. Alvarez, Y. Matzumiya, H. K. Rasmussen, H. Watanabe, and O. Hassager, “Extensional rheology of entangled polystyrene solutions suggests importance of nematic interaction”, ACS Macro Letters 2, 741–744 (2013b).

Huang, Q., M. Mangnus, N. J. Alvarez, R. Koopmans, and O. Hassager, “A new look at extensional rheology of low-density polyethylene”, Rheol. Acta 55(5), 343–350 (2016).

Ianniruberto, G., A. Brasiello, and G. Marrucci, “Simulations of fast shear flows of PS oligomers confirm monomeric friction reduction in fast elongational flows of monodisperse PS melts as indicated by rheooptical data”, Macromolecules 45, 8058–8066 (2012).

Ianniruberto, G. and G. Marrucci, "Entangled melts of branched PS behave like linear PS in the steady state of fast elongational flows", Macromolecules 46, 267–275 (2013).

Ianniruberto, G., "Extensional Flows of Solutions of Entangled Polymers Confirm Reduction of Friction Coefficient", Macromolecules 48, 6306–6312 (2015).

Jackson, J. K. and H. H. Winter, "Entanglement and Flow Behavior of Bidisperse Blends of Polystyrene and Polybutadiene", Macromolecules 28, 3146–3155 (1995).

Khaliullin, R. N. and J. D. Schieber, "Application of the Slip-link Model to Bidisperse Systems", Macromolecules 43, 6201–6212 (2010).

Kolte, M. I., H. K. Rasmussen, and O. Hassager, "Transient filament stretching rheometer II: Numerical simulation", Rheol. Acta 36, 285–302 (1997).

Kornfield, J. A., G. Fuller, and D. S. Pearson, "Dichroism Measurements of Molecular Relaxation in Binary Blend Melt Rheology", Macromolecules 22, 1334–1345 (1989).

Lee, J. H., L. J. Fetters, and L. A. Archer, "Branch–point motion in asymmetric star polymers", Macromolecules 38, 4484–4494 (2005).

Likhtman, A. E. and T. C. B. McLeish, "Quantitative theory for linear dynamics of linear entangled polymers", Macromolecules 35, 6332–6343 (2002).

Luap, C., C. Müller, T. Schweizer, and D. C. Venerus, "Simultaneous stress and birefringence measurements during uniaxial elongation of polystyrene melts with narrow molecular weight distribution", Rheol. Acta 45, 83–91 (2005).

Lyhne, A., H. K. Rasmussen, and O. Hassager, "Simulation of Elastic Rupture in Extension of Entangled Monodisperse Polymer Melts", Phys. Rev. Lett. 102, 138301 (2009).

Marrucci, G., "Relaxation by reptation and tube enlargement: A model for polydisperse polymers", J. Polym. Sci. Polym. Phys. Ed. 23, 159–177 (1985).

Marrucci, G. and N. Grizzuti, "Fast flows of concentrated polymers: Prediction of the tube model on chain stretching", Gazz. Chim. Ital. 118, 179–185 (1988).

Marrucci, G., "A nonlinear model consistent with the Cox-Merz rule", J. Non-Newtonian Fluid Mech. 62, 279–289 (1996).

Marrucci, G. and G. Ianniruberto, "On compatibility of the Cox-Merz rule with the model of Doi and Edwards", J. Non-Newtonian Fluid Mech. 65, 241–246 (1996).

Marrucci, G. and G. Ianniruberto, "Convective orientational renewal in entangled polymers", J. Non-Newtonian Fluid Mech. 95, 363–374 (2000).

Marrucci, G. and G. Ianniruberto, “Interchain pressure effect in in extensional flows of entangled polymer melts”, Macromolecules 37, 3934–3942 (2004).

Marrucci, G. and G. Ianniruberto, “Modelling non-linear polymer rheology is still challenging”, Korea-Australia Rheol. J. 17(3), 111–116 (2005).

Masubuchi, Y.; Matsumiya, Y.; Watanabe, H., “Test of Orientation/Stretch-Induced Reduction of Friction via Primitive Chain Network Simulations for Polystyrene, Polyisoprene, and Poly(n-butyl acrylate)”, Macromolecules 47, 6768–6775 (2014).

Matta, J. E. and R. P. Tytus, “Liquid stretching using a falling cylinder”, J. Non-Newtonian Fluid Mech. 35, 215–229 (1990).

McKinley, G. H. and T. Sridhar, “Filament stretching rheometry of complex fluids", Annu. Rev. Fluid Mech. 34, 375–415 (2002).

McLeish, T.C.B., “Tube theory of entangled polymer dynamics”, Adv. Phys. 51(6), 1379–1527 (2002).

Meissner, J., “Dehnungsverhalten von polyäthylen-schmelzen”, Rheologica Acta 10, 230–242 (1971).

Meissner, J., “Development of a universal extensional rheometer for the uniaxial extension of polymer melts”, Transactions of the society of rheology 16(3), 405–420 (1972).

Meissner, J. and J. Hostettler, “A new elongational rheometer for polymer melts and other highly viscoelastic liquids”, Rheol. Acta 33, 1–21 (1994).

Milner, S. T. and T. C. B McLeish, “Reptation and Contour-Length Fluctuations in Melts of Linear Polymers”, Phys. Rev. Lett. 81, 725–728 (1998).

Münstedt, H. and H. Laun, ‘Elongational behaviour of a low density polyethylene melt Part I. Strain rate and stress dependence of viscosity and recoverable strain in the steady-state”, Rheol. Acta 17, 415–425 (1978).

Münstedt, H., “New universal extensional rheometer for polymer melts, measurements on a polystyrene sample”, J. Rheol. 23, 421–436 (1979).

Ndoni, S., Ch. M. Papadakis, F. S. Bates, and K. Almdal, “Laboratory–scale setup for anionic polymerization under inert atmosphere”, Rev. Sci. Instrum. 66(2), 1090–1095 (1995).

Nielsen, J. K., H. K. Rasmussen, O. Hassager, and G. H. McKinley, “Elongational viscosity of monodisperse and bidisperse polystyrene melts”, J. Rheol. 50, 453–476 (2006).

Nielsen, J. K., H. K. Rasmussen, M. Denberg, K. Almdal, and O. Hassager, "Nonlinear Branch-Point Dynamics of Multiarm Polystyrene", Macromolecules 39, 8844–8853 (2006b).

Nielsen, J. K., H. K. Rasmussen, and O. Hassager, "Stress relaxation of narrow molar mass distribution polystyrene following uniaxial extension", J. Rheol. 52(4), 885–899 (2008).

Orr, N. V. and T. Sridhar, "Probing the dynamics of polymeric solutions in extensional flow using step strain rate experiments", J. Non-Newtonian Fluid Mech. 82, 203–232 (1999).

Ott, M., R. Perez-Aparicio, H. Schneider, P. Sotta, and K. Saalwachter, "Microscopic Study of Chain Deformation and Orientation in Uniaxially Strained Polymer Networks: NMR Results versus Different Network Models", Macromolecules 47, 7597-7611 (2014).

Pyckhout-Hintzen, W., S. Westermann, A. Wischnewski, M. Monkenbusch, D. Richter, E. Straube, B. Farago, and P. Lindner, "Direct Observation of Non affine Tube Deformation in Strained Polymer Networks", Phys. Rev. Lett. 110, 196002 (2013).

Park, S. J. and R. G. Larson, " Tube dilation and reptation in binary blends of monodisperse linear polymers", Macromolecules 37, 597–604 (2004).

Rasmussen, H. K., J. K. Nielsen, A. Bach, and O. Hassager, "Viscosity overshoot in the start-up of uniaxial elongation of low density polyethylene melts", J. Rheol. 49(2), 369–381 (2005).

Rasmussen, H. K., A. G. Bejenariu, O. Hassager, and D. Auhl, "Experimental evaluation of the pure configurational stress assumption in the flow dynamics of entangled polymer melts", J. Rheol. 54(6), 1325–1336 (2010).

Rasmussen, H. K., "Interchain tube pressure effect in the flow dynamics of bi-disperse polymer melts", Rheol. Acta 54, 9–18 (2014).

Read, D.J. and T.C.B. McLeish, "Microscopic theory for the "lozenge" contour plots in scattering from stretched polymer networks", Macromolecules 30, 6376–6384 (1997a).

Read, D.J. and T.C.B. McLeish, "Lozenge contour plots in scattering from polymer networks ", Phys. Rev. Lett. 79, 1, 87–90 (1997b).

Read, D.J. and T.C.B. McLeish, "Comment on "Lozenge" contour plots in scattering from polymer networks' - Reply", Phys. Rev. Lett. 80, 24, 5450 (1998).

Read, D. J., K. Jagannathan, S. K. Sukumaran, and D. Auhl, "A full-chain constitutive model for bidisperse blends of linear polymers", J. Rheol. 56(4), 827–873 (2012).

Román Marín, J. M., J. K. Huusom, N. J. Alvarez, Q. Huang, H. K. Rasmussen, A. Bach, A. L. Skov, and O. Hassager, "A control scheme for filament stretching rheometers with application to polymer melts", J. Non-Newtonian Fluid Mech. 194, 14–22 (2013).

Rouse, P. E., "A theory of the linear viscoelastic properties of dilute solutions of coiling polymers", J. Chem. Phys. 21, 1272–1280 (1953).

Rubinstein, M. and S. Panyukov, "Nonaffine Deformation and Elasticity of Polymer Networks", Macromolecules 30, 8036–8044 (1997).

Rubinstein, M. and R. H. Colby, "Polymer Physics", Oxford University Press(2003).

Sentmanat, M., "Miniature universal testing platform: from extensional melt rheology to solid-state deformation behaviour", Rheol. Acta 43, 657–669 (2004).

Spiegelberg, S. H., D. C. Ables, and G. H. McKinley, "The role of end–effects on measurements of extensional viscosity in filament stretching rheometers", J. Non–Newtonian Fluid Mech. 64, 229–267 (1996).

Sridhar, T. V. Tirtaatmadja, D. A. Nguyen, and R. K. Gupta, "Measurement of extensional viscosity of polymer solutions", J. Non-Newtonian Fluid Mech. 40, 271–280 (1991).

Sridhar, T., Acharya, M., Nguyen, D. A., Bhattacharjee, P. K., "On the Extensional Rheology of Polymer Melts and Concentrated Solutions", Macromolecules 47, 379–386 (2014).

Straube, E., "Small-Angle Neutron Scattering Investigation of Topological Constraints and Tube Deformation in Networks", Phys.Rev. Lett. 74, 22, 4464–4467 (1995).

Struglinski, M. J., and W. W. Graessley, "Effect of polydispersity on the linear viscoelastic properties of entangled polymers. 1. Experimental observation for binary mixtures of linear polybutadiene", Macromolecules 18, 2630–2643 (1985).

Struglinski, M. J., and W. W. Graessley, "Effect of polydispersity on the linear viscoelastic properties of entangled polymers. 2. Comparison of viscosity and recoverable compliance with tube model predictions", Macromolecules 19, 1754–1760 (1986).

Szabo, P., "Transient filament stretching rheometer part I: Force balance analysis", Rheol. Acta 36, 277–284 (1997).

Szabo, P., G. H. McKinley, "Filament stretching rheometer: Inertia compensation revisited", Rheol. Acta 42, 269–271 (2003).

Tirtaatmadja, V. and T. Sridhar, "A filament stretching device for measurement of extensional viscosity", J. Rheol. 37(6), 1081–1102 (1993).

Tsenoglou C., "Viscoelasticity of binary polymer blends", ACS Polym. Preprints 28, 185–186 (1987).

van Krevelen, D. V., "Properties of Polymers", Elsevier (1990).

van Ruymbeke, E., C. Y. Liu, and C. Bailly, "Quantitative tube model predictions for the linear viscoelasicity of linear polymers", Rheol. Reviews, 53–134 (2007).

van Ruymbeke, E., J. K. Nielsen, and O. Hassager, "Linear and nonlinear viscoelastic properties of bidisperse linear polymers: Mixing law and tube pressure effect", J. Rheol. 54(5), 1155–1172 (2010).

van Ruymbeke, E., Y. Masubuchi, H. Watanabe, "Effective value of the dynamic dilution exponent in bidisperse linear polymers: from 1 to 4/3". Macromolecules 45, 2085–2098 (2012).

van Ruymbeke, E., V. Shchetnikava, Y. Matsumiya, H. Watanabe, "Dynamic dilution effect in binary blends of linear polymers with well-separated molecular weights", Macromolecules 47, 7653–7665 (2014).

Viovy, J. L. , M. Rubinstein, and R. H. Colby, "Constraint release in polymer melts: tube reorganization versus tube dilation", Macromolecules 24, 3587–3596 (1991).

Wagner, M. H., S. Kheirandish, K. Koyama, A. Nishioka , A. Minegishi, T. Takahashi, " Modelling strain hardening of polydisperse polystyrene melts by molecular by molecular stress function theory", Rheol. Acta 44, 235–243 (2005).

Wagner, M. H., S. Kheirandish, and O. Hassager, "Quantitative prediction of transient and steady-state elongational viscosity of nearly monodisperse polystyrene melts", J. Rheol. 49(6), 1317–1327 (2005).

Wagner, M. H., V. H. Rolón-Garrido, J. K. Nielsen, H. K. Rasmussen, and O. Hassager, "A constitutive analysis of transient and steady-state elongational viscosities of bidisperse polystyrene blends", J. Rheol. 52, 67–86 (2008).

Wagner, M. H., "The effect of dynamic tube dilation on chain stretch in nonlinear polymer melt rheology", J. of Non-Newtonian Fluid Mech. 166, 915–924 (2011).

Wagner, M. H., "Scaling relations for elongational flow of polystyrene melts and concentrated solutions of polystyrene in oligomeric styrene", Rheol Acta 53, 765–777 (2014).

Wagner, M.H., "An extended interchain tube pressure model for elongational flow of polystyrene melts and concentrated solutions", Journal of Non-Newtonian Fluid Mechanics 222, 121–131 (2015).

Wang, Y., P. Boukany, S. Q. Wang, and X. Wang, "Elastic breakup in uniaxial extension of entangled polymer melts", Phys. Rev. Lett. 99, 237801 (2007).

Warner, M and S. F. Edwards, "Neutron scattering from strained polymer networks", J. Phys. A: Math. Gen. 11, 8, 1649–1655 (1978).

Watanabe, H., S. Ishida, Y. Matsumiya, and T. Inoue, "Viscoelastic and dielectric behavior of entangled blends of linear polyisoprenes having widely separated molecular weights: Test of tube dilation picture", Macromolecules 37, 1937–1951 (2004a).

Watanabe, H., S. Ishida, Y. Matsumiya, and T. Inoue, "Test of full and partial tube dilation pictures in entangled blends of linear polyisoprenes", Macromolecules 37, 6619–6631 (2004b).

Watanabe, H., Y. Matzumiya, E. V. Ruymbeke, "Component relaxation times in entangled binary blends of linear chains: reputation/CLF along partially or fully dilated tube", Macromolecules 46, 9296–9312 (2013).

Westermann, S., V. Urban, W. Pyckhout-Hintzen, D. Richter, and E. Straube, "Comment on "Lozenge" Contour Plots in Scattering from Polymer Networks", Phys. Rev. Lett. 80, 24, 5449 (1998).

Yaoita, T., T. Isaki, Y. Masubuchi, H. Watanabe, G. Ianniruberto, and G. Marrucci, "Primitive chain network simulation of elongational flows of entangled linear chains: stretch/orientation–induced reduction of monomeric friction", Macromolecules 45, 2773–2782 (2012).

Ye, K., R. G. Larson, C. Pattamaprom, and T. Sridhar, "Extensional properties of monodisperse and bi-disperse polystyrene solutions ", J. Rheol. 47, 443–468 (2003).

Department of Chemical and Biochemical Engineering
Danish Polymer Centre
Technical University of Denmark
Søltofts Plads, Building 227
2800 Kgs. Lyngby
Denmark

Phone: +45 45 25 68 01
Web: www.kt.dtu.dk/english/Research/DPC